

**A Comprehensive Study of Rock Glacier  
Distribution, Velocities, and Water Storage  
in High Mountain Asia**

**SUN, Zhangyu**

A Thesis Submitted in Partial Fulfillment  
of the Requirements for the Degree of  
Doctor of Philosophy  
in  
Earth and Atmospheric Sciences

The Chinese University of Hong Kong  
May 2025

## **Thesis Assessment Committee**

Professor CHOW Alex (Chair)

Professor LIU Lin (Thesis Supervisor)

Professor TAN Yen Joe (Committee Member)

Professor HUANG Lingcao (Committee Member)

Professor DELALOYE Reynald (External Examiner)

# Abstract

---

Abstract of thesis entitled:

A Comprehensive Study of Rock Glacier Distribution, Velocities, and Water Storage in High Mountain Asia

Submitted by SUN, Zhangyu

for the degree of Doctor of Philosophy

at The Chinese University of Hong Kong in May 2025

Rock glaciers are debris landforms resulting from the former or current gravity-driven creep of permafrost. They hold significant scientific and practical values for permafrost studies, mountain hydrology, and disaster assessment. However, fundamental knowledge about their distribution, kinematics, and hydrological significance as water stores in High Mountain Asia (HMA) remains limited due to the absence of a comprehensive inventory and scarce studies on their velocities and water storage. To fill the knowledge gap, this thesis aims to use optical remote sensing, deep learning and InSAR techniques to comprehensively investigate rock glaciers' characteristics across large regions in HMA.

In our first work, we developed a deep-learning-based mapping method that utilizes the DeepLabv3+ semantic segmentation model. We trained our deep learning model with Planet Basemaps images and existing rock glacier local inventories from six regions, and then applied this model to map rock glaciers for the entire Tibetan Plateau. Based on the deep-learning-mapped areas, we compiled a comprehensive inventory of rock glaciers for the Tibetan Plateau, i.e., TPRoGI [v1.0]. This inventory consists of a total of 44,273 rock glaciers, covering approximately 6,000 km<sup>2</sup>, with a mean area of 0.14 km<sup>2</sup>. Rock glaciers on the Tibetan Plateau are predominantly situated at elevations between 4,000 and 5,500 m a.s.l., with a mean of 4,729 m a.s.l. They tend to occur on slopes with gradients between 10° and 25°, with a mean of 17.7°. Across the plateau, rock glaciers are widespread in the northwestern and southeastern areas, with dense concentrations in the Western Pamir and Nyainqêntanglha, while more sparsely distributed in the inner plateau.

In our second work, we developed a multi-temporal and multi-geometry InSAR framework for large-scale rock glacier velocity assessment. Our approach facilitates the rapid and systematic generation of rock glacier velocity fields by integrating interferograms from multiple acquisition dates and both ascending and descending orbits. To rigorously validate

the method, we compared the InSAR-derived velocities with those derived from three independent datasets including very high-resolution optical imagery (Pléiades satellite and aerial imagery) and Global Navigation Satellite System (GNSS) measurements. The results demonstrate statistically significant correlations between our InSAR-derived velocities and all comparison datasets, whereas our method tends to underestimate the magnitudes. The mean relative difference is approximately 20% when compared to velocities from Pléiades and aerial images, whereas increasing to 50% for GNSS point measurements. Applying our method to Sentinel-1 SAR images acquired between July and August 2022, we produced the first large-scale regional rock glacier velocity dataset, encompassing downslope velocity fields for 19,727 rock glaciers on the Tibetan Plateau. The median velocity of all assessed rock glaciers is 17 cm/yr. Notably, we found a striking velocity contrast between different climatic domains: rock glaciers in the westerlies domain move on average faster (median = 30 cm/yr) than those in the monsoon domain (median = 13 cm/yr).

In our third work, we integrated deep learning techniques with high-resolution satellite imagery to map rock glaciers and, for the first time, comprehensively evaluated their water storage across the entire HMA region. To mitigate the estimation uncertainty of water storage caused by mapping inaccuracies, we calibrated our results using TPRoGI, applying linear scaling to refine region-wide estimates. Our findings reveal that while rock glaciers are not a substitute water resource for glaciers in most of HMA, yet their role in specific subregions is critical and cannot be neglected. Rock glaciers in HMA collectively store  $189.7 \pm 21.7$  km<sup>3</sup> of water volume equivalent (WVEQ), representing ~2.5% (1:39 ratio) of the water stored in glaciers. Notably, the Hengduan Shan holds the largest rock glacier WVEQ ( $22.0 \pm 8.9$  km<sup>3</sup>) and exhibits the highest rock-glacier-to-glacier storage ratio (1:3), driven by the widespread presence of rock glaciers and limited glacier coverage. Moreover, as climate change accelerates glacier mass loss, the relative hydrological importance of rock glaciers is expected to grow in the coming decades.

In summary, this thesis presents a deep learning approach for mapping rock glaciers and an InSAR method for assessing their velocities, both of which are readily transferable to other regions worldwide. We developed the first comprehensive rock glacier inventory for the Tibetan Plateau, produced the first large-scale velocity dataset, and conducted the inaugural assessment of water storage across HMA. The outputs of this thesis constitute a significant contribution towards understanding, monitoring, and assessment of permafrost dynamics and associated hydrological impacts in HMA under climatic warming.

# 摘要

---

石冰川是凍土在重力作用下緩慢蠕動形成的岩屑地貌。它們在多年凍土研究、山地水文效應、以及災害風險評估中具有重要的科學與實用價值。然而，由於缺乏全面的編目數據集以及對石冰川運動速度與儲水量的相關研究匱乏，目前對亞洲高山地區石冰川的分布特徵、運動機制與水文意義的認識仍相當有限。為了填補知識空白，本論文旨在利用遙感、深度學習和InSAR技術，全面研究亞洲高山地區大範圍區域石冰川的特徵。

在第一項研究中，我們開發了一種基於深度學習的石冰川製圖方法。該方法採用DeepLabv3+語義分割模型。我們使用 Planet Basemaps 影像與六個地區現有石冰川局部目錄來訓練我們的深度學習模型，然後將此模型應用於繪製整個青藏高原的石冰川分佈。基於深度學習的預測結果，我們建立了首個青藏高原全域石冰川目錄TPRoGI [v1.0]，共包含44,273條石冰川，總面積約6,000平方公里，平均單體面積為0.14平方公里。這些石冰川主要分布於海拔4,000至5,500米之間（平均4,729米），坡度集中在10°至25°範圍內（平均17.7°）。空間分布上呈現明顯的區域差異：西北部的西帕米爾地區與東南部的念青唐古拉山脈分布最為密集，而高原內部則相對稀疏。

在第二項研究中，我們開發了一套多時相、多幾何構型的InSAR分析框架，用於大範圍石冰川運動速度評估。該方法通過整合不同獲取時間、升軌與降軌的干涉圖，實現了石冰川速度場的高效系統化生成。為驗證方法的可靠性，我們將InSAR反演的速度結果與三組獨立數據集（包括Pléiades衛星超高分辨率光學影像、航空影像以及全球導航衛星系統GNSS實測數據）進行比對。結果顯示InSAR速度與所有對照數據均具有統計顯著性相關，但存在系統性低估現象：與Pléiades和航空影像的相對差異約為20%，與GNSS單點測量的差異則達50%。應用該方法處理2022年7月至8月的Sentinel-1 SAR影像後，我們成功建立了涵蓋青藏高原19,727條石冰川的首個大範圍速度數據集，其運動速度中位數為17厘米/年。值得注意的是，不同氣候帶之間存在顯著的速度差異：西風帶影響區的石冰川運動速度（中位數30厘米/年）明顯快於季風影響區（中位數13厘米/年）。

在第三項研究中，我們整合深度學習技術與高分辨率衛星影像，首次對整個亞洲高山

地區的石冰川儲水量進行全面評估。為降低製圖不確定性對儲水量估算的影響，我們採用TPRoGI目錄進行線性比例校正。研究結果表明，雖然在大部分亞洲高山地區石冰川的水文貢獻無法與冰川相比，但在某些特定區域（如橫斷山脈）其作用不容忽視。亞洲高山地區石冰川的總儲水量達 $189.7 \pm 21.7$ 立方公里水當量（WVEQ），約佔冰川總儲水量的2.5%（比例為1:39）。其中，橫斷山脈以 $22.0 \pm 8.9$ 立方公里WVEQ的儲量位居首位，由於該區域石冰川分布廣泛而冰川覆蓋有限，其石冰川與冰川的儲量比例更達到1:3。隨著氣候變化加劇冰川消退，預計未來數十年石冰川的水文重要性將可能持續提升。

本研究提出的深度學習製圖方法與InSAR速度評估技術具有全球適用性。我們不僅建立了青藏高原首個全域石冰川目錄、首個大範圍運動速度數據集，更完成了亞洲高山地區石冰川儲水量的開創性評估。這些研究成果為理解與監測氣候變化背景下亞洲高山地區多年凍土的演變提供了重要的科學基礎。

# Acknowledgements

---

The completion of this dissertation marks the culmination of four transformative years that would not have been possible without the unwavering support, guidance, and encouragement of countless individuals. To all who walked alongside me in this journey—whether through intellectual inspiration, camaraderie, or steadfast belief—I offer my deepest gratitude.

Foremost, I would like to thank my supervisor, Prof. Lin Liu, for being the cornerstone of my academic growth. Your patience, motivation, and profound expertise have shaped not only this thesis but also my identity as a researcher. Beyond equipping me with technical skills, you taught me how to think—how to distill complexity into clarity, how to defend ideas with rigor, and how to embrace uncertainty as part of the scientific process. Your comforting words, “Don’t worry too much, Joe”, have become my anchor during moments of self-doubt. Thank you for investing your time, ideas, and resources to make my doctoral journey both productive and inspiring. Thank you for showing me that research is not just about answers but about asking better questions.

I am also immensely thankful to my host supervisor, Prof. Tobias Bolch at the Technical University of Graz, for welcoming me into your research group and providing an enriching academic environment. Your constructive suggestions, expert guidance, and willingness to share your vast knowledge greatly enhanced the quality of my work. Your thoughtful feedback and encouragement gave me a fruitful experience during my time at TU Graz.

I also want to thank the committee members of my dissertation: Prof. Alex Chow, Prof. Yen Joe Tan, Prof. Lingcao Huang, and Prof. Reynald Delaloye. I am deeply grateful for your generosity in reviewing this work and serving as examiners. Your insightful comments and constructive suggestions elevated the quality of this dissertation and broadened my perspective.

I would like to express my gratitude to my former and current groupmates—Yan Hu, Xingyu Xu, Zhuoxuan Xia, Billy Tsang, Chengyan Fan, Zhuoyi Zhao, Xiaofan Zhu, Jianlong He, Wensong Zhang, and Mengze Li—for their invaluable support in resolving technical issues, coding challenges, and writing difficulties throughout my studies and research. I also extend my thanks to my friends Hui Liu, Tiangang Yuan and all the EASC members who have supported me during my academic journey and enriched my campus life. Thank you all for giving me such joyful and cherished memories in Hong Kong. I also want to thank Prof. Kunpeng Wu and Yanfei Peng, whom I met during my exchange period in Graz. Thanks a lot for your help during my studies at TU Graz.

Finally, no words could ever fully express the depth of my gratitude. The journey to a doctoral degree has been challenging, marked by moments of doubt and perseverance. Yet through it all, your unconditional love and unwavering support were my refuge, giving me strength to endure the toughest days of these four years.

As I turn the page on this chapter, I carry with me a profound truth: science is not a solitary endeavor, but a tapestry woven from collaboration, curiosity, and the generosity of others. To everyone who has been part of this journey—whether through guidance, encouragement, or simple kindness—thank you for helping write my story.

# Table of Contents

---

<b>Abstract.....</b>	<b>I</b>
<b>摘要.....</b>	<b>III</b>
<b>Acknowledgements.....</b>	<b>V</b>
<b>Table of Contents .....</b>	<b>VII</b>
<b>List of Figures.....</b>	<b>XI</b>
<b>List of Tables .....</b>	<b>XIV</b>
<b>Chapter 1 Introduction.....</b>	<b>1</b>
<b>Abstract.....</b>	1
<b>1.1 Definition and scientific values of rock glaciers .....</b>	1
<b>1.2 Introduction of High Mountain Asia.....</b>	5
<b>1.3 Literature review .....</b>	6
1.3.1 Mapping and inventorying rock glaciers .....	6
1.3.2 Assessing rock glacier velocities using InSAR .....	9
1.3.3 Assessing hydrological significance of rock glaciers as water stores.....	12
<b>1.4 Research gaps.....</b>	15
1.4.1 Inventory task .....	15
1.4.2 Velocity assessment.....	16
1.4.3 Water storage estimate.....	16
<b>1.5 Objectives.....</b>	17
<b>1.6 Roadmap.....</b>	17
<b>Chapter 2 Inventorying rock glaciers on the Tibetan Plateau using deep learning .....</b>	<b>18</b>
<b>Abstract.....</b>	18
<b>2.1 Introduction.....</b>	18
<b>2.2 Study area .....</b>	20
<b>2.3 Data .....</b>	21
2.3.1 Planet Basemaps .....	21
2.3.2 Existing rock glacier local inventories for training .....	21
2.3.3 Topo-climatic datasets .....	23

2.3.4 Auxiliary data .....	23
<b>2.4 Methods.....</b>	<b>24</b>
2.4.1 Deep-learning-based rock glacier mapping approach .....	24
2.4.2 Adding attributes of the final revised rock glaciers .....	28
2.4.3 Spatial analysis of rock glaciers .....	31
<b>2.5 Results .....</b>	<b>31</b>
2.5.1 Performance of deep learning-based rock glacier mapping approach .....	32
2.5.2 Rock glacier inventory on the Tibetan Plateau: TPRoGI [v1.0].....	37
2.5.3 Spatial distribution characteristics of rock glaciers .....	38
<b>2.6 Discussion.....</b>	<b>41</b>
2.6.1 Limitations of the deep learning-based mapping approach .....	41
2.6.2 Comparison with existing local inventories.....	43
2.6.3 Significance of the inventory and future work .....	47
<b>2.7 Conclusions.....</b>	<b>48</b>
<b>Chapter 3 Assessing rock glacier velocities on the Tibetan Plateau using InSAR</b>	<b>50</b>
<b>Abstract.....</b>	<b>50</b>
<b>3.1 Introduction.....</b>	<b>51</b>
<b>3.2 InSAR methods for rock glacier velocity assessment .....</b>	<b>53</b>
3.2.1 Wrapped method.....	53
3.2.2 Single unwrapped method .....	53
3.2.3 Time-series methods.....	54
<b>3.3 Study area .....</b>	<b>54</b>
<b>3.4 Methods and materials .....</b>	<b>55</b>
3.4.1 Assessing rock glacier velocities using multi-temporal and multi-geometry InSAR .....	55
3.4.2 Comparing InSAR-derived velocities with other velocity datasets .....	64
3.4.3 Assessing rock glacier velocities on the Tibetan Plateau .....	67
<b>3.5 Results .....</b>	<b>67</b>
3.5.1 Comparison with other velocity datasets .....	67
3.5.1.1 Comparison with velocities derived from Pléiades imagery in Muztagh Ata, western Nyainqêntanglha, and central Ile Alatau .....	67
3.5.1.2 Comparison with velocities derived from aerial imagery in the western U.S.	70
3.5.1.3 Comparison with GNSS-derived velocities in the Swiss Alps .....	73
3.5.2 Contrasting rock glacier velocity patterns on the Tibetan Plateau .....	74
<b>3.6 Discussion.....</b>	<b>76</b>

3.6.1 Advantages and limitations of our InSAR approach .....	76
3.6.1.1 Advantages .....	76
3.6.1.2 Limitations.....	77
3.6.2 Environmental controls on rock glacier velocities .....	79
3.6.3 Significance of our large-scale rock glacier velocity dataset.....	80
<b>3.7 Conclusion .....</b>	<b>82</b>
<b>Chapter 4 Assessing rock glacier water storage in High Mountain Asia .....</b>	<b>84</b>
<b>Abstract.....</b>	<b>84</b>
<b>4.1 Introduction.....</b>	<b>84</b>
<b>4.2 Study area and data .....</b>	<b>86</b>
4.2.1 Study area .....	86
4.2.2 Data.....	87
<b>4.3 Methods.....</b>	<b>88</b>
4.3.1 Mapping rock glaciers using deep learning .....	88
4.3.2 Estimating water storage.....	89
4.3.3 Refining estimates using Tibetan Plateau inventory.....	91
<b>4.4 Results .....</b>	<b>93</b>
4.4.1 Rock glacier WVEQ .....	93
4.4.2 Rock-glacier-to-glacier WVEQ ratios .....	94
<b>4.5 Discussion.....</b>	<b>98</b>
4.5.1 Uncertainty and limitations.....	98
4.5.2 Comparison of rock-glacier-to-glacier WVEQ ratio with other regions .....	99
4.5.3 Future rock glacier water storage .....	99
4.5.4 Implications for hydrological models and water management strategies .....	100
<b>4.6 Conclusions .....</b>	<b>101</b>
<b>Chapter 5 Conclusions and outlook .....</b>	<b>103</b>
<b>Abstract.....</b>	<b>103</b>
<b>5.1 Conclusions .....</b>	<b>103</b>
<b>5.2 Innovative merits and potential impacts.....</b>	<b>105</b>
<b>5.3 Future work.....</b>	<b>106</b>
5.3.1 Enhancement of the deep-learning-based rock glacier mapping method .....	107
5.3.2 Enhancement and application of the InSAR-based rock glacier velocity assessment method .....	108
5.3.3 Investigating the environmental controls on rock glacier velocities .....	109
5.3.4 Investigating the long-term evolutions of selected rock glaciers.....	110

<b>Outputs.....</b>	<b>112</b>
<b>Publications .....</b>	<b>112</b>
<b>Conferences .....</b>	<b>112</b>
<b>Data .....</b>	<b>113</b>
<b>Bibliography .....</b>	<b>114</b>

# List of Figures

---

Figure 1.1: Photos of rock glaciers in (a) Andes (Janke and Bolch, 2021), (b) Tien Shan (photograph by S. Titkov), (c) western U.S. (photograph by Constance Millar), and (d) Swiss Alps (photograph by R. Frauenfelder).....	2
Figure 1.2: (a) Field photo and (b) anatomy of a rock glacier in Vallone di Sort (Italy), 45.5605°N, 7.1589°E, 2500–2800 m a.s.l. This figure is modified from Hu et al. (2025) and RGIK (2023). .....	3
Figure 1.3: High Mountain Asia. The glacier outlines are from (RGI Consortium, 2023). The permafrost extent is from (Obu et al., 2018).....	5
Figure 1.4: Permafrost distribution (Obu et al., 2018) and locations of rock glacier inventories in HMA published before this thesis.....	15
Figure 2.1: Study area (the Tibetan Plateau). The Hindu-Kush Himalayan region is excluded from this study. The permafrost extent map is from Obu et al. (2018).....	20
Figure 2.2: Flowchart of the deep learning-based approach for mapping rock glaciers.....	24
Figure 2.3: (a) Deep-learning-mapped candidate rock glacier polygons. (b) Rock glacier inventory on the Tibetan Plateau (TPRoGI). The permafrost in Hengduan Shan is overlapped by the rock glaciers thus not visible on the map. The permafrost extent map is from Obu et al. (2018).....	32
Figure 2.4: IoU scores during the training and validation processes. ....	33
Figure 2.5: Examples of the candidate rock glaciers are shown in (a) training and (b) validation regions using the well-trained deep learning model. The IoU scores are labelled on the mapped rock glaciers.....	33
Figure 2.6: (a) An example area in Western Pamir showing the deep learning outputs (in red) and manually revised rock glacier boundaries (in green). Clean and debris-covered glacier extents (light blue) are from the Randolph Glacier Inventory (RGI v.6) (Pfeffer et al., 2014); (b-c) enlarged views of the areas showing good agreement between deep learning outputs and revised boundaries; (d) enlarged view showing a false detection example in the center; (e) enlarged view showing multiple missing identifications. ....	36
Figure 2.7: Statistical summaries of the geomorphic and current climatic features of rock glaciers in the study region. (a) The areal histogram of all the rock glaciers on the Tibetan Plateau. The inset shows the areas smaller than 0.5 km <sup>2</sup> . (b)–(h) are histograms of the minimum elevations, slopes, aspects of the rock glaciers with the radial axis representing the counts, Mean Annual Air Temperature (MAAT), Mean Annual Ground Temperature (MAGT), annual precipitation, and annual Potential Incoming Solar Radiation (PISR), respectively.....	38
Figure 2.8: Rock glacier (a) density, (b) area, (c) minimum elevation and (d) slope averaged over grid cells of 50 km × 50 km.....	40

Figure 2.9: Rock glacier aspects in different subregions of the study area.....	41
Figure 3.1: The locations of rock glaciers, mapped in the TPRoGI by Sun et al. (2024), on the Tibetan Plateau. The northernmost boundary of monsoon domain and the southernmost boundary of westerlies domain are from Huang et al. (2023). Also shown are mean annual precipitation from 1979 to 2020 obtained from Jiang et al. (2023). ...	55
Figure 3.2: Workflow of the InSAR approach for assessing rock glacier velocities using multi-temporal and multi-geometry interferograms.....	58
Figure 3.3: Distribution of rock glaciers presented in TPRoGI [v1.0] and Sentinel-1 frames in ascending and descending orbits.....	59
Figure 3.4: Sentinel-1 frames in ascending and descending orbits in the Northern Tien Shan. (b) Enlarged view of the studied rock glaciers. The basemap is from Bing Maps. ....	60
Figure 3.5: (a) Distribution of 16 rock glaciers studied by Kääb and Røste (2024) and Sentinel-1 frames in ascending and descending orbits in the United States. Enlarged views of the rock glaciers: (b) Star Peak, (c) Pine Creek, (d) Birch Min, (e) Cardinal Mt North and South, (f) Old Hyndman Peak, (g) Galena creek, (h) Sulphur creek, (i) Cater Mtn, (j) Ferguson ranch W, (k) Thomas lake W, (l) Arapaho Peak, (m) Mt Mears, (n) Mt Sneffels, (o) Teakettle Mtn, (p) Twin Sisters. The basemap is Bing Maps.....	62
Figure 3.6: (a) Distribution of nine rock glaciers and Sentinel-1 frames in ascending and descending orbits in the Swiss Alps. Enlarged views of the rock glaciers: (b) Aget, (c) Alpage de Mille, (d) Yettes Condjà, (e) Gruben, (f) Monte Prosa, (g) Stabbio di Largario, (h) Valle di Sceru, (i) Murtèl-Corvatsch, (j) Rechy. The basemap is Bing Maps.....	63
Figure 3.7: Rock glacier boundaries (first column) and velocity fields derived from Pléiades imagery (second column) and InSAR (third column) in the Muztagh Ata, western Nyainqêntanglha, and central Ile Alatau. The background images are from Bing Maps. .....	69
Figure 3.8: Scatter plot between the 75th percentile pixel values from the velocity fields derived from Pléiades imagery and InSAR for the rock glaciers in the Muztagh Ata, western Nyainqêntanglha, and central Ile Alatau .....	70
Figure 3.9: Scatter plot between the 75th percentile pixel values from the InSAR-derived velocity fields and the velocities derived from aerial imagery by Kääb and Røste (2024). .....	71
Figure 3.10: InSAR-derived velocity fields for the rock glaciers in the United States: (a) Star Peak, (b) Pine Creek, (c) Birch Min, (d) Cardinal Mt North and South, (e) Old Hyndman Peak, (f) Galena creek, (g) Sulphur creek, (h) Cater Mtn, (i) Ferguson ranch W, (j) Thomas lake W, (k) Arapaho Peak, (l) Mt Mears, (m) Mt Sneffels, (n) Teakettle Mtn, (o) Twin Sisters. The basemap is from Bing Maps. ....	72
Figure 3.11: Scatter plot between the mean velocities of InSAR-derived pixel velocities and GNSS-measured point velocities. The uncertainty represents the standard deviation. The uncertainty bars in (c) indicate standard deviations derived from GNSS-measured and	

sampled InSAR-derived velocities at all the TGS points. The uncertainty bars in (c) indicate standard deviations derived from GNSS-measured and sampled InSAR-derived velocities at all the TGS points.....	73
Figure 3.12: InSAR-derived velocity fields for the rock glaciers in the Swiss Alps: (a) Aget, (b) Alpage de Mille, (c) Yettes Condjà, (d) Gruben, (e) Monte Prosa, (f) Stabbio di Largario, (g) Valle di Sceru, (h) Murtèl-Corvatsch, (i) Rechy. The basemap is from Bing Maps.....	74
Figure 3.13: (a) Averaged rock glacier downslope velocities in grid cells of 50 km×50 km and in 50 km bins along (b) longitudinal and (c) latitudinal directions. The northernmost boundary of monsoon domain and the southernmost boundary of westerlies domain in (a) are from Huang et al. (2023). The gray-shaded areas in (b) and (c) denote the standard deviation of all velocities in the bins.....	75
Figure 3.14: Distributions of rock glacier downslope velocities in (a) the entire study region and different climatic domains, and different ranges of (b) rock glacier area, (c) minimum elevation, and (d) slope. IQR is interquartile range.....	76
Figure 4.1: (a) Study area (High Mountain Asia).....	87
Figure 4.2: (a) Deep-learning-mapped rock glacier polygons across High Mountain Asia (HMA). (b-g) Examples of deep-learning-mapped rock glacier polygons.....	89
Figure 4.3: Workflow of assessing rock glacier water storage in High Mountain Asia using deep learning. The Tibetan Plateau inventory (TPRoGI) is employed to calibrate the WVEQ estimates from deep-learning-mapped polygons using a linear scaling approach. ....	92
Figure 4.4: Subregion-based linear relationship between rock glacier WVEQs derived from rock glacier inventory (TPRoGI) and deep-learning-mapped polygons.....	93
Figure 4.5: Grid-based linear relationship between rock glacier WVEQs derived from rock glacier inventory (TPRoGI) and deep-learning-mapped polygons.....	93
Figure 4.6: Rock glacier WVEQs and rock-glacier-to-glacier WVEQ ratios of different subregions in HMA.....	97
Figure 4.7: Rock glacier WVEQs and rock-glacier-to-glacier WVEQ ratios at $1^\circ \times 1^\circ$ grids in HMA.....	97

# List of Tables

---

Table 1.1: Summary of previous rock glacier inventory works in HMA .....	8
Table 1.2: Summary of methods for assessing rock glacier velocities using InSAR.....	12
Table 1.3: Summary of previous studies of assessing rock glacier hydrological significance as water stores.....	14
Table 2.1: Information of rock glacier local inventories selected for training deep learning model.....	22
Table 2.2: Attribute data dictionary for Tibetan Plateau rock glacier inventory shapefile....	30
Table 2.3: Performance of deep learning mapped polygons in different subregions.....	35
Table 2.4: Independent validation results of sampled Tibetan Plateau rock glacier inventory (n = 2110 samples).....	37
Table 2.5: Comparisons of the numbers of inventoried rock glaciers with existing local inventories.....	45
Table 3.1: Information of nine rock glaciers and terrestrial survey point (TGS) points in Swiss Alps.....	66
Table 3.2: Number of rock glaciers with areas larger than 0.1 km <sup>2</sup> compiled in TPRoGI [v1.0] and number with a successful generation of downslope velocity fields.....	75
Table 4.1: Rock glacier water volume equivalents (WVEQs), glacier WVEQs, and rock- glacier-to-glacier WVEQ ratios of different subregions in HMA.....	95

# Chapter 1 Introduction

---

## Abstract

Rock glaciers are debris landforms generated by the former or current creep of mountain permafrost showing distinct geomorphological characteristics of front, lateral margins, and ridge-and-furrow surface topography. They hold significant scientific and practical value for permafrost modeling, mountain hydrology, climate change impact assessments in periglacial environments, and geohazard evaluation. However, knowledge about their distribution, kinematics, and hydrological significance as water stores in High Mountain Asia (HMA) remains limited due to the absence of a comprehensive inventory and scarce studies on their kinematics and water storage. This chapter first introduces the definition and scientific values of rock glaciers. We then review existing studies in three aspects: (1) mapping and inventorying rock glaciers, (2) assessing rock glacier velocities using InSAR, and (3) assessing the hydrological significance of rock glaciers as water stores. Following this review, we identify current research gaps and present the objectives and roadmap of this thesis.

### 1.1 Definition and scientific values of rock glaciers

Rock glaciers are widespread debris landforms in high mountain environments (Figure 1.1). Understanding of rock glaciers within the scientific community has been evolving since the publication of [Spencer \(1900\)](#)'s initial article on "*a peculiar form of talus*". Over the past century, the identification of rock glaciers has been the subject of ongoing debate, and the criteria for identifying them has evolved with an increasing number of studies worldwide ([Capps, 1910](#); [Barsch, 1996](#); [Haeberli et al., 2006](#); [Berthling, 2011](#); [Jones et al., 2019a](#); [Janke and Bolch, 2021](#)). In the last decade, the identification and compilation of rock glacier inventories has sparked heated debate due to the intricate nature of these landforms ([Berthling, 2011](#); [Brardinoni et al., 2019](#)). In response to the challenge posed by inconsistencies in the identification and compilation of rock glaciers, the International Permafrost Association (IPA) Action Group Rock Glacier Inventories and Kinematics (RGIK) was established in

2018 with the aim of developing widely accepted guidelines for rock glacier inventorying, thereby fostering a globally consistent and comprehensive approach to rock glacier inventories ([Delaloye et al., 2018](#); [RGIK, 2023](#)). Through the efforts of RGIK, the baseline and practical guidelines have been documented and updated in several versions, which greatly promote the global assemblage and uniform completion of rock glacier inventories ([RGIK, 2023](#)). This thesis closely follows the RGIK guidelines in the conceptual definition of rock glaciers as “*debris landforms generated by the former or current creep of frozen ground (permafrost), detectable in the landscape with the following morphologies: front, lateral margins and optionally ridge-and-furrow surface topography*” (Figure 1.2, [RGIK, 2023](#)). These landforms hold substantial significance for inferring permafrost distribution, understanding mountainous hydrology, evaluating climate impacts, and assessing geohazards.

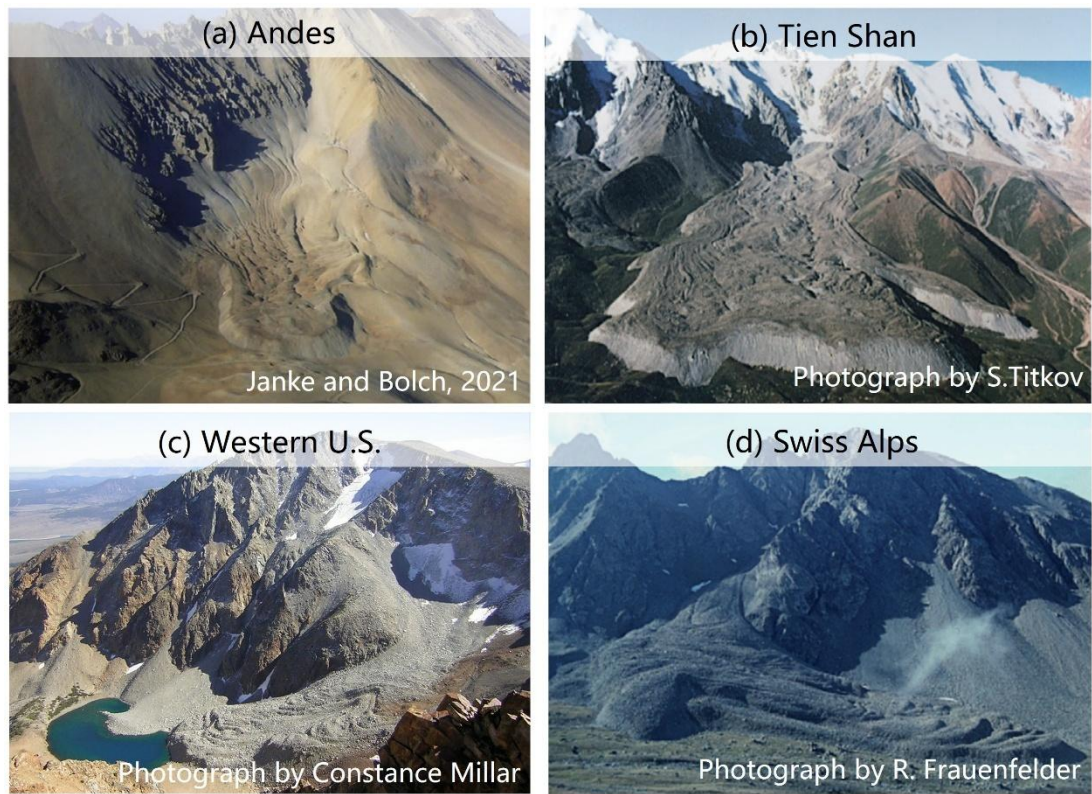


Figure 1.1: Photos of rock glaciers in (a) Andes ([Janke and Bolch, 2021](#)), (b) Tien Shan (photograph by S. Titkov), (c) western U.S. (photograph by Constance Millar), and (d) Swiss Alps (photograph by R. Frauenfelder).

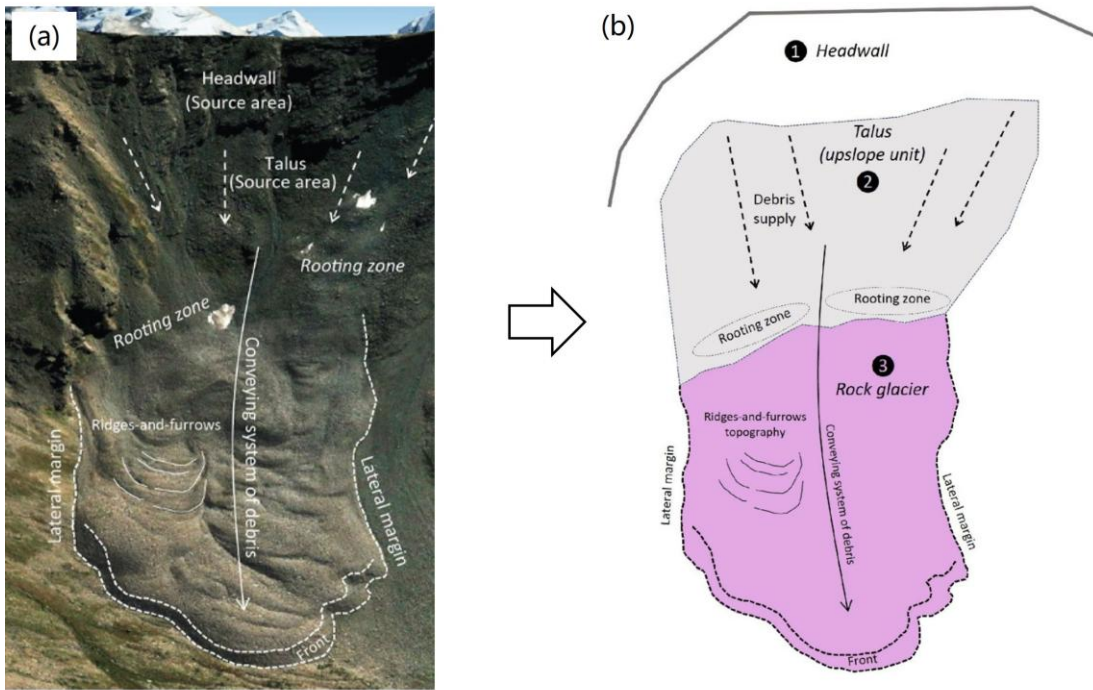


Figure 1.2: (a) Field photo and (b) anatomy of a rock glacier in Vallone di Sort (Italy), 45.5605°N, 7.1589°E, 2500–2800 m a.s.l. This figure is modified from [Hu et al. \(2025\)](#) and [RGIK \(2023\)](#).

Firstly, rock glaciers serve as a proxy for permafrost occurrence. These landforms serve as visible indicators of frozen ground, thereby providing essential information about the presence and extent of mountain permafrost ([Barsch, 1996](#); [Haeberli et al., 2006](#)). [Schmid et al. \(2015\)](#) used the distribution of rock glaciers to assess permafrost maps in the Hindu Kush Himalayan region. [Li et al. \(2024\)](#) compared the rock glacier inventory with permafrost maps and found they align well in regions with a Permafrost Zonation Index greater than 0.5. Many other studies have used rock glacier inventories to construct permafrost maps for their own study areas (e.g., [Boeckli et al., 2012a,b](#); [Marcer et al., 2017](#); [Hassan et al., 2021](#); [Hu et al., 2024](#)).

Secondly, rock glaciers hold hydrological significance as water stores. The identification of massive amounts of ground ice within rock glaciers from field-based measurements suggests their potential as important water reservoirs ([Corte, 1976](#); [Arenson et al., 2002](#); [Croce and Milana, 2002](#); [Hausmann et al., 2007, 2012](#); [Bolch et al., 2019a](#)). In arid regions, rock glaciers could contain more significant water stores than glaciers ([Azócar and Brenning, 2010](#); [Bodin et al., 2010](#); [Janke et al., 2017](#)). Furthermore, the insulating effect of the active surface layer slows the melting of

rock glaciers compared to ice glaciers, suggesting that their relative hydrological importance could increase under future climate warming ([Jones et al., 2019b](#); [Schaffer et al., 2019](#)).

Thirdly, rock glaciers serve as an indicator of permafrost response to climate change. Long-term observations have identified decadal to multi-decadal acceleration trends in rock glacier velocities across various regions worldwide. The European Alps host the most extensive long-term in-situ surveys on rock glacier kinematics, consistently reporting accelerating trends in rock glacier velocities since the 1990s across different regions ([Delaloye et al., 2010](#); [Kellerer-Pirklbauer et al., 2024](#)). Since 2000, continuous monitoring of rock glaciers in the Swiss Alps has been established, with nearly all study sites documenting increasing velocities over the past two decades ([PERMOS, 2024](#)). Feature tracking has also been widely employed to reconstruct long-term velocity time series of rock glaciers, revealing increases in decadal velocities across various regions worldwide ([Vivero et al., 2021](#); [Kääb et al., 2021](#); [Kääb and Røste, 2024](#)). These findings underscore that changes in rock glacier velocities can serve as indicators of climate change impacts on creeping mountain permafrost. Therefore, Rock Glacier Velocity (RGV), defined as “a time series of annualized surface velocity values measured or computed on a rock glacier unit or a part of it”, has been recognized as a new product associated with the Essential Climate Variable (ECV) Permafrost by the Global Climate Observing System (GCOS) ([RGIK, 2022b](#); [Hu et al., 2025](#)).

Fourthly, rock glaciers can cause geohazards. Rapid movement or destabilization of rock glaciers can trigger disasters such as rockfalls, debris flows, and lake outbursts, posing a potential risk to nearby human infrastructure and facilities ([Janke and Bolch, 2021](#); [Marcer et al., 2021](#)). In Karakoram, Tien Shan, and Altai mountains, 5–14% of the 2,000 rock glaciers affect 95 km of river channels. In Hunza Basin, one rock glacier dam in the upper Hunza Basin, 35 rock glaciers could form dams, while 68 have interacted with river channels ([Hassan et al., 2021](#)). The advance of these rock glaciers could lead to lake outbursts if the dams become unstable ([Blöthe et al., 2019](#)). Therefore, monitoring rock glaciers is beneficial for assessing and monitoring potential geohazards in high mountain environments.

## 1.2 Introduction of High Mountain Asia

HMA is a vast and complex mountainous region encompassing the Tibetan Plateau, the Himalayas, the Karakoram, the Hindu Kush, and surrounding ranges ([Bolch et al., 2019b](#)). This region is termed as ‘Asian Water Tower’, because it serves as a primary freshwater source for over a billion people through major river systems such as the Indus, Ganges, Brahmaputra, and Yangtze ([Immerzeel et al., 2020](#), Figure 1.3). HMA is also referred to as the ‘the Third Pole’ because it holds the largest frozen water outside the Antarctic and Arctic, featuring extensive glaciers and permafrost systems ([Bolch et al., 2019b](#)), which hosts more than 130,000 glaciers ([RGI Consortium, 2023](#)) and  $\sim 2,000,000 \text{ km}^2$  permafrost areas ([Obu et al., 2018](#)). However, compared to other cryospheric components such as glaciers and permafrost, rock glaciers remain understudied in this critical cold region.

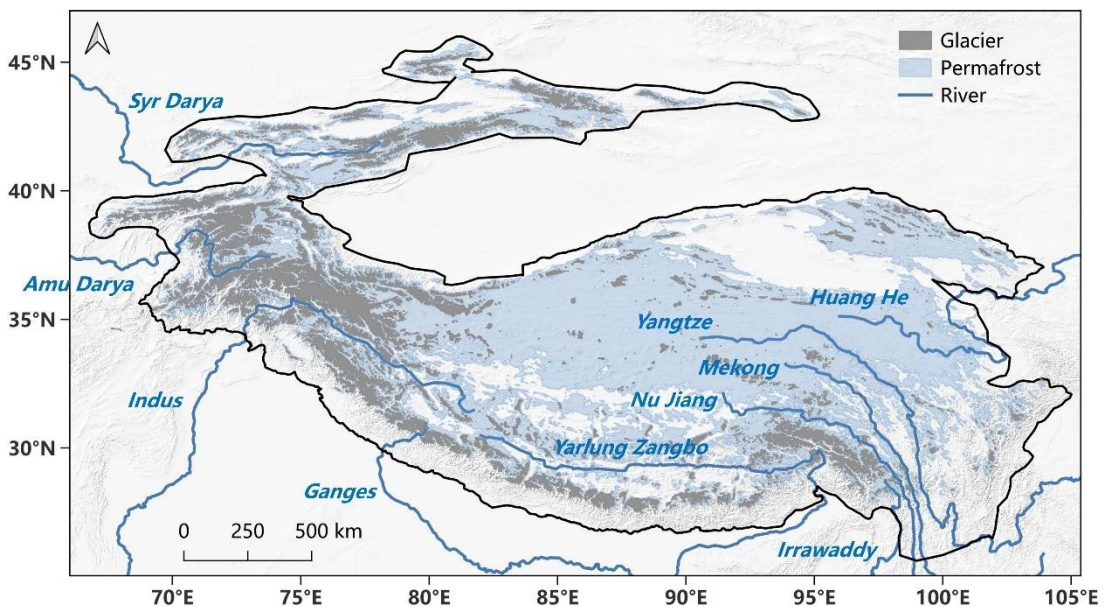


Figure 1.3: High Mountain Asia. The glacier outlines are from ([RGI Consortium, 2023](#)). The permafrost extent is from ([Obu et al., 2018](#)).

## 1.3 Literature review

### 1.3.1 Mapping and inventorying rock glaciers

#### 1.3.1.1 Manual interpretation methods

In HMA, most regional-scale rock glacier inventories have been created through the visual interpretation of high-resolution optical satellite imagery (Table 1.1). By analyzing Google Earth imagery, [Jones et al. \(2018b\)](#) produced a rock glacier inventory for the Nepalese Himalaya, identifying 6,239 locations and 1,137 boundaries. Building on this work, they later expanded their efforts to cover the entire Himalaya, resulting in an inventory of 24,968 locations and 2,070 boundaries ([Jones et al., 2021](#); [Harrison et al., 2024](#)). Similarly, [Ran and Liu \(2018\)](#) visually analyzed Google Earth imagery to catalog 295 rock glaciers in Daxue Shan, while [Pandey \(2019\)](#) inventoried 516 rock glaciers in the Himachal Himalaya. Additional inventories include 616 rock glaciers in the Hunza River Basin ([Hassan et al., 2021](#)), 5,057 rock glaciers in Guokalariju ([Li et al., 2024](#)), and 3,082 rock glaciers in the Northwestern Himalayas ([Pandey et al., 2024](#)). Using a combination of Google Earth and Pléiades images, [Bolch et al. \(2022\)](#) mapped 370 rock glaciers in the Poiqu River Basin. [Zhang et al. \(2022\)](#) employed LocaSpace Viewer to delineate the boundaries of 132 rock glaciers, while [Hu et al. \(2024\)](#) utilized multiple image sources, including Google Earth, ESRI maps, Bing Maps, and Yandex images, to map 1,530 rock glaciers in the Qilian Mountains.

Some other studies have incorporated InSAR data alongside optical imagery to inventory rock glaciers. [Wang et al. \(2017\)](#) combined InSAR and optical images from Google Earth to map 261 rock glaciers in the northern Tien Shan of China. [Kääb et al. \(2021\)](#) utilized interferograms from multiple satellite sources and high-resolution optical imagery from Google Earth and Bing Maps to inventory 551 rock glaciers in the Northern Tien Shan. Similarly, [Reinosch et al. \(2021\)](#) combined InSAR data and optical imagery to map 1,433 rock glaciers in the Western Nyainqêntanglha Range. Employing Sentinel-1 InSAR data and high-resolution optical imagery, [Cai et al. \(2021\)](#) identified 344 rock glaciers in Daxue Shan, [Zhang et al. \(2021\)](#) inventoried 4,962 rock glaciers in the Central Himalayas, [Zhang et al. \(2023\)](#) mapped 20,531 rock glaciers in the Nyainqêntanglha, and [Hassan et al. \(2024\)](#) cataloged 2,290 rock glaciers in the Shigar and Shayok basins.

### 1.3.1.2 Deep-learning-based methods

The production of a rock glacier inventory through visual interpretation requires substantial geomorphological expertise and is both labor-intensive and time-consuming ([Barsch, 1996](#); [RGIK, 2023](#)). In recent years, several studies have successfully leveraged deep learning techniques to automate the detection of rock glaciers. [Robson et al. \(2020\)](#) combined convolutional neural networks (CNNs) with object-based image analysis to detect rock glaciers using Sentinel-2 optical imagery, Sentinel-1 interferometric coherence maps, and DEMs in the La Laguna catchment of the Chilean semi-arid Andes and the Poiqu catchment in the central Himalayas. Similarly, [Marcer et al. \(2020\)](#) demonstrated that CNNs can accurately classify unshadowed and snow-free rock glaciers using optical imagery. [Erharter et al. \(2022\)](#) trained a U-Net model using orthophotos and DEM-derived slope maps as inputs, and an inventory of 5,769 rock glaciers in the Austrian Alps as output. [Hu et al. \(2023a\)](#) trained the DeepLabv3+ network using rock glaciers mapped from InSAR data and Google Earth images, and subsequently applied the well-trained model to Sentinel-2 imagery for rock glacier detection in the Western Kunlun Mountains.

Table 1.1: Summary of previous rock glacier inventory works in HMA.

Method	Reference	Study area	Dataset	Rock glacier number
Visual interpretation	<a href="#">Jones et al. (2018b)</a>	Nepalese Himalaya	Google Earth	6,239
	<a href="#">Ran and Liu (2018)</a>	Daxue Shan	Google Earth	295
	<a href="#">Pandey (2019)</a>	Himachal Himalaya	Google Earth	516
	<a href="#">Jones et al. (2021)</a>	Himalaya	Google Earth	24,968
	<a href="#">Hassan et al. (2021)</a>	Hunza River Basin	Google Earth	616
	<a href="#">Bolch et al. (2022)</a>	Poiqu River Basin	Pléiades, Google Earth	370
	<a href="#">Zhang et al. (2022)</a>	Gangdise Mountains	LocaSpace Viewer	132
	<a href="#">Li et al. (2024)</a>	Guokalariju	Google Earth	5,057
	<a href="#">Hu et al. (2024)</a>	Qilian Mountains	Google Earth, ESRI maps, Bing maps, and Yandex images	1,530
InSAR, visual analysis	<a href="#">Pandey et al. (2024)</a>	Northwestern Himalayas	Google Earth	3,082
	<a href="#">Wang et al. (2017)</a>	Northen Tien Shan of China	Google Earth, ALOS-1 PALSAR-1	261
	<a href="#">Kääb et al. (2021)</a>	Northern Tien Shan	ERS-1/2 tandem mission, ALOS-1 PALSAR-1, ALOS-2 PALSAR-2, Sentinel-1, Google Earth, Bing Maps	551
	<a href="#">Reinosch et al. (2021)</a>	Western Nyainqêntanglha Range	Sentinel-1, Sentinel-2, Landsat 8, TanDEM-X, Bing Maps, Google Earth, Zoom Earth	1,433
	<a href="#">Cai et al. (2021)</a>	Daxue Shan	Sentinel-1, Google Earth	344
	<a href="#">Zhang et al. (2021)</a>	Central Himalayas	Sentinel-1, Bing Maps, Google Earth, ESRI satellite maps	4,962
	<a href="#">Zhang et al. (2023)</a>	Nyainqêntanglha	Sentinel-1, Gaofen-2	20,531
	<a href="#">Hassan et al. (2024)</a>	Shigar and Shayok basins	Google Earth, Sentinel-1	2290
Deep learning, InSAR, visual analysis	<a href="#">Hu et al. (2023a)</a>	Western Kunlun Mountains	ALOS-1 PALSAR-1, Sentinel-2, Google Earth	413

### 1.3.2 Assessing rock glacier velocities using InSAR

Three primary methods are typically used to assess rock glacier velocities using InSAR, referred to as (1) wrapped method, (2) single unwrapped method, and (3) time-series methods (Table 1.2).

#### 1.3.2.1 Wrapped method

The wrapped method involves analyzing multiple wrapped interferograms generated from various satellite data over different time intervals. [Barboux et al. \(2014\)](#) introduced a systematic procedure for interpreting interferometric signals from extensive InSAR datasets. This method enabled the detection and displacement rate estimation of moving zones in the Western Swiss Alps, resulting in the identification of 1,500 moving objects, of which 908 were attributed to rock glaciers. Similarly, [Kääb et al. \(2021\)](#) analyzed numerous interferograms, identifying over 900 moving landforms in the northern Tien Shan, with 551 interpreted as rock glaciers. To standardize the integration of kinematic information into rock glacier inventories, the European Space Agency (ESA) Permafrost Climate Change Initiative (CCI) developed guidelines for systematically incorporating such data ([RGIK, 2022a](#)). Adopting these guidelines, [Bertone et al. \(2022\)](#) incorporated InSAR kinematics into over 3,600 rock glaciers across 11 regions worldwide. Through comprehensive analysis of multiple wrapped interferograms from diverse sources, this method provides a robust classification of rock glacier velocities. However, it requires substantial manual effort, making it impractical for assessing velocities across large quantities (e.g., tens of thousands) of rock glaciers in extensive regions.

#### 1.3.2.2 Single unwrapped method

The single unwrapped method employs unwrapped interferograms to calculate the line-of-sight (LOS) velocity from a single interferometric pair, which is then projected into the surface-parallel direction to estimate the downslope creep rates of rock glaciers. [Liu et al. \(2013\)](#) used this approach to quantify the velocities of 59 rock glaciers in Sierra Nevada, California, USA, reporting movement speeds ranging from 14 to 87 cm/yr, with a regional mean velocity of 53 cm/yr. Similarly, [Wang et al. \(2017\)](#) applied the method to 261 rock glaciers in the northern Tien Shan of China, revealing substantial spatial variation in downslope velocities, with a maximum of approximately 114 cm/yr and a mean of about 37 cm/yr. More recently, [Hu et al.](#)

([2023a](#)) calculated downslope velocities for 413 rock glaciers across the Western Kunlun Mountains, finding mean and maximum velocities of approximately 17 cm and 127 cm/yr, respectively. [Hassan et al. \(2024\)](#) estimated the downslope velocities of rock glaciers in the Shigar and Shayok basins, reporting maximum velocities of approximately 101 cm/yr and 114 cm/yr and median velocities of around 27 cm/yr and 29 cm/yr in the Shigar and Shayok basins, respectively. This method facilitates direct calculation of downslope velocity from interferograms and demands less manual effort compared to the wrapped method. However, using single interferograms introduces challenges from unfavorable viewing geometries, atmospheric errors, and phase decorrelation.

### 1.3.2.3 Time-series methods

Time-series InSAR is widely used because it effectively mitigates errors caused by atmospheric effects and decorrelation. Among time-series algorithms, the Small Baseline Subset (SBAS) approach is the most used for rock glacier studies. [Barboux et al. \(2015\)](#) used SBAS to investigate the slope movements in the Western Swiss Alps and found that SBAS employed with 11 days TerraSAR X-band summer interferograms has the detectable movement rates of 35 cm/yr in the LOS with a root mean squared error of 6.7 cm/yr. [Necsoiu et al. \(2016\)](#) applied SBAS to nine rock glaciers located in Retezat Mountain and estimated the displacement rates at a few centimeters per year. [Cai et al. \(2021\)](#) applied the SBAS technique to estimate mean annual surface displacement velocities over the Daxue Shan, Southeast Tibetan Plateau. Their study resulted in an inventory of 344 rock glaciers, with mean downslope velocities ranging from 2.8 mm/yr to 107.4 mm/yr. Later, [Cai et al. \(2024\)](#) introduced a strategy for estimating Three-Dimensional (3D) velocities of rock glaciers using SBAS. They mapped the 3D surface creeping velocities of 1,084 rock glaciers in Daxue Shan and estimated the maximum and average annual velocities of 30.1 cm/yr and 3.0 cm/yr. [Reinosch et al. \(2021\)](#) presented the first rock glacier inventory for the western Nyainqêntanglha Range containing 1,433 rock glaciers based on surface velocity estimations from SBAS. [Zhang et al. \(2023\)](#) used SBAS to evaluate the velocities of 20,531 rock glaciers in the Nyainqêntanglha region, finding that 32.1% exhibited velocities exceeding 10 cm/yr. SBAS selects SAR image pairs with small spatial and temporal baselines, making it particularly suitable for detecting slow deformation. However, the velocities of active rock glaciers typically

range from centimeters to meters per year ([Hu et al., 2025](#)). When SBAS incorporates interferograms with longer temporal baselines, unwrapping errors become more severe, leading to underestimated velocities ([Fan et al., 2025](#)).

Another algorithm, Persistent Scatterer Interferometry (PSI), relies on highly coherent scatterers, making it effective for very slow deformation but often unsuitable for active rock glaciers due to severe decorrelation in long-time-span interferograms. [Barboux et al. \(2015\)](#) found that PSI is only able to precisely detect only points moving with velocities below 3.5 cm/yr in the LOS. As a result, very few studies have applied PSI to rock glaciers. [Zhang et al. \(2021\)](#) developed a multi-baseline Persistent Scatterer and Distributed Scatterer InSAR approach to monitor rock glacier activity in the central Himalayas. Their analysis show that the deformation rate of rock glaciers in the central Himalayas is experiencing spatial variations, with velocities ranging from 0 to 75 mm/yr. [Guerrero et al. \(2025\)](#) used SqueeSAR algorithm to process seven years of Sentinel-1 high-resolution InSAR data and produced the first kinematic database of rock glaciers for the Pyrenean region.

Stacking methods are another commonly used algorithm to measure rock glacier velocities. [Brencher et al. \(2021\)](#) used stacking velocity maps from ascending and descending interferograms to assess the velocities of 205 rock glaciers in the Uinta Mountains, Utah, USA. [Rouyet et al. \(2021b\)](#) employed a multi-temporal baseline InSAR stacking method to create a regional morpho-kinematic inventory of slope movements in Northern Norway, identifying 414 rock glacier units and assigning kinematic attributes to each. [Buchelt et al. \(2023\)](#) employed the stacking algorithm to investigate the small-scale spatial patterns of rock glacier velocities and found good spatial agreement compared with annual movement derived from orthophotos and unpiloted aerial vehicle data. However, conventional stacking typically uses interferograms from a single orbital geometry (e.g., ascending or descending), thus averaging LOS measurements in the same One-Dimensional (1D) directions.

Table 1.2: Summary of methods for assessing rock glacier velocities using InSAR.

Method	Algorithm	Advantages	Disadvantages	Selected references
Wrapped method		Robust attribution of velocity classes	Significant manual effort	<a href="#">Barboux et al. (2014)</a> ; <a href="#">Kääb et al. (2021)</a> ; <a href="#">Bertone et al. (2022)</a>
Single unwrapped method		Direct calculation of downslope velocity; less manual effort	Large uncertainties from unfavourable viewing geometries, atmospheric errors, and phase decorrelation	<a href="#">Liu et al. (2013)</a> ; <a href="#">Wang et al. (2017)</a> ; <a href="#">Hu et al. (2023a)</a> ; <a href="#">Hassan et al. (2024)</a>
Time series method	SBAS	Error mitigation caused by atmospheric effects and decorrelation; suitable for detecting slow deformation	Incorporation of interferograms with longer temporal baselines can cause underestimated velocities due to unwrapping errors	<a href="#">Barboux et al. (2015)</a> ; <a href="#">Nescioiu et al. (2016)</a> ; <a href="#">Cai et al. (2021, 2024)</a> ; <a href="#">Reinosch et al. (2021)</a> ; <a href="#">Zhang et al. (2023)</a>
	PSI	Effective for very slow deformation	Unsuitable for measuring the velocities of active rock glaciers	<a href="#">Barboux et al. (2015)</a> ; <a href="#">Zhang et al. (2021)</a> ; <a href="#">Guerrero et al. (2025)</a>
	Stacking	Suitable for measuring the velocities of active rock glaciers	Rely on single-geometry data	<a href="#">Brencher et al. (2021)</a> ; <a href="#">Rouyet et al. (2021b)</a> ; <a href="#">Buchelt et al. (2023)</a>

### 1.3.3 Assessing hydrological significance of rock glaciers as water stores

The water volume equivalent (WVEQ) of a rock glacier can be calculated by multiplying its surface area, mean thickness, ice content, and an ice density conversion factor. The thickness of a rock glacier can be estimated using either an area-thickness power-law scaling method ([Brenning, 2005b](#)) or a slope-dependent model ([Cicoira et al., 2021](#)).

In the Andes, the hydrological significance of rock glaciers as water stores has been extensively studied (Table 1.3). In the Andes of Santiago (33°–35°S), [Brenning \(2005a\)](#) estimated a rock-glacier-to-glacier ice volume ratio of 1:7. [Azócar and Brenning \(2010\)](#) reported that rock glaciers are more significant water stores than glaciers in the Chilean Andes between 29° and 32°S (ratio 3:1), though their importance decreases northward (27°–29°S, ratio 1:3) and southward (32°–33°S,

ratio 1:7). [Bodin et al. \(2010\)](#) found that rock glaciers dominate water storage over glaciers in the Andes of Santiago at 33.5°S, with a water equivalent ratio of 1.5:1. [Perucca and Esper Angillieri \(2011\)](#) examined the Dry Andes of Argentina (28°S) and identified a water equivalent ratio of 1:8. [Rangecroft et al. \(2015\)](#) assessed the Bolivian Andes (15°–22°S) and found a significantly lower rock-glacier-to-glacier water equivalent ratio of 1:33. [Janke et al. \(2017\)](#) estimated that rock glaciers account for 48–64% of total water resources in the Aconcagua River Basin, Chile.

Regional-scale assessments of the hydrological significance of rock glaciers as water stores have also been conducted worldwide. [Jones et al. \(2018a\)](#) compiled a near-global rock glacier database and estimated a global rock-glacier-to-glacier WVEQ ratio of 1:456. In the Great Basin, USA, [Millar and Westfall \(2019\)](#) found that rock glaciers contribute 93% of the total frozen water volume. In the Austrian Alps, [Wagner et al. \(2021\)](#) estimated a WVEQ ratio of 1:12 between rock glaciers and glaciers.

In HMA, most studies on the hydrological significance of rock glaciers as water stores have focused on the Himalayas. [Jones et al. \(2018b\)](#) compiled the first comprehensive Nepalese rock glacier inventory (~6,000 locations, ~1,000 outlines) and estimated a rock-glacier-to-glacier WVEQ ratio of 1:9 using a statistical upscaling method. Extending this approach to the entire Himalayas, [Jones et al. \(2021\)](#) calculated a ratio of 1:25. [Hu et al. \(2023b\)](#) developed a method for estimating rock glacier ice content based on velocity and used it to assess WVEQ in the Khumbu and Lhotse valleys. [Pandey et al. \(2024\)](#) evaluated the water storage of rock glaciers in the northwestern Himalayas using an inventory of 3,082 rock glaciers. Localized studies have been performed in other parts of HMA. [Bolch and Marchenko \(2009\)](#) examined the water storage of rock glaciers in a localized area in the Northern Tien Shan. [Li et al. \(2024\)](#) assessed rock glacier water storage in Guokalariju, finding comparable subsurface ice stored in rock glaciers and glaciers, with a WVEQ ratio of 1:1.69.

Table 1.3: Summary of previous studies of assessing rock glacier hydrological significance as water stores.

Region	Study area	Rock-glacier-to-glacier WVEQ ratio	Reference
	Global	1:456	<a href="#">Jones et al. (2018a)</a>
	Andes of Santiago ( $33^{\circ}$ – $35^{\circ}$ S)	1:7	<a href="#">Brenning (2005a)</a>
	Andes of Santiago, Chile ( $33.5^{\circ}$ S)	1.5:1	<a href="#">Bodin et al. (2010)</a>
Andes	Chilean Andes ( $27^{\circ}$ – $29^{\circ}$ S)	1:3	<a href="#">Azócar and Brenning (2010)</a>
	Chilean Andes ( $29^{\circ}$ – $32^{\circ}$ S)	3:1	<a href="#">Azócar and Brenning (2010)</a>
	Chilean Andes ( $32^{\circ}$ – $33^{\circ}$ S)	1:7	
	Cerro El Potro ( $28^{\circ}$ S)	1:8	<a href="#">Perucca and Esper Angillieri (2011)</a>
	Bolivian Andes ( $15^{\circ}$ – $22^{\circ}$ S)	1:33	<a href="#">Rangecroft et al. (2015)</a>
	Aconcagua River Basin, Chile	1:1–2:1	<a href="#">Janke et al. (2017)</a>
Europe	Austrian Alps	1:12	<a href="#">Wagner et al. (2021)</a>
U.S.	The Great Basin, USA	14:1	<a href="#">Millar and Westfall (2019)</a>
High Mountain Asia	Nepalese Himalaya	1:9	<a href="#">Jones et al. (2018b)</a>
	Western Himalaya	1:34	
	Central Himalaya	1:17	<a href="#">Jones et al. (2021)</a>
	Eastern Himalaya	1:43	
	Himalaya	1:25	
High Mountain Asia	Khumbu and Lhotse valleys	1:17	<a href="#">Hu et al. (2023b)</a>
	Northwestern Himalayas	Unknown	<a href="#">Pandey et al. (2024)</a>
	Northern Tien Shan	Unknown	<a href="#">Bolch and Marchenko (2009)</a>
	Guokalariju	1:1.69	<a href="#">Li et al. (2024)</a>

## 1.4 Research gaps

### 1.4.1 Inventory task

Existing studies utilizing deep learning for the automatic detection of rock glaciers remain in the trial stage, primarily focusing on localized areas or individual mountain ranges ([Robson et al., 2020](#); [Marcer et al., 2020](#); [Erhardt et al., 2022](#); [Hu et al., 2023a](#)). Before this thesis work, none have employed deep learning to map rock glaciers across uncharted or extensive regions. Consequently, a systematic, deep-learning-based method that is both applicable and transferable for mapping rock glaciers in uncharted regions is still absent.

While a substantial number of rock glacier inventories have been produced through manual interpretation (Table 1.1), many are not openly accessible. Furthermore, some inventories lack comprehensiveness. For instance, the Himalayan inventory includes 24,968 locations, but only 2,070 have delineated boundaries ([Jones et al., 2021](#); [Harrison et al., 2024](#)). [Li et al. \(2024\)](#) compiled a rock glacier inventory for the Qinghai-Tibet Plateau and adjacent mountainous regions, yet it only includes rock glaciers located in front of glaciers, omitting those connected to talus. Additionally, some inventories may miss many rock glaciers by interpreting InSAR data or low-resolution imagery ([Wang et al., 2017](#); [Zhang et al., 2022](#); [Hu et al., 2023a](#)). As a result, the availability of open-access and comprehensive rock glacier inventories remains patchy (Figure 1.4), and a comprehensive, plateau-wide, and open-access inventory is still lacking.

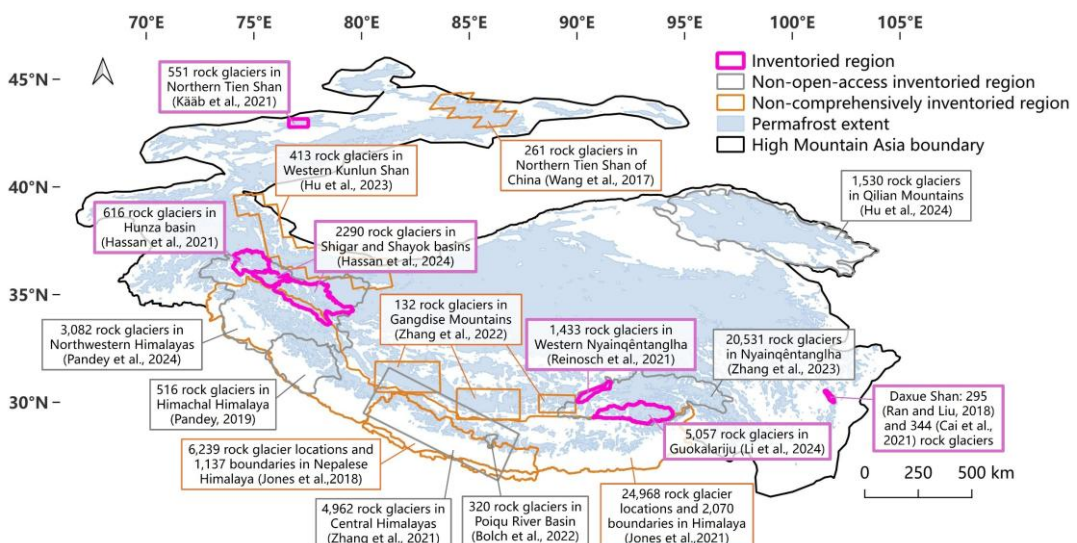


Figure 1.4: Permafrost distribution ([Obu et al., 2018](#)) and locations of rock glacier inventories in HMA published before this thesis.

### 1.4.2 Velocity assessment

Current InSAR methods face significant challenges in assessing rock glacier velocities over large regions. The wrapped method recommended by the IPA RGIK ([RGIK, 2022a](#)) can reliably classify rock glacier velocities but requires substantial manual effort, making it impractical for analyzing tens of thousands of rock glaciers across extensive areas. While the single unwrapped method can directly calculate downslope velocities, it is prone to significant uncertainties due to unfavorable viewing geometries, atmospheric errors, and decorrelation noise. Similarly, time-series methods have limitations: neither SBAS nor PSI is well-suited for detecting active rock glacier movement rates, and conventional stacking algorithms rely on single-geometry data, averaging LOS measurements along the same 1D direction.

As a result of these methodological limitations, most studies have focused on small-scale regions or individual mountains. Furthermore, due to the scarcity of in-situ rock glacier velocity measurements, comprehensive validation of InSAR-derived velocities remains very limited. As a result, the accuracy and reliability of rock glacier velocity products derived from InSAR have not yet been adequately evaluated. Currently, there is no method for systematically assessing rock glacier velocities across large regions. The large-scale velocity characteristics, particularly in large regions such as High Mountain Asia, remain poorly quantified and understood. This knowledge gap also impedes a comprehensive understanding of the environmental factors influencing rock glacier velocities at broader spatial scales.

### 1.4.3 Water storage estimate

Existing studies assessing rock glacier water storage have primarily focused on the Himalaya ([Jones et al., 2018b, 2021; Pandey et al., 2024](#)) or on localized areas outside this region ([Bolch and Marchenko, 2009; Li et al., 2024](#)). However, the hydrological role of rock glaciers across other areas in HMA remains poorly understood. While [Jones et al. \(2021\)](#) assessed the water storage of rock glaciers across the entire Himalaya, their analysis relied on an upscaling method that inferred total water storage based on the boundaries of a subsample from the inventory. Therefore, a more robust and comprehensive assessment of rock glacier water storage across the entire HMA is needed.

## 1.5 Objectives

To fill the knowledge gap about the characteristics of rock glaciers in HMA, we aim to use optical remote sensing, deep learning and InSAR techniques to comprehensively investigate the distribution, velocities, and water storage of rock glaciers across large regions. Specifically, the objectives include:

- 1) To develop a systematic and automated deep-learning-based method for consistent mapping and inventorying rock glaciers.
- 2) To compile a comprehensive rock glacier inventory for the Tibetan Plateau.
- 3) To develop a framework for systematically generating rock glacier velocity fields over large-scale regions using multi-temporal and multi-geometry InSAR.
- 4) To assess rock glacier velocities on the Tibetan Plateau.
- 5) To comprehensively estimate rock glacier water storage in HMA.

## 1.6 Roadmap

The remainder of this thesis is organized as follows:

Chapter [2](#) explores the distribution of rock glaciers on the Tibetan Plateau by developing a deep-learning-based method utilizing the DeepLabv3+ network to map rock glaciers from high-resolution (~5 m) Planet Basemaps imagery. Applying this method across the entire study area, we compile the first comprehensive inventory of rock glaciers for the Tibetan Plateau.

Chapter [3](#) introduces a multi-temporal and multi-geometry InSAR framework for large-scale rock glacier velocity assessment. Using this approach, we generate the first large-scale velocity estimates for rock glaciers on the Tibetan Plateau.

Chapter [4](#) extends the deep learning model developed in Chapter [2](#) to map rock glaciers across the entire HMA. Based on the deep-learning-mapped polygons and using the compiled inventory for calibration, we provide the first comprehensive estimate of rock glacier water storage in HMA.

Chapter [5](#) presents the conclusions of this thesis and outlines future research.

# Chapter 2 Inventorying rock glaciers on the Tibetan Plateau using deep learning

---

## Abstract

Inventories of rock glaciers remain patchy in many alpine regions, and as a result their distributions are poorly understood in High Mountain Asia. To assist the mapping of rock glaciers, we developed a deep learning-based mapping method that utilizes the DeepLabv3+ semantic segmentation model. By training the model with Planet Basemaps images and existing rock glacier local inventories from six regions, we achieved an intersection over union score of 0.76 and 0.70 on the training and validation datasets, respectively. Based on the deep learning-mapped areas, we compiled the first comprehensive inventory of rock glaciers for the Tibetan Plateau, i.e., TPRoGI [v1.0]. This inventory consists of a total of 44,273 rock glaciers, covering approximately 6,000 km<sup>2</sup>, with a mean area of 0.14 km<sup>2</sup>. Rock glaciers in this region are predominantly situated at elevations between 4,000 and 5,500 m a.s.l., with a mean of 4,729 m above sea level (m a.s.l.). They tend to occur on slopes with gradients between 10° and 25°, with a mean of 17.7°. Across the plateau, rock glaciers are widespread in the northwestern and southeastern areas, with dense concentrations in the Western Pamir and Nyainqêntanglha, while more sparsely distributed in the inner plateau. Our inventory serves as a benchmark dataset, which constitutes a significant contribution towards understanding, future monitoring and assessment of permafrost on the Tibetan Plateau in the context of climate change.

## 2.1 Introduction

Mapping and inventorying rock glaciers are motivated by providing valuable baseline knowledge for addressing various scientific questions associated with periglacial realm, including permafrost occurrence inference, water storage estimation, climate response evaluation, and natural geohazards assessment. A comprehensive inventory of rock glaciers also lays the foundation for improving our understanding of their spatial distribution, topo-climatic environment, kinematic activity, and temporal evolution.

In early times, aerial photographs were the main source for producing rock glacier

inventories ([Wahrhaftig & Cox, 1959](#)). More recently, the advent of remotely sensed satellite data allows to elaborate rock glacier inventories over broad regions by visually interpreting high-resolution optical satellite images such as Google Earth imagery or Interferometric Synthetic Aperture Radar (InSAR) images. As a result, a significant number of rock glacier inventories emerged around the globe, especially in European Alps (e.g., [Scotti et al., 2013](#); [Wagner et al., 2020](#)), Andes (e.g., [Rangecroft et al., 2014](#); [Janke et al., 2015](#)), High Mountain Asia including the Himalaya and Tien Shan (e.g., [Schmid et al., 2015](#); [Jones et al., 2021](#); [Kääb et al., 2021](#)). However, despite the existence of rock glacier inventories in many parts on the earth, no global-scale complete rock glacier inventory has yet been compiled.

Due to the complexity of rock glaciers, there has been contentious debate about their identification and compilation ([Berthling, 2011](#); [Brardinoni et al., 2019](#)), making it challenging to create a fully coherent global inventory. To address this issue, the IPA established an action group on rock glacier inventories and kinematics ([Delaloye et al., 2018](#)), with the goal of creating widely accepted standard guidelines for inventorying rock glaciers to promote the global assemblage and uniform completion of rock glacier inventories ([RGIK, 2023](#)).

However, the production of a rock glacier inventory through visual interpretation requires strong geomorphological expertise, and is labour-intensive and time-consuming ([Barsch, 1996](#); [RGIK, 2023](#)). Rock glaciers exhibit spectral properties similar to their surrounding environment, making it challenging to identify optical remote sensing images ([Robson et al., 2020](#)). Moreover, in high mountain environments, there are various landforms that resemble rock glaciers, such as debris-covered glaciers, rock avalanches, debris flows, and fluvial landforms ([Haeberli et al., 2006](#); [Robson et al., 2020](#)). As a result, inexperienced analysts are prone to making erroneous judgments. With the development of artificial intelligence, deep learning models have become valuable tools for mapping complex landforms such as rock glaciers. Deep learning models can learn the visual patterns of objects and identify features in previously unseen images with high accuracy and have been successfully applied to map permafrost landforms ([Huang et al., 2020](#)). In recent years, several studies have successfully employed deep learning techniques for the automatic detection of rock glaciers, yielding satisfactory results ([Robson et al., 2020](#); [Marcer et al., 2020](#); [Erharder et al., 2022](#); [Hu et al., 2023a](#)). However, the methods

employed in previous studies are not systematic over large areas, leading to inconsistencies and patchy coverage.

In this study, we created the most extensive plateau-wide inventory of rock glaciers on the Tibetan Plateau, i.e., TPRoGI [v1.0], using a deep learning method based on DeepLabV3+ model. It is expected that the benchmark dataset produced by this study will be maintained and updated in the future and will facilitate the investigation into many scientific questions related to rock glaciers and mountain permafrost on the Tibetan Plateau.

## 2.2 Study area

The Tibetan Plateau is part of High Mountain Asia, covering an area of approximately 2.5 million km<sup>2</sup> with an average elevation of over 4,500 m above sea level. [Bolch et al. \(2019b\)](#) split High Mountain Asia into 22 subregions based on their topographical and climatological characteristics, of which 13 were situated in the Tibetan Plateau. We selected all the 13 subregions as study areas for this work, thus covering most of the Tibetan Plateau (Figure 2.1), as well as the Qaidam basin, which was not a subregion in [Bolch et al. \(2019b\)](#)'s study.

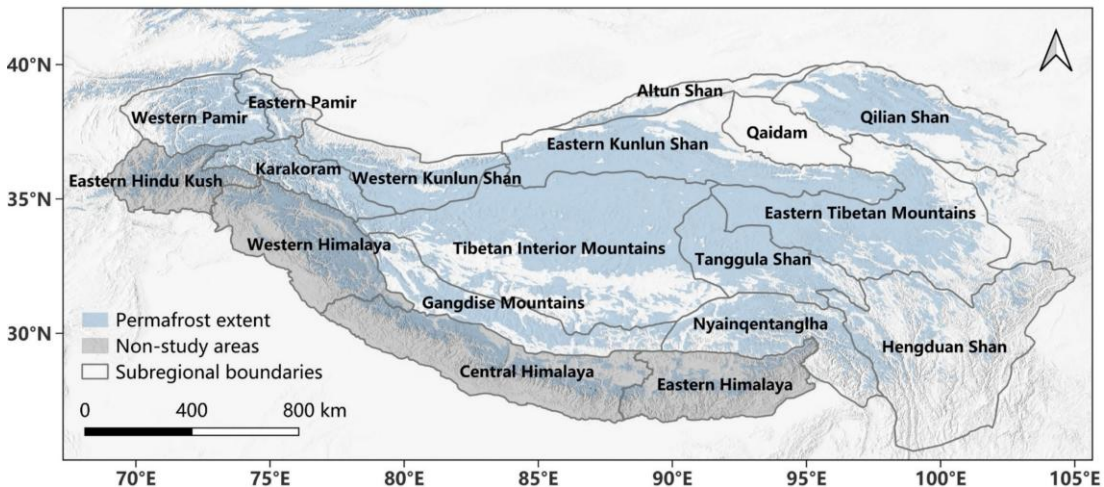


Figure 2.1: Study area (the Tibetan Plateau). The Hindu-Kush Himalayan region is excluded from this study. The permafrost extent map is from [Obu et al. \(2018\)](#).

## 2.3 Data

### 2.3.1 Planet Basemaps

We used a large volume of optical imagery from high-resolution satellite data, i.e., Planet Basemaps, as training images. Planet Labs Inc. generates the Basemaps product using imagery and data from its fleet with over 200 earth imaging satellites ([Nass et al., 2019](#)). The three-band (red, green, blue) imagery contains well-processed, scientifically accurate, and analyses-ready mosaics with a 4.77 m spatial resolution, visual consistency, and cloud mitigation ([Nass et al., 2019](#)). The visual consistency of Planet Basemaps is crucial for developing a comprehensive map of rock glaciers over broad regions. Furthermore, we chose images from a single sensor to ensure consistent quality and time stamp of the source images. To train the deep learning model and infer new rock glaciers, we mostly utilized the Planet Basemaps mosaics from the third quarter (July-September 2021) supplemented with images from the fourth quarter (October-December 2021) when needed to mitigate image quality problems in the third-quarter images, such as shadows and image distortion.

### 2.3.2 Existing rock glacier local inventories for training

To create a set of robust and diverse training data, we compiled existing rock glacier local inventories from multiple regions. Utilizing a multi-source approach helps increase the volume and diversity of the training dataset while mitigating the subjectivity and possible biases introduced by individual inventories. To incorporate more high-quality data, we included rock glaciers not only from the Tibetan Plateau but also from other regions, with a total of six local inventories comprising both intact and relict rock glaciers ([Table 2.1](#)).

## CHAPTER 2. DISTRIBUTION

Table 2.1: Information of rock glacier local inventories selected for training deep learning model.

Location	Number of rock glaciers	Number of intact rock glaciers	Number of relict rock glaciers	Image sources	Method	Reference
Western Kunlun Shan	413	413	0	ALOS-1 PALSAR-1, Sentinel-2, Google Earth	InSAR, deep learning, visual analysis	<a href="#">Hu et al. (2023a)</a>
Hunza River Basin	616	450	166	Google Earth	Visual analysis	<a href="#">Hassan et al. (2021)</a>
Poiqu River Basin	370	370	0	Pléiades, Google Earth	Visual analysis	<a href="#">Bolch et al. (2022)</a>
Daxue Shan	295	Unknown	Unknown	Google Earth	Visual analysis	<a href="#">Ran and Liu (2018)</a>
Northern Tien Shan	551	Unknown	Unknown	ERS-1/2 tandem mission, ALOS-1 PALSAR-1, ALOS-2 PALSAR-2, Sentinel-1, Google Earth, Bing Maps	InSAR, visual analysis	<a href="#">Kääb et al. (2021)</a>
French Alps	3,281	1,498	1,783	IGN ortho-imagery	Visual analysis	<a href="#">Marcer et al. (2017)</a>

Prior to generating the final training dataset, we performed quality control to account for the various source images and compilation strategies employed among these inventories. As a result, we manually checked and modified rock glacier boundaries by overlaying and visually checking the previously inventoried rock glaciers on our Planet Basemaps images. For example, rock glaciers that were difficult to recognize at places where the image quality was poor or covered by shadows were removed; when we identified missing rock glaciers in previous inventories, these were manually added. Since the front is a critical feature of a rock glacier, we followed the RGIK guidelines to use the extended geomorphological footprints to delineate rock glacier training samples ([RGIK, 2023](#)). We finally collected 4,085 rock glacier polygons as training samples.

### 2.3.3 Topo-climatic datasets

To analyse the patterns of rock glacier distribution and the associated environmental factors, we used several topo-climatic datasets including (1) the 30-m-resolution National Aeronautics and Space Administration Digital Elevation Model (NASADEM) ([Crippen et al., 2016](#)), (2) the  $0.1^\circ \times 0.1^\circ$  monthly mean annual air temperature (MAAT) data from January 1982 to the present derived from the Noah 3.6.1 model in the Famine Early Warning Systems Network (FEWS NET) Land Data Assimilation System (FLDAS) ([McNally and NASA/GSFC/HSL, 2018](#)), (3) the mean annual ground temperature (MAGT) data from 2000 to 2016 at 1-km spatial resolution produced by [Obu et al. \(2018\)](#), and (4) the  $0.1^\circ \times 0.1^\circ$  monthly precipitation data from 2001 to 2020 from the Integrated Multi-satellitE Retrievals for GPM (IMERG) ([Huffman et al., 2023](#)).

### 2.3.4 Auxiliary data

We also incorporated additional data sources including Google Earth images, ESRI basemaps, and the information on glacier and permafrost distributions. Google Earth images and ESRI basemaps were used as supplementary data to aid in the identification and validation of rock glaciers by using high-resolution images ([Yu and Gong, 2012](#)). For the glacier and debris-covered glacier data, we utilized the widely recognized Randolph Glacier Inventory (RGI v6.0), which provides global coverage of glacier outlines ([Pfeffer et al., 2014](#)). The RGI offers a valuable reference for distinguishing rock glaciers from adjacent glaciers. Regarding

permafrost extent, we relied on the map for the northern hemisphere produced by [Obu et al. \(2018\)](#).

## 2.4 Methods

### 2.4.1 Deep-learning-based rock glacier mapping approach

We propose a systematic deep-learning-based approach for mapping rock glaciers on the Tibetan Plateau. The workflow of the mapping approach is illustrated in Figure 2.2. The mapping process comprises two primary stages: (i) deep learning mapping and (ii) manual improvement, which will be elaborated in the following subsections.

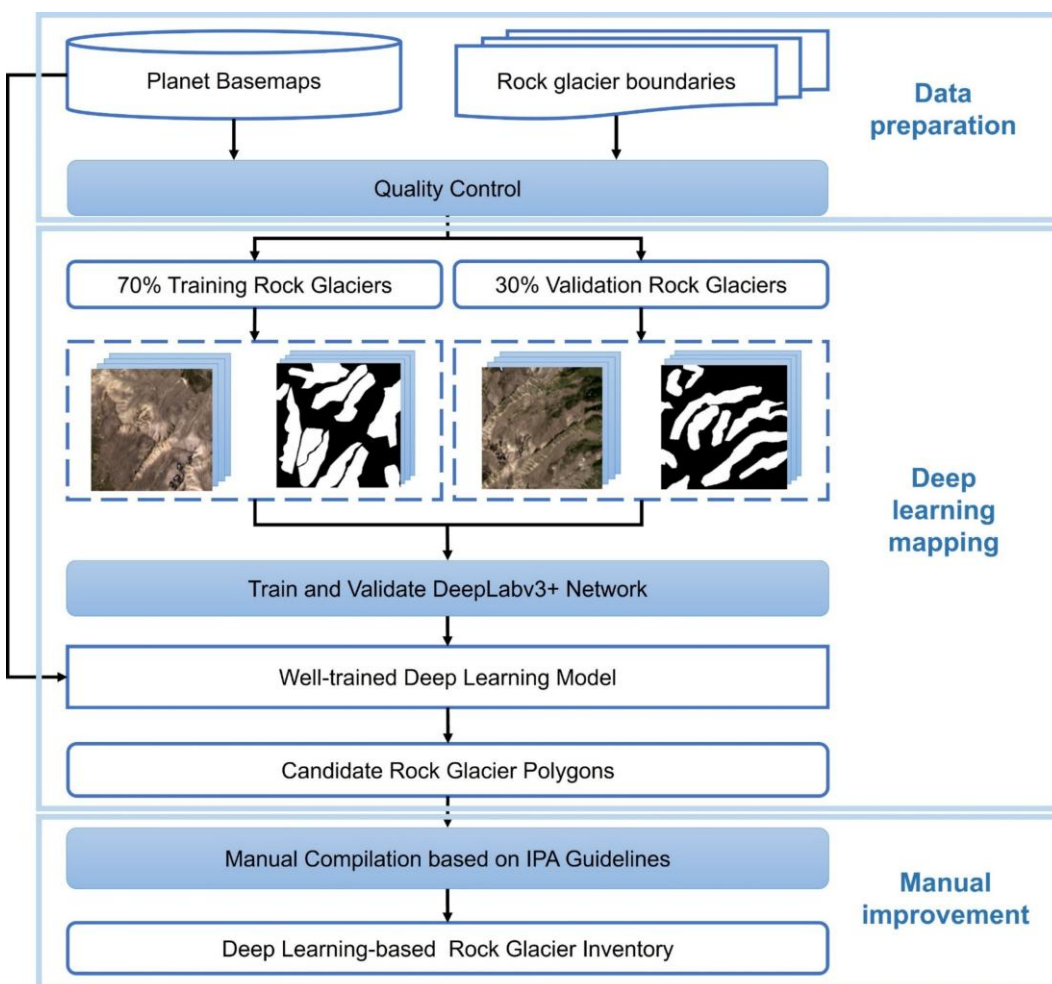


Figure 2.2: Flowchart of the deep learning-based approach for mapping rock glaciers.

#### 2.4.1.1 Deep learning mapping

DeepLabv3+, introduced by [Chen et al. \(2018\)](#), was selected as the neural network

architecture for the deep learning model, with Xception71 serving as its backbone ([Chollet, 2017](#)). DeepLabv3+ is specifically designed for semantic segmentation tasks and has been proven to excel in mapping permafrost landforms ([Huang et al., 2020; Hu et al., 2023a](#)). Xception71 is a convolutional neural network architecture consisting of 71 layers and encompasses approximately 42 million parameters ([Chollet, 2017](#)).

Our deep learning model takes a three-channel image with red, green, and blue (RGB) bands as input and outputs a binary image indicating the occurrence of rock glaciers. Topographic information such as slope or elevation was not used because this model only accepts three image bands as input. The model first processes the RGB image and captures color and texture information. Then a convolutional neural network extracts spatial and spectral features (e.g., shape, texture, color patterns) that distinguish rock glaciers from other terrain. Finally, the model classifies pixels or regions as ‘rock glacier’ or ‘not rock glacier’ based on learned patterns from training data.

For the model training, 70% of rock glacier boundaries from the six local inventories were extracted, with the remaining 30% kept for validation. The intersection over union (IoU) was employed as the accuracy metric of validation, which is defined as:

$$\text{IoU}(A, B) = \text{area}(A \cap B) / \text{area}(A \cup B) \quad (2.1)$$

where A denotes the mapped polygon and B is the reference polygon. The IoU scores range from 0 to 1, and a higher value indicates a higher accuracy ([Huang et al., 2020](#)).

We supplemented our training dataset with negative samples, incorporating non-rock glacier polygons to address potential misclassifications by the deep learning model, particularly when encountering landforms exhibiting similar characteristics to rock glaciers. These non-rock glacier polygons encompass diverse features such as debris-covered glaciers, rock avalanches, and water bodies. To incorporate context information from the surrounding area of a rock glacier, we established a buffer area to extract a subset of Planet images. A small buffer area may fail to provide sufficient contextual information, resulting in an increased occurrence of false positives; while an overly large buffer area risks inundating the model with excessive background information, potentially compromising its ability to accurately detect rock glaciers ([Huang et al., 2018; Huang et al., 2020](#)). We conducted experiments

with buffer area sizes ranging from 500 meters to 2000 meters. The results showed no significant increase in the IoU metric once the buffer area exceeded 1500 meters. Therefore, we selected 1500 meters as the buffer area. The subset of images was then subdivided into patches of  $480 \times 480$  pixels with an overlap of 160 pixels. The binary label patches were created by rasterizing rock glacier polygons ([Huang et al., 2020](#)).

Once trained, the deep learning model was validated using images across the Tibetan plateau. We calculated the areas of true positives (TP), false positives (FP), and false negatives (FN), and then calculated the precision, recall, and F1 score using the following equations ([Huang et al., 2020](#)):

$$\text{Precision} = \text{TP}/(\text{TP} + \text{FP}) \quad (2.2)$$

$$\text{Recall} = \text{TP}/(\text{TP} + \text{FN}) \quad (2.3)$$

$$F_1 = 2 \times \text{Precision} \times \text{Recall}/(\text{Precision} + \text{Recall}) \quad (2.4)$$

Since the predicted polygons are subject to uncertainties due to varying qualities of imagery, training inventories, and model accuracy, initial results are referred to as “candidate rock glacier polygons”. These polygons were not considered definitive rock glacier inventories but rather served as preliminary detection of rock glaciers, along with the locations and boundaries, which were then refined as described below.

#### **2.4.1.2 Manual improvement and independent validation**

To ensure the accuracy and reliability of the dataset, a manual checking and improving process was carried out on the candidate rock glacier polygons. By utilizing these polygons as a starting point, the efforts for manual compilation were significantly reduced. The manual improvement process followed the standard guidelines recommended by the IPA Action Group RGIK ([RGIK, 2023](#)). According to these guidelines, the mapped rock glaciers were visually checked based on specific geomorphological features, notably the visible accumulation of talus material at the front and the presence of a lateral extension of this talus material along the sides of the rock glacier. Additionally, certain rock glaciers may exhibit noticeable convex-downslope or longitudinal-surface undulations, creating a ridge-and-furrow topography. We considered the extended footprints of rock glaciers while restricting the horizontal distance between the upper front edge and the frontal talus base within

50 m to exclude the possible exaggerated front. Following the global glacier inventory standards and given the resolution limitations of Planet Basemaps (4.77 m), rock glaciers smaller than 10,000 m<sup>2</sup> (0.01 km<sup>2</sup>) were excluded from the inventory ([RGIK, 2023](#)).

We proposed four “R” operations to manually check the rock glacier candidate polygons:

- “Remain”: no operation if the polygon accurately outlines the rock glacier
- “Remove”: remove the polygon if it is not a rock glacier
- “Refine”: modify the polygon if it was correctly identified as a rock glacier but the boundaries were not correctly outlined
- “Retrieve”: add a missing rock glacier and outline its boundary

The "Remove" operation is designed to exclude landforms that have been incorrectly identified as rock glaciers by the deep learning model. These misidentified landforms commonly include debris-covered glaciers and rock avalanches. Debris-covered glaciers are glaciers that are partially covered by variable layers of debris (from a few centimeters to two meters) and are characterized by supraglacial features such as thermokarst features, supraglacial lakes, streams, and ice cliffs ([Jones et al., 2019b](#); [Racoviteanu et al., 2022](#); [RGIK, 2023](#)). Outlines from the RGI v6.0 inventory were used to visually remove polygons overlapping debris-covered glaciers. Rock avalanches, on the other hand, are composed of fragmented rocks that flow downhill following large rock slope failures ([Hungr et al., 2014](#)). Unlike rock glaciers, rock avalanches typically lack any discernible pattern or order on the surface. The "Refine" operation involved the manual editing of the deep learning predicted rock glacier outlines to ensure that the polygon boundaries closely matched the observed boundaries of rock glaciers in the images. The "Retrieve" operation serves the purpose of adding missing rock glaciers to the inventory. Some rock glaciers can be overlooked by the deep learning model, either due to their subtle features or low-quality image data. When missing rock glaciers were identified during the manual inspection of nearby candidate polygons, they were added to the inventory. Furthermore, in high mountain environments, the convergence of multiple rock glacier units into a complex system is a frequent occurrence ([RGIK, 2023](#)). However,

the deep learning model often tends to predict this system as a singular rock glacier. To anticipate such issues, we manually separated the system into smaller rock glacier units if their lateral boundaries were clearly observed in Planet Basemaps images.

Our team consisted of seven mappers and two independent reviewers. Each candidate rock glacier polygon was manually examined and refined by visual interpretation of Planet Basemaps images following the four “R” operations by each mapper. In cases where the features of rock glaciers were uncertain and not clearly observable in Planet images, high-resolution Google Earth images and ESRI basemaps were utilized for more accurate visual inspection and analysis. An extended footprint of each rock glacier was yielded, from which we generated the primary marker, which is a point identifying a unique rock glacier unit or system ([RGIK, 2023](#)).

We proceeded with an independent validation process to assess the quality of the revised inventory. Given the difficulty in accurately evaluating the delineated boundaries, our validation focused primarily on verifying the primary markers. To conduct this validation, we randomly selected 2,110 samples (approximately 5% of the primary markers). Two independent reviewers examined all the selected samples using Google Earth images. Based on their independent assessments, each reviewer provided one of four decisions: "yes," indicating that the rock glaciers were correctly identified; "no," suggesting an incorrect identification; "uncertain," denoting a lack of certainty in the identification; and "undefined," used when the examined rock glaciers could not be clearly observed due to factors such as heavy snow cover, shadows, or the unavailability of high-quality images.

#### **2.4.2 Adding attributes of the final revised rock glaciers**

According to the IPA RG IK guidelines, there are three mandatory attributes for a rock glacier unit (RGU): the primary ID, the associated rock glacier system (RGS), and the metadata ([RGIK, 2023](#)). In our inventory, the attribute ID is equivalent to the primary ID, which is formed by combining "RGU" with the World Geodetic System 84 (WGS84) coordinates of the rock glacier, expressed in decimal degrees with four digits ([RGIK, 2023](#)). We were unable to provide the RGS information in our current inventory due to image resolution limitations and instance segmentation issues. We have included the metadata attribute, which contains information of source data, date

of mapping, mapper's name, reviewer's name, and additional information, which are separately stored in SOUR\_DATA, MAP\_DATE, MAPPER, REVIEWER, and ADDI\_INF attributes ([RGIK, 2023](#)). The ADDI\_INF provides information on whether the rock glacier has been recognized as a false identification by the reviewers. Furthermore, we computed the geomorphic and climatic attributes of each inventoried rock glacier to analyse their spatial distribution characteristics and the associated topo-climatic conditions. We derived the rock glacier area based on the polygon extent. The NASADEM was used to calculate the elevation, slope, and aspect of the rock glaciers ([Crippen et al., 2016](#)). The climatic information, including MAAT, MAGT, and annual precipitation, of each rock glacier was extracted from the climatic data. We also calculated the annual potential incoming solar radiation (PISR) using the model described by [Kumar et al. \(1997\)](#). Table [2.2](#) lists all the attributes of the inventory.

Table 2.2: Attribute data dictionary for Tibetan Plateau rock glacier inventory shapefile.

Attribute name	Description	Units
ID <sup>1</sup>	Rock glacier ID	
SOUR_DATA <sup>2</sup>	Source data	
MAP_DATE <sup>2</sup>	Date of mapping	
MAPPER <sup>2</sup>	Mapper's name	
REVIEWER <sup>2</sup>	Reviewer's name	
ADDI_INF <sup>2</sup>	Additional information	
LAT	Latitude	Degrees
LON	Longitude	Degrees
SUBREGION	Subregion of rock glacier	
AREA	Rock glacier area	m <sup>2</sup>
ELE_MEAN <sup>3</sup>	Mean elevation of rock glacier	m
ELE_MEDIAN <sup>3</sup>	Median elevation of rock glacier	m
ELE_MIN <sup>3</sup>	Minimum elevation of rock glacier	m
ELE_MAX <sup>3</sup>	Maximum elevation of rock glacier	m
SLO_MEAN <sup>3</sup>	Mean slope of rock glacier	Degrees
SLO_MEDIAN <sup>3</sup>	Median slope of rock glacier	Degrees
SLO_MIN <sup>3</sup>	Minimum slope of rock glacier	Degrees
SLO_MAX <sup>3</sup>	Maximum slope of rock glacier	Degrees
ASPECT <sup>3</sup>	Aspect of rock glacier	Degrees
MAAT <sup>4</sup>	Mean annual air temperature	°C
MAGT <sup>5</sup>	Mean annual ground temperature	°C
AP <sup>6</sup>	Annual precipitation	mm
PISR <sup>3</sup>	Annual potential incoming solar radiation	kWh/m <sup>2</sup>

<sup>1</sup>ID is identical to the Primary ID attribute in the IPA RGIK guidelines.

<sup>2</sup>SOUR\_DATA, MAP\_DATE, MAPPER, REVIEWER, and ADDI\_INF contain the information of Metadata attribute in the IPA RGIK guidelines.

<sup>3</sup>ELE\_MEAN, ELE\_MEDIAN, ELE\_MIN, ELE\_MAX, SLO\_MEAN, SLO\_MEDIAN, SLO\_MIN, SLO\_MAX, ASPECT, and PISR are attributed based on the 30-m-resolution National Aeronautics and Space Administration Digital Elevation Model (NASADEM) ([Crippen et al., 2016](#)) (<https://search.earthdata.nasa.gov/search>, last access: 3 December 2024).

<sup>4</sup>MAAT is attributed based on the  $0.1^\circ \times 0.1^\circ$  monthly mean annual air temperature (MAAT) data from January 1982 to the present derived from the Noah 3.6.1 model in the Famine Early Warning Systems Network (FEWS NET) Land Data Assimilation System (FLDAS) ([McNally and NASA/GSFC/HSL, 2018](#)) ([https://disc.gsfc.nasa.gov/datasets/FLDAS\\_NOAH01\\_C\\_GL\\_M\\_001/summary?keywords=MERRA-2%20and%20CHIRPS](https://disc.gsfc.nasa.gov/datasets/FLDAS_NOAH01_C_GL_M_001/summary?keywords=MERRA-2%20and%20CHIRPS), last access: 3 December 2024).

<sup>5</sup>MAGT is attributed based on mean annual ground temperature (MAGT) data from 2000 to 2016 at 1-km spatial resolution produced by [Obu et al. \(2018\)](#) (<https://apgc.awi.de/dataset/pex>, last access: 3 December 2024).

<sup>6</sup>AP is attributed based on the  $0.1^\circ \times 0.1^\circ$  monthly precipitation data from 2001 to 2020 from the Integrated Multi-satellitE Retrievals for GPM (IMERG) ([Huffman et al., 2023](#)) (<https://doi.org/10.5067/GPM/IMERG/3B-MONTH/07>, last access: 3 December 2024).

### 2.4.3 Spatial analysis of rock glaciers

To investigate the spatial distribution characteristics of rock glaciers on the Tibetan Plateau, we conducted statistical analyses of their geomorphic features within a 50 km × 50 km grid cell. In each cell, we counted the number of rock glaciers and calculated the average values for their areas, minimum elevations, and slopes. We also analysed the distribution patterns of their aspects in different subregions.

## 2.5 Results

Across the entire study area, the deep learning model predicted a total of 48,767 candidate rock glacier polygons (Figure [2.3a](#)). After the manual improvement (see Section [2.4.1.2](#)), we produced an inventory consisting of 44,273 rock glaciers (Figure [2.3b](#) and further described in Sections [2.5.2](#) and [2.5.3](#)). Below we first present the validation of our results from three perspectives: (i) validation of the deep learning model based on training and validation datasets (Section [2.5.1.1](#)); (ii) validation of the deep learning predicted rock glacier outlines based on manually improved rock glaciers used as our ground truth (Section [2.5.1.1](#)); (iii) independent validation of inventoried rock glaciers based on visual examination (Section [2.5.1.2](#)).

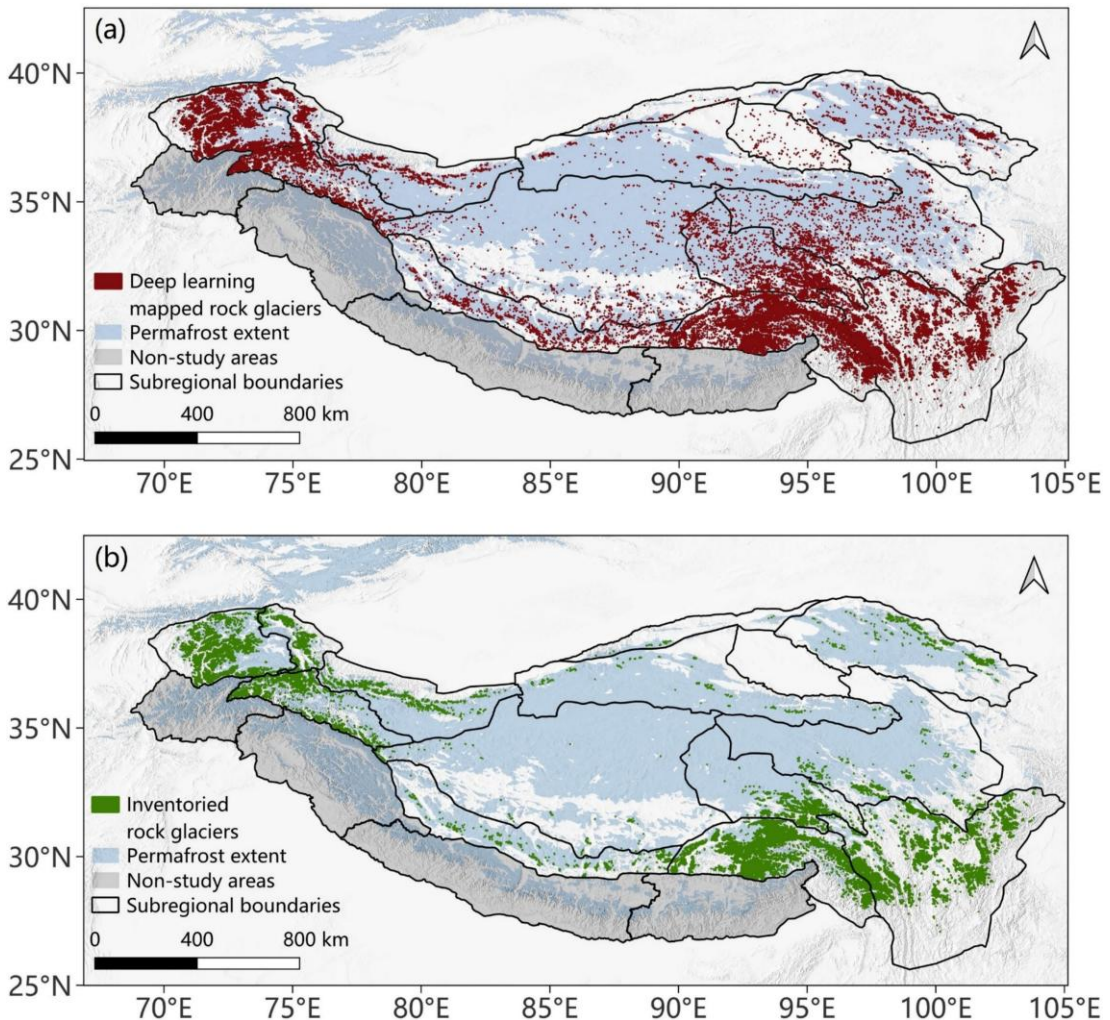


Figure 2.3: (a) Deep-learning-mapped candidate rock glacier polygons. (b) Rock glacier inventory on the Tibetan Plateau (TPRoGI). The permafrost in Hengduan Shan is overlapped by the rock glaciers thus not visible on the map. The permafrost extent map is from [Obu et al. \(2018\)](#).

## 2.5.1 Performance of deep learning-based rock glacier mapping approach

### 2.5.1.1 Deep learning model performance and output

Figure 2.4 shows the IoU scores achieved by the deep learning model during the training and validating processes. Initially, both the training and validation IoU scores exhibit an upward trend, followed by a gradual stabilization. By the last iteration, the model achieved an IoU score of 0.76 on the training dataset and 0.70 on the validation dataset, indicating that the model learned effectively from the training data and generalized well to the validation data.

To further evaluate the model performance, we applied the well-trained model to

predict the rock glacier boundaries on both the training and validation datasets. The deep learning model accurately captured rock glacier characteristics within the training dataset, as evidenced by the close alignment between the predicted boundaries and the training polygons (Figure 2.5a). Figure 2.5b further confirms that the model could generalize well to new datasets, with good agreement between predicted boundaries and validation polygons. However, difficulties in mapping rooting regions led to misalignment in those areas ([Brardinoni et al., 2019](#)).

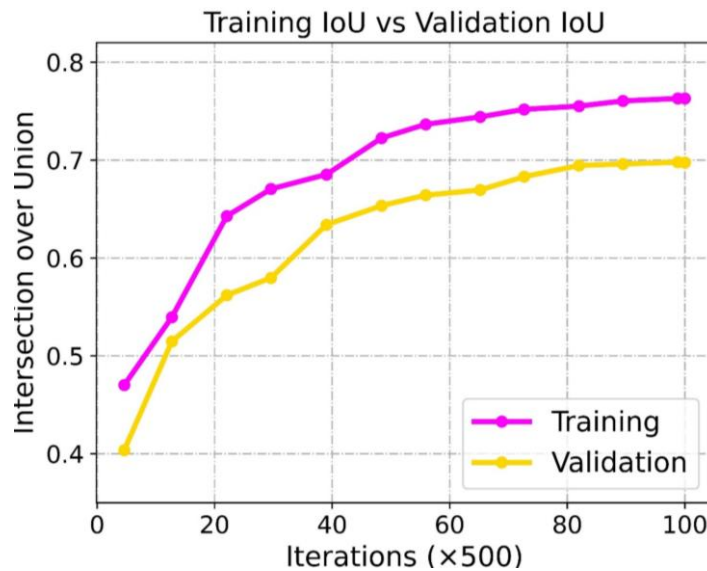


Figure 2.4: IoU scores during the training and validation processes.

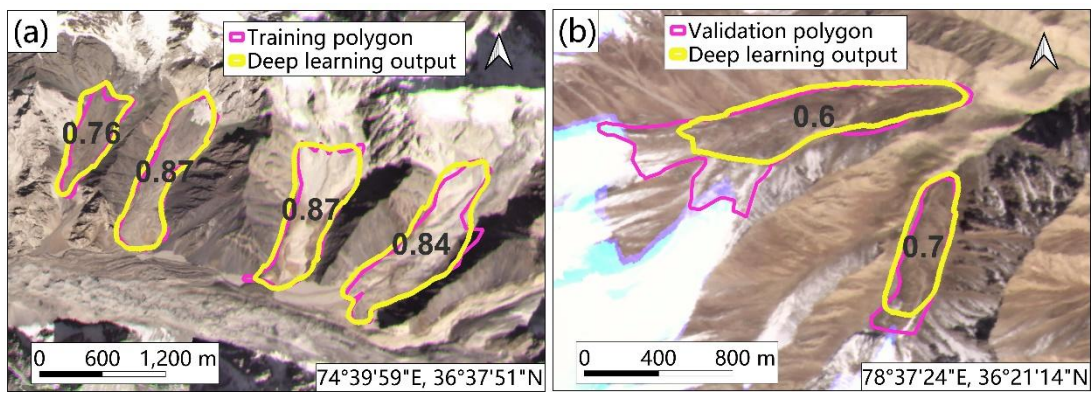


Figure 2.5: Examples of the candidate rock glaciers are shown in (a) training and (b) validation regions using the well-trained deep learning model. The IoU scores are labelled on the mapped rock glaciers.

Table 2.3 presents the calculated recall, precision, and  $F_1$  score of the deep learning mapped polygons for each subregion, as well as for the entire study area. Over the entire study area, the  $F_1$  score was 0.63, which we consider satisfactory for rock glacier mapping. The highest performance was for the Hengduan Shan ( $F_1 = 0.76$ ), with  $F_1$  scores of the Eastern Pamir, Karakoram, Nyainqêntanglha, Western Kunlun Shan, Western Pamir, and Hengduan Shan subregions above 0.6, lower  $F_1$  scores for the Altun Shan, Eastern Kunlun Shan, Eastern Tibetan Mountains, Gangdise Mountains (0.27–0.36), and the lowest for Tibetan Interior Mountains subregion (0.16) (Table 2.3). This disparity arises from the scarcity of rock glaciers in certain subregions, where the deep learning model generated many falsely detected polygons and subsequently produced high false positives. Recall scores are generally higher than the precision scores, indicating that the false positives outweigh the false negatives in the model predictions. This finding suggests that the deep learning model possesses a strong capability for detecting rock glaciers.

However, deep learning alone also generates numerous falsely detected polygons, highlighting the need for manual improvement. For example, Figure 2.6 demonstrates the performance of the well-trained deep learning model in detecting and delineating rock glaciers in a new area – the Western Pamir, which was not included in the training process. As shown in Figure 2.6a–c, there is good agreement between the deep learning output and the manually revised boundaries for a significant proportion of the rock glaciers in this area. However, Figure 2.6 also illustrates some uncertainties associated with inaccurate boundary delineation, false detections, and missing identifications. For instance, as shown in Figure 2.6d, a debris-covered glacier was falsely identified as a rock glacier, while Figure 2.6e highlights several missing rock glaciers, possibly due to their poorly developed geomorphological features.

## CHAPTER 2. DISTRIBUTION

Table 2.3: Performance of deep learning mapped polygons in different subregions.

Subregion	Number of deep learning mapped polygons	Number of manually revised rock glaciers	TP <sup>1</sup> (km <sup>2</sup> )	FP <sup>1</sup> (km <sup>2</sup> )	FN <sup>1</sup> (km <sup>2</sup> )	Precision	Recall	F1 score
Altun Shan	82	32	3.55	9.03	3.45	0.28	0.51	0.36
Eastern Kunlun Shan	517	180	22.81	60.57	33.46	0.27	0.41	0.33
Eastern Pamir	1,060	1,330	230.76	115.40	143.12	0.67	0.62	0.64
Eastern Tibetan Mountains	2,569	1,095	43.97	200.09	32.34	0.18	0.58	0.27
Gangdise Mountains	1,572	816	49.91	128.50	66.82	0.28	0.43	0.34
Karakoram	2,873	2,612	415.89	344.57	133.41	0.55	0.76	0.64
Nyainqêntanglha	14,161	16,222	1,095.42	876.49	465.46	0.56	0.70	0.62
Qilian Shan	1,367	1,047	77.21	129.90	68.68	0.37	0.53	0.44
Tibetan Interior Mountains	1,158	150	15.71	130.23	35.13	0.11	0.31	0.16
Western Kunlun Shan	779	1,019	116.44	69.40	87.56	0.63	0.57	0.60
Western Pamir	4,989	4,957	685.50	549.56	266.32	0.56	0.72	0.63
Tanggula Shan	4,010	2,402	166.92	288.34	61.34	0.37	0.73	0.49
Hengduan Shan	13,387	12,411	1,478.55	678.96	268.31	0.69	0.85	0.76
Qaidam	243	0	0	15.95	0	0	N/A	N/A
Entire study area	48,767	44,273	4,403.43	3,596.49	1,664.61	0.55	0.73	0.63

<sup>1</sup>TP (true positive), FP (false positive) and FN (false negative) are expressed as the total areas.

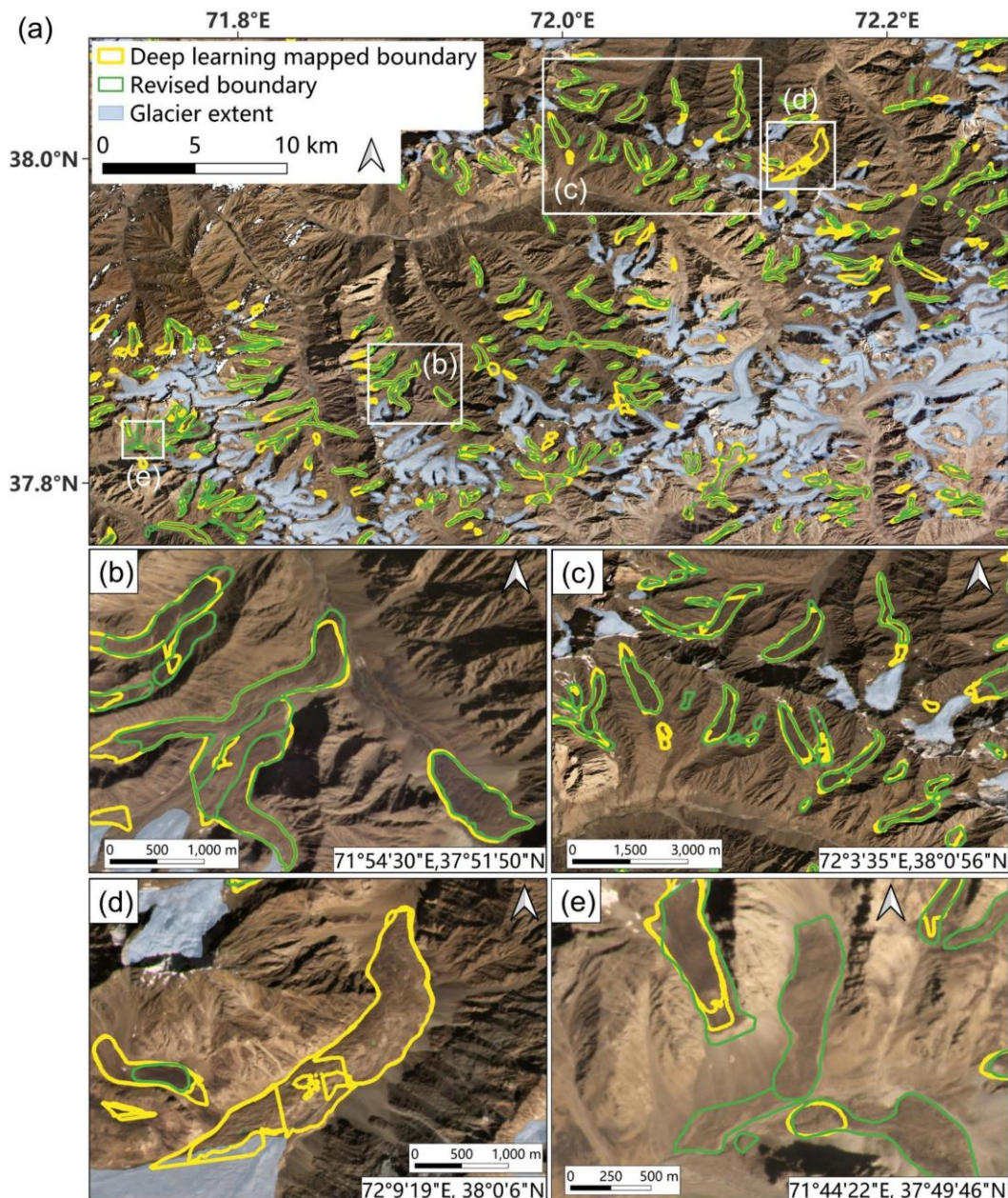


Figure 2.6: (a) An example area in Western Pamir showing the deep learning outputs (in red) and manually revised rock glacier boundaries (in green). Clean and debris-covered glacier extents (light blue) are from the Randolph Glacier Inventory (RGI v.6) (Pfeffer et al., 2014); (b-c) enlarged views of the areas showing good agreement between deep learning outputs and revised boundaries; (d) enlarged view showing a false detection example in the center; (e) enlarged view showing multiple missing identifications.

### 2.5.1.2 Independent validation of the inventoried rock glaciers

Results of the independent review based on the 2110 rock glacier primary markers are presented in Table 2.4 and show that approximately 87% of the primary markers were assigned as correctly identifying rock glaciers by both reviewers. This indicates that most of the sampled features met the criteria and characteristics of rock glaciers. Additionally, the evaluation process identified that only approximately 1% and 6% of the primary markers were assigned as false identifications by the two reviewers, respectively. This signifies that the occurrence of misclassifications or false positives within the inventory is relatively low (below 10%). The discrepancy in the "no" decision numbers between the two reviewers can be attributed to the differences in the operators' judgments (Brardinoni et al., 2019).

Table 2.4: Independent validation results of sampled Tibetan Plateau rock glacier inventory (n = 2110 samples).

Reviewer	Number of “yes”	Number of “no”	Number of “uncertain”	Number of “undefined”
Reviewer 1	1,836	17	42	215
Reviewer 2	1,844	127	44	95

### 2.5.2 Rock glacier inventory on the Tibetan Plateau: TPRoGI [v1.0]

After manual improvement, our plateau-wide inventory encompasses 44,273 rock glaciers, including both intact and relict types (Figure 2.3b). The inventoried rock glaciers cover a total area of approximately 6,000 km<sup>2</sup> (6,068,043,348 m<sup>2</sup>). The mean area is 0.14 km<sup>2</sup>. The largest rock glacier occupies 4.6 km<sup>2</sup>, whereas most of them (90.6%) are smaller than 0.3 km<sup>2</sup> (Figure 2.7a). In terms of elevation, most rock glaciers (95.0%) exhibit minimum elevations between 4,000 m and 5,500 m above sea level (m a.s.l.), with an average value of 4,729 m a.s.l. (Figure 2.7b). The highest rock glacier is situated at an elevation of 5,839 m a.s.l. in the Tibetan Interior Mountains, whereas the lowest lies at 2,717 m a.s.l. in Western Pamir. Rock glaciers develop on slopes with varying gradients, and approximately 90% of them occur on slopes between 10° to 25° with an average slope angle of 17.7° (Figure 2.7c). Also, the compiled rock glaciers are distributed across various slope orientations with preferences at the north- and west-facing slopes (Figure 2.7d).

Rock glaciers predominantly occur in cold environments with temperatures at or slightly below freezing. A significant proportion of rock glaciers (66.3%) thrive in

areas where the MAAT ranges between  $-5$  and  $0$   $^{\circ}\text{C}$  (Figure 2.7e). Furthermore, 71.7% of the rock glaciers exhibit MAGT between  $-5$  and  $0$   $^{\circ}\text{C}$  (Figure 2.7f). On average, the MAAT and MAGT for these rock glaciers are  $-2.7$  and  $-1.6$   $^{\circ}\text{C}$ , respectively. Approximately 82% of the rock glaciers are situated in regions with annual precipitation ranging from 300 to 1,000 mm, with an average of 597 mm (Figure 2.7g). About 85% of the rock glaciers receive PISR between 2,500 and 3,500  $\text{kWh}/\text{m}^2$  annually, with a mean value of 2,930  $\text{kWh}/\text{m}^2$  (Figure 2.7h).

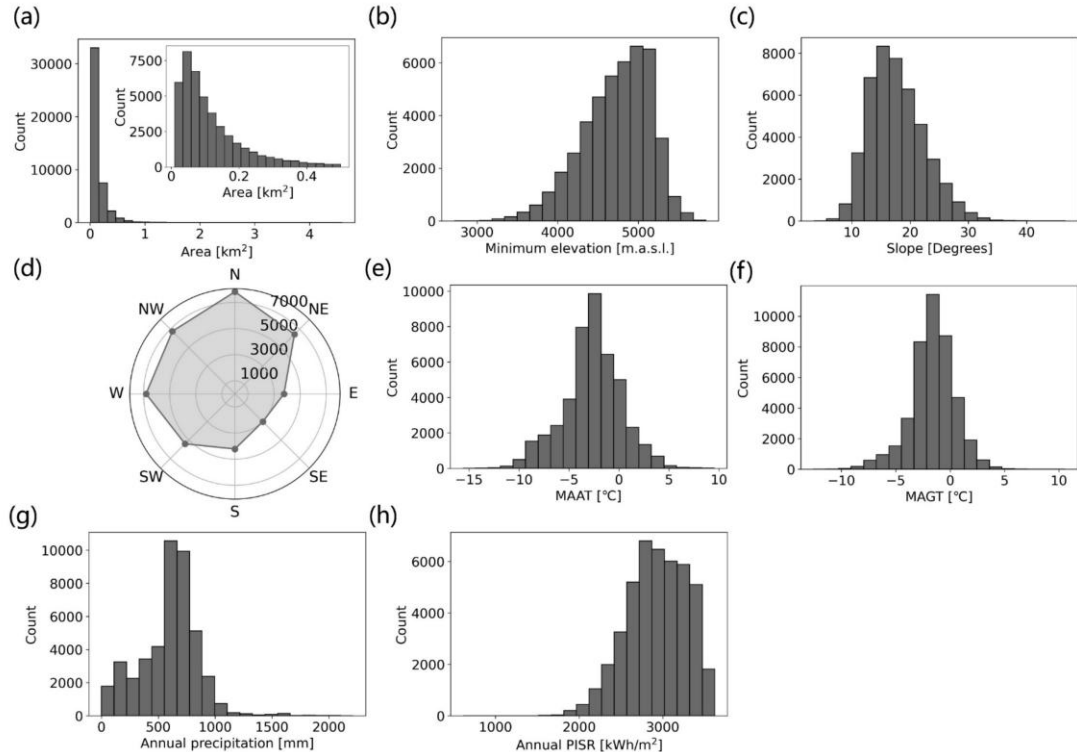


Figure 2.7: Statistical summaries of the geomorphic and current climatic features of rock glaciers in the study region. (a) The areal histogram of all the rock glaciers on the Tibetan Plateau. The inset shows the areas smaller than  $0.5 \text{ km}^2$ . (b)–(h) are histograms of the minimum elevations, slopes, aspects of the rock glaciers with the radial axis representing the counts, Mean Annual Air Temperature (MAAT), Mean Annual Ground Temperature (MAGT), annual precipitation, and annual Potential Incoming Solar Radiation (PISR), respectively.

### 2.5.3 Spatial distribution characteristics of rock glaciers

Figure 2.8 presents the spatial distribution and geomorphic characteristics of rock glaciers on the Tibetan Plateau within 50 km grid cells. Rock glaciers are widespread in the northwestern and southeastern plateau and densely distributed in the Western Pamir and Nyainqêntanglha, while they are scarce in the inner plateau (Figure 2.8a).

No rock glacier was found in the Qaidam region, presumably due to the absence of permafrost and the occurrence of few mountains there. Rock glaciers in the western plateau have larger areas (mean =  $0.21 \text{ km}^2$ ) than in the eastern plateau (mean =  $0.11 \text{ km}^2$ ), as evident in Figure [2.8b](#). Notably, a decreasing gradient is observed in minimum elevations of rock glaciers, with higher elevations in the Gangdise Mountains and lower elevations towards the east and west directions (Figure [2.8c](#)). The average slopes of rock glaciers are larger in northwestern Karakoram and southeastern plateau, suggesting a tendency for rock glaciers to develop on steeper slopes in these areas (Figure [2.8d](#)).

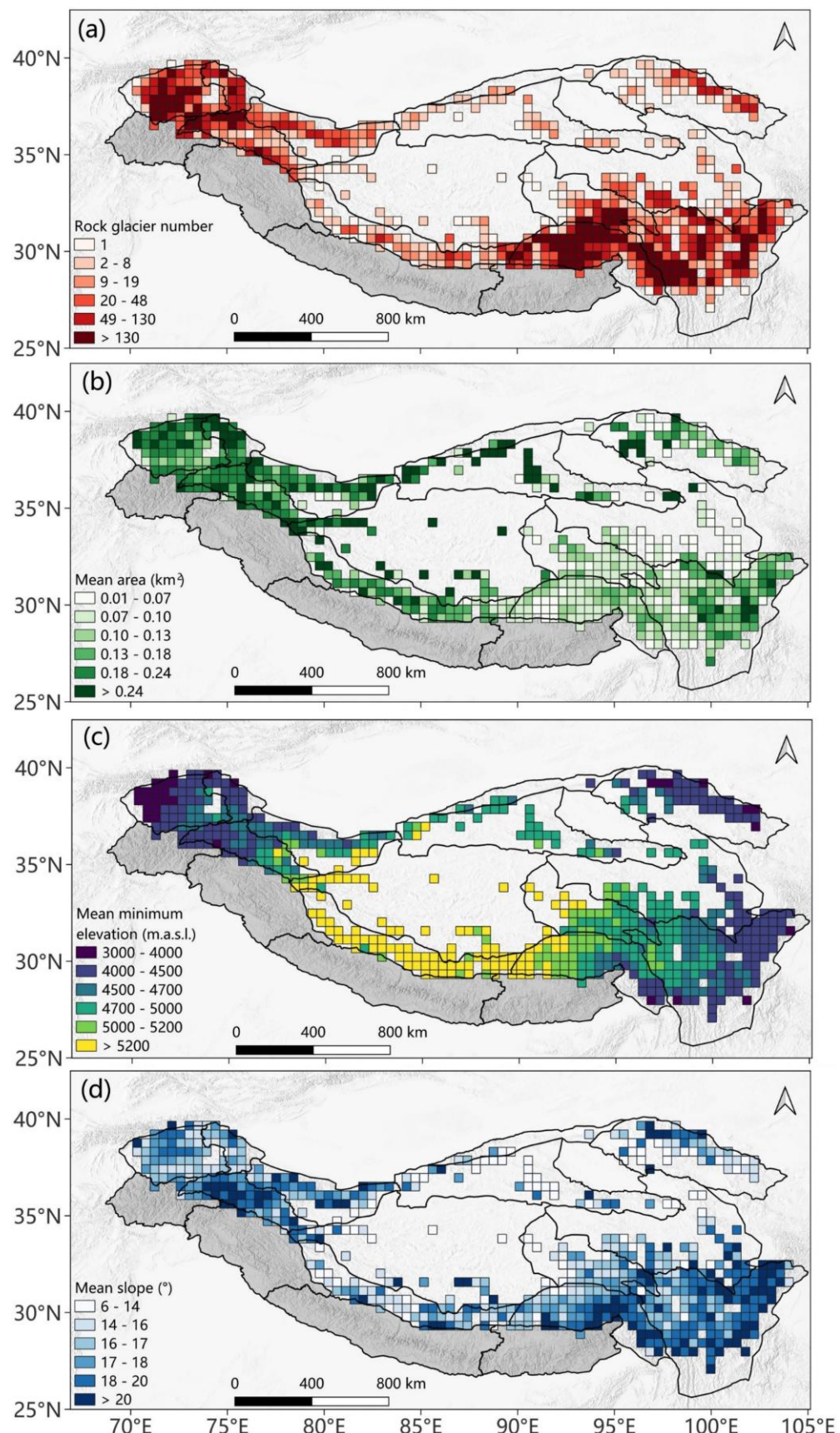


Figure 2.8: Rock glacier (a) density, (b) area, (c) minimum elevation and (d) slope averaged over grid cells of  $50 \text{ km} \times 50 \text{ km}$ .

Rock glacier aspects across different subregions are depicted in Figure 2.9, characterized by a discernible west-east gradient and similarities between neighbouring subregions. Specifically, the ones found in the western plateau (Western Kunlun Shan, Karakoram, Eastern Pamir, Western Pamir) display no distinct preference towards any specific orientation, whereas those situated in the central part of the plateau (Altun Shan, Eastern Kunlun Shan, Tibetan Interior Mountains, Gangdise Mountains) primarily face north. Conversely, rock glaciers in the eastern plateau (Qilian Shan, Eastern Tibetan Mountains, Tanggula Shan, Hengduan Shan, Nyainqêntanglha) exhibit a prevalent preference for north and west orientations.

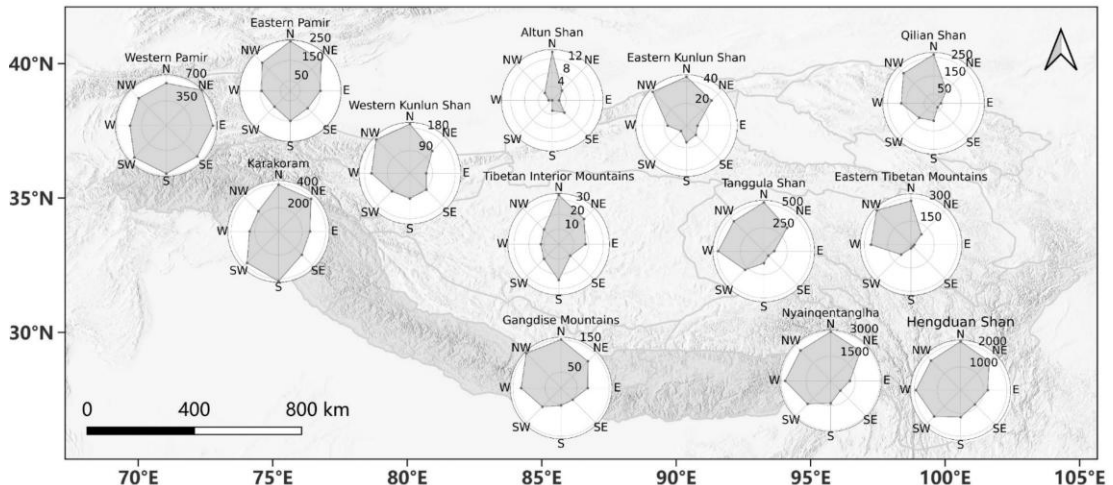


Figure 2.9: Rock glacier aspects in different subregions of the study area.

## 2.6 Discussion

### 2.6.1 Limitations of the deep learning-based mapping approach

#### 2.6.1.1 Limitations of Planet Basemaps imagery

The quality of the source images plays a crucial role in the uncertainty of the predicted results as the deep learning model accuracy heavily relies on high-quality input images. However, rock glaciers are frequently found in regions characterized by poor image quality due to factors associated with cloud cover, shadows, and distortions, which are common in mountainous areas. These challenges have a substantial impact on the accuracy of predictions. Consequently, when the deep learning model is input with images suffering severe quality issues, it may fail to

identify rock glaciers within that region.

### 2.6.1.2 Limitations of the deep learning model

The mapped results generated by the deep learning model still have significant uncertainties associated with inaccurately predicted boundaries, false detections, and missing identifications (Figure 2.6). Despite utilizing the powerful neural network DeepLabv3+ as the model structure, the training and validation IoU scores fall below 0.8 (Figure 2.4). When applied to the entire study area, the uncertainty increases further, with a precision of 0.55, a recall of 0.73, and  $F_1$  score of 0.63 (Table 2.3). These results are comparable to [Robson et al. \(2020\)](#)'s results, which obtained a precision of 63.9% to 68.9% and a recall of 75% to 75.4%. Both results highlighted the challenges of using deep learning to map rock glaciers fully automatically in high mountain environment.

A key limitation of the current deep learning model is the restricted number of input bands. Our model only utilizes RGB bands, while inherently excluding crucial topographic information such as slope and elevation. As rock glacier occurrence is closely related to topography and underlying geology, the absence of morphometric inputs like terrain roughness and slope, as well as lithological data, may hinder the model performance.

Furthermore, the learning performance of the model can be hindered by limited and biased training samples. Our training samples were derived from six local inventories, encompassing 4,085 rock glacier polygons. Due to the limited quantity of our training dataset, the model may struggle to fully capture the complexity and diversity of the training samples. Consequently, its generalization ability and accuracy may be compromised when presented with unfamiliar images ([Rice et al., 2020](#)). Additionally, the six local inventories were compiled by different operators from various institutes. The divergent knowledge and expertise among these operators can introduce inconsistencies in judgments, resulting in subjectivity and bias within the training dataset. As a result, inconsistent and biased training samples can potentially confuse the model, thereby impairing its ability to accurately identify rock glaciers ([Ren et al., 2018](#)).

Additionally, it is important to note that the deep learning model can only map the areas of rock glaciers and is not capable of performing instance segmentation, which

would accurately segment individual rock glacier units ([Erharder et al., 2022](#)). Consequently, the model tends to predict the entire rock glacier system, composed of several adjacent rock glacier units, as a single entity.

### **2.6.1.3 Limitations of manual improvement**

The manual examination and refinement were assigned by multiple individuals with varying levels of experience, which inevitably introduced subjectivity, human errors, and potential inconsistencies ([Brardinoni et al., 2019](#)). Moreover, accurately depicting the boundaries of rock glaciers via manual delineation can be challenging due to the 4.77 m resolution of the interpreted images and thus the mapped rock glaciers inherently contain uncertainties ([Jones et al., 2018b](#)).

Furthermore, delineating the upper and lateral boundaries within rock glacier systems presents even greater uncertainties ([Brardinoni et al., 2019](#)). In comparison to the lower boundary in the front and lateral margin regions, the upper boundary in the rooting zone and the lateral boundary between rock glaciers within a system often lack pronounced geomorphological features and thereby require more precise interpretation of surface texture and color variations. As a result, the delineation of upper and lateral boundaries is inherently ambiguous and subjective ([Schmid et al., 2015](#); [Jones et al., 2018b](#); [Erharder et al., 2022](#)). Due to the difficulty in delineating lateral boundaries and the limitations imposed by image resolution, the separation of rock glacier systems is uncertain. Therefore, some rock glacier systems, particularly the smaller ones lacking pronounced features of lateral boundaries, may not be effectively separated.

Additionally, the "Retrieve" operation focused on areas where missing rock glaciers were observed near the polygons identified by the deep learning model. Consequently, some rock glaciers may have been missed without conducting an exhaustive examination of the entire study region.

### **2.6.2 Comparison with existing local inventories**

We compared the number of inventoried rock glaciers in our study with existing local inventories on the plateau, including Daxue Shan ([Ran and Liu, 2018](#); [Cai et al., 2021](#)), Nyainqêntanglha ([Reinosch et al., 2021](#); [Zhang et al., 2023](#); [Li et al., 2024](#)), Hunza Basin ([Hassan et al., 2021](#)), Gangdise Mountains ([Zhang et al., 2022](#)), West

Kunlun Shan ([Hu et al., 2023a](#)), and Qilian Mountains ([Hu et al., 2024](#)) as shown in Table [2.5](#). The number of inventoried rock glaciers in our study is generally comparable to those in Daxue Shan and Hunza Basin. However, our inventory has more rock glaciers than the inventories in Gangdise Mountains and West Kunlun Shan, and fewer rock glaciers than the inventories in Nyainqêntanglha and Qilian Mountains.

## CHAPTER 2. DISTRIBUTION

Table 2.5: Comparisons of the numbers of inventoried rock glaciers with existing local inventories.

Location	Reference of existing local inventory	Number of inventoried rock glaciers in previous inventory	Number of inventoried rock glaciers in this study
Daxue Shan	<a href="#">Ran and Liu (2018)</a>	295	256
Daxue Shan	<a href="#">Cai et al. (2021)</a>	344	256
Western Nyainqêntanglha Range	<a href="#">Reinosch et al. (2021)</a>	1,433	798
Hunza Basin	<a href="#">Hassan et al. (2021)</a>	616	647
Gangdise Mountains	<a href="#">Zhang et al. (2022)</a>	132	816
Western Kunlun Shan	<a href="#">Hu et al. (2023a)</a>	413	2,145
Nyainqêntanglha	<a href="#">Zhang et al. (2023)</a>	20,531	16,222
Guokalariju	<a href="#">Li et al. (2024)</a>	5,057	4,000
Qilian Mountains	<a href="#">Hu et al. (2024)</a>	1,530	1,047

These discrepancies can be explained by inherent sources of error within each dataset. As highlighted in the RGIK guidelines ([RGIK, 2023](#)), operator judgment in compiling rock glacier inventories can vary over time, leading to discrepancies between inventories created at different time periods. Even within the same time frame, differences in operator experience can result in significant variations in judgment ([Brardinoni et al., 2019](#)). For example, the delineation of the upper boundary of rock glaciers in rooting regions is challenging and can vary among different operators ([Brardinoni et al., 2019](#)). In the Hunza Basin, our delineated rock glaciers had lower upper boundaries compared to the results of [Hassan et al. \(2021\)](#). Additionally, small rock glaciers can be difficult to recognize due to the lack of distinct characteristics. In the Nyainqntanglha region, some small landforms were included as rock glaciers in the inventories of [Reinosch et al. \(2021\)](#) and [Li et al. \(2024\)](#) but were excluded from our inventory. Moreover, it is common in mountainous environments for several rock glacier units to merge into a complex system ([RGIK, 2023](#)). Some operators may delineate this system as a single polygon, while others may separate it into smaller polygons. This can be observed in the case of Daxue Shan, where some systems were delineated as single polygons in our inventory but were separated into smaller polygons in the inventories of [Ran and Liu \(2018\)](#) and [Cai et al. \(2021\)](#).

Another significant factor contributing to discrepancies in inventories is the use of different image sources. Images with varying types, resolutions, and qualities can greatly influence the inventory results. The use of InSAR images, for example, is beneficial for detecting actively moving rock glaciers but may have poor performance in identifying slowly moving or relict rock glaciers ([Liu et al., 2013](#); [Hu et al., 2023a](#)). Moreover, images with low resolution used in some of the previous inventories may not clearly reveal the morphological characteristics of rock glaciers, increasing the probability of missing identifications. In the Western Kunlun Shan region, our inventory compiled more rock glaciers by using Planet Basemaps images (4.77 m resolution) compared to [Hu et al. \(2023a\)](#), whose inventory was based on Sentinel-2 images (10 m resolution). Additionally, images with quality issues caused by clouds, snow, shadows, and image distortion can lead to missed identifications of rock glaciers. In some areas of Nyainqntanglha, for instance, some rock glaciers were obscured by clouds in Planet Basemaps images and were missed in our

inventory, but they were visible in Google Earth images and had been included in the inventories of [Reinosch et al. \(2021\)](#) and [Li et al. \(2024\)](#). Since the discrepancies between inventories can arise from various sources, conducting further quantitative comparisons on the accuracies of rock glacier locations and boundaries poses challenges.

### 2.6.3 Significance of the inventory and future work

To our knowledge, the creation of the new inventory on the Tibetan Plateau represents the most extensive collection of rock glaciers published worldwide. This large dataset offers exciting prospects for advancing various research areas related to rock glaciers, including permafrost distribution, mountain hydrology, climate impacts on the permafrost environment, and geohazards as introduced in Section 1.

First, our new inventory enables more accurate assessments of permafrost distribution, allowing researchers to refine existing permafrost maps and enhance our understanding of permafrost characteristics on the Tibetan Plateau ([Hu et al., 2024](#)). We underline that the lack of comprehensive rock glacier information on the plateau had previously limited permafrost assessment studies in this region. [Cao et al. \(2021\)](#) found that a model driven by rock glacier observations led to an overestimation of permafrost extent by about 8.4–13.1% on the Tibetan Plateau compared to a model using in situ measurements. Nevertheless, they used datasets from the Himalayan range as an alternative due to the limited availability of rock glacier observations on the plateau.

With respect to hydrology, [Jones et al. \(2018a\)](#) had estimated the global water contribution from rock glaciers and highlighted the lack of rock glacier data in certain regions, including the Tibetan Plateau. Our inventory fills the data gap in this critical region of High Mountain Asia, providing an opportunity to investigate the potential water storage available within rock glaciers ([Corte, 1976](#); [Azócar and Brenning, 2010](#); [Jones et al., 2019a](#); [Schaffer et al., 2019](#); [Wagner et al., 2020a, 2021](#)) and the contribution of rock glacier meltwater to streamflow ([Geiger et al., 2014](#); [Wagner et al., 2016](#)).

Moreover, our inventory serves as a guide for establishing rock glacier monitoring sites on the plateau, contributing to the study of the long-term evolution of rock glaciers and the impacts of climate change on mountain permafrost in this region.

Long-term monitoring of rock glacier velocities has been established in the European Alps ([PERMOS, 2024](#)), Northern Tien Shan ([Kääb et al., 2021](#)), and the Andes ([Vivero et al., 2021](#)), and the United States ([Kääb et al., 2024](#)). Currently no such monitoring sites exist on the Tibetan Plateau due to the lack of information on rock glacier distribution.

Lastly, the new inventory developed in this study will contribute to the evaluation of rock glacier hazards and risks, providing important information for geohazard management and enabling informed decision-making regarding infrastructure planning on the Tibetan Plateau ([Hassan et al., 2021](#); [Janke and Bolch, 2021](#)).

## 2.7 Conclusions

In this study, we proposed a deep learning-based approach for mapping rock glaciers and created the first plateau-wide inventory i.e., TPRoGI [v1.0], encompassing 44,273 rock glaciers. This inventory fills the gap in the rock glacier data on the Tibetan Plateau and provides a baseline dataset for monitoring mountain permafrost in this region.

Findings from the current study are summarized as follows:

- (1) the deep learning model demonstrates a promising capability in detecting and outlining rock glaciers and can serve as a valuable tool for inventorying rock glaciers across large regions;
- (2) rock glaciers are widespread in the northwestern and southeastern plateau and densely distributed in the Western Pamir and Nyainqêntanglha, while they are scarce in the inner plateau;
- (3) the majority of rock glaciers are situated at elevations from 4,000 to 5,500 m a.s.l. and on slopes between 10° and 25° with north and west preferences;
- (4) rock glaciers show a north-west preference in the eastern plateau, a north-only orientation in the central plateau, and no specific preference in the western plateau;
- (5) rock glaciers on the Tibetan Plateau cover a total area of 6,000 km<sup>2</sup> with a mean area of 0.14 km<sup>2</sup>, with rock glaciers in the western plateau exhibiting larger areas compared to those in other areas.

However, limitations inherent in imagery, deep learning model, and manual improvement introduce uncertainties in the current inventory. We expect that the

benchmark dataset produced by this study will facilitate the investigation into many scientific questions related to rock glaciers and mountain permafrost on the Tibetan Plateau.

# Chapter 3 Assessing rock glacier velocities on the Tibetan Plateau using InSAR

---

## Abstract

The kinematics of rock glaciers provide critical insights for permafrost studies, mountain hydrology, and hazard assessment. Previous studies have measured rock glacier velocities using field-based terrestrial geodetic surveys, repeat photogrammetry, and Interferometric Synthetic Aperture Radar (InSAR). However, these methods have typically been confined to local regions, leaving the large-scale velocity characteristics underexplored. In this study, we developed a multi-temporal and multi-geometry InSAR framework for large-scale rock glacier velocity assessment. Our approach facilitates systematic generation of rock glacier velocity fields by integrating interferograms from multiple acquisition dates and both ascending and descending orbits. To rigorously validate the method, we compared the InSAR-derived velocities with those derived from three independent datasets including very high-resolution optical imagery (Pléiades satellite and aerial imagery) and Global Navigation Satellite System (GNSS) measurements. The results demonstrate statistically significant correlations between our InSAR-based velocities and all comparison datasets, whereas our method tends to underestimate the magnitudes. The mean relative difference is approximately 20% when compared to velocities from Pléiades and aerial images, whereas increasing to 50% for GNSS point measurements. Applying our method to Sentinel-1 SAR images acquired between July and August 2022, we produced the first large-scale regional rock glacier velocity dataset, encompassing downslope velocity fields for 19,727 rock glaciers on the Tibetan Plateau. The median velocity of all assessed rock glaciers is 17 cm/yr. Notably, we found a striking velocity contrast between different climatic domains: rock glaciers in the westerlies domain move on average clearly faster (median = 30 cm/yr) than those in the monsoon domain (median = 13 cm/yr). This disparity is likely driven by differences in glacial influence and rock glacier sizes between the two domains. Our study presents a methodological framework for assessing rock glacier velocities using InSAR and demonstrates its capability for large-scale applications. This approach can be readily adapted to other regions

worldwide to support the assessment and monitoring of rock glacier dynamics in a changing climate.

### 3.1 Introduction

Rock glaciers are debris landforms resulting from the former or current gravity-driven creep of frozen ground ([RGIK, 2023](#)). Comprising a mixture of ice and debris, intact rock glaciers display a notable sensitivity to climate fluctuations ([Haeberli et al., 2006](#); [Janke and Bolch, 2021](#)). The movement of rock glaciers is a combination of shear processes and internal deformation ([Haeberli et al., 2006](#); [Wirz et al., 2016](#); [Cicoira et al., 2021](#)). The observed surface displacements are primarily attributed to permafrost creep within a layer referred to as the 'shear horizon', located at depths between 15 and 30 meters in alpine rock glaciers ([Arenson et al., 2002](#); [Haeberli et al., 2006](#); [Cicoira et al., 2021](#)).

Rock glacier kinematics can offer valuable insights into the ice content of rock glaciers and hence, their hydrological significance relative to glaciers ([Hartl et al., 2016](#); [Hu et al., 2023b](#)). They are also important for hazard assessment ([Janke and Bolch, 2021](#)) and permafrost distribution modeling ([Cao et al., 2021](#); [Li et al., 2024](#)) in high mountain regions. Long-term observations across various regions have shown that changes in rock glacier velocities can reveal the impacts of climate change on creeping mountain permafrost ([Kääb et al., 2021](#); [Kellerer-Pirklbauer et al., 2024](#); [Kääb and Røste, 2024](#)). Thus, Rock Glacier Velocity (RGV), defined as "a time series of annualized surface velocity values measured or computed on a rock glacier unit or a part of it", has been recognized as a new product associated with the Essential Climate Variable (ECV) Permafrost by the Global Climate Observing System (GCOS) ([RGIK, 2022b](#); [Hu et al., 2025](#)).

Field-based terrestrial geodetic surveys (TGS) have been conducted to measure rock glacier velocities using theodolite (e.g., [Wahrhaftig and Cox, 1959](#)) and repeat or continuous Global Navigation Satellite System (GNSS) (e.g., [Berthling et al., 1998](#); [Lambiel and Dylaloye, 2004](#); [Wirz et al., 2014](#); [Cicoira et al., 2022](#); [Kellerer-Pirklbauer et al., 2024](#)). These surveys provide precise 3D measurements of surface displacement on rock glaciers but are often limited to few individual rock glaciers with sparse sampling due to challenging field conditions in remote and harsh environments ([Cicoira et al., 2022](#)). Additionally, repeat photogrammetry has been

widely used to measure rock glacier velocities (e.g., [Kääb et al., 2021](#); [Robson et al., 2022](#); [Manchado et al., 2024](#); [Kääb and Røste, 2024](#); [Cusicanqui et al., 2024](#)), but these studies have also typically been conducted in small local areas or a limited number of selected rock glaciers.

Interferometric Synthetic Aperture Radar (InSAR) has proven effective in measuring rock glacier velocities at both local (e.g., [Delaloye et al., 2008](#); [Necsoiu et al., 2016](#); [Strozzi et al., 2020](#)) and regional scales (e.g., [Liu et al., 2013](#); [Kääb et al., 2021](#); [Reinosch et al., 2021](#)). According to the specific types of algorithms, various InSAR methods developed for mapping rock glacier velocities can be generally divided into three groups: (1) using wrapped interferograms (wrapped method in short), (2) using a single unwrapped interferogram (single unwrapped method in short), and (3) time-series methods. However, each of these methods has its own limitations when applied to large-scale assessments, as will be elaborated in the next section. Consequently, existing InSAR studies have predominantly focused on localized areas or individual mountain ranges. Furthermore, due to the scarcity of in-situ rock glacier velocity measurements, comprehensive validation of InSAR-derived velocities remains very limited. As a result, the accuracy and reliability of rock glacier velocity products derived from InSAR have not yet been adequately evaluated.

Currently, there is no method for systematically assessing rock glacier velocities across large regions. The large-scale velocity characteristics, particularly in large regions such as High Mountain Asia (HMA), remain poorly quantified and understood. Leveraging deep learning techniques and high-resolution satellite optical imagery, [Sun et al. \(2024\)](#) have identified more than 40,000 rock glaciers on the Tibetan Plateau. While previous studies have utilized InSAR to evaluate rock glacier velocities in localized areas of southeastern Tibet ([Reinosch et al., 2021](#); [Cai et al., 2021, 2024](#); [Zhang et al., 2023](#)), the kinematic status of rock glaciers in other regions remains largely unknown.

In this study, we developed a multi-temporal and multi-geometry InSAR approach for systematic generation of rock glacier velocity fields. To rigorously validate our method, we compared the InSAR-derived results with independent velocity datasets derived from high-resolution satellite and aerial imagery, as well as GNSS measurements, across various regions. By applying this approach to a plateau-wide rock glacier inventory, we successfully generated downslope velocity fields for

almost 20,000 rock glaciers larger than 0.1 km<sup>2</sup> across the Tibetan Plateau region. This study represents the first of its kind that reveals the regional-scale spatial characteristics of rock glacier velocities over an area exceeding 10<sup>6</sup> km<sup>2</sup>.

## 3.2 InSAR methods for rock glacier velocity assessment

### 3.2.1 Wrapped method

Rock glacier velocities can be estimated by manually interpreting wrapped interferograms ([Barboux et al., 2014](#); [Kääb et al., 2021](#)). This method involves the visual analysis of wrapped interferograms from a large InSAR dataset, generated using various satellite data over different time intervals, to identify moving areas associated with rock glaciers and estimate their displacement rates ([Barboux et al., 2014](#)). Building on this approach, the International Permafrost Association (IPA) Rock Glacier Inventory and Kinematics (RGIK) initiative standardized a strategy for classifying rock glacier movement rates through manual interpretation of wrapped interferograms ([RGIK, 2022a](#)). [Bertone et al. \(2022\)](#) has successfully applied this method to incorporate InSAR kinematics into over 3,600 rock glaciers across 11 regions worldwide. Through comprehensive analysis of multiple wrapped interferograms from diverse sources, this method provides robust classification of rock glacier velocities. However, it requires substantial manual effort, making it impractical for assessing velocities across large quantities (e.g., tens of thousands) of rock glaciers in extensive regions. Additionally, this method can only provide velocity classes and cannot derive specific velocity values, limiting its utility for generating quantitative RGV products.

### 3.2.2 Single unwrapped method

[Liu et al. \(2013\)](#) employed unwrapped interferograms to calculate the line-of-sight (LOS) velocity from a single interferometric pair, which is then projected into the surface-parallel direction to estimate the downslope creep rates of rock glaciers. This method has been successfully applied to map rock glaciers and estimate their downslope velocities in individual mountain ranges or basins in parts of HMA ([Wang et al., 2017](#); [Hu et al., 2023a](#); [Hassan et al., 2024](#)). This method allows direct calculation of downslope velocities from interferograms and demands less manual effort compared to the wrapped method. However, using single interferograms introduces challenges from unfavorable viewing geometries, atmospheric errors, and

phase decorrelation.

### 3.2.3 Time-series methods

Time-series InSAR is widely used because it effectively mitigates errors caused by atmospheric effects and decorrelation. Among time-series algorithms, the Small Baseline Subset (SBAS) approach is the most commonly used for rock glacier studies (e.g., [Necsoiu et al., 2016](#); [Cai et al., 2021, 2024](#); [Reinosch et al., 2021](#); [Zhang et al., 2021, 2023](#)). SBAS selects SAR image pairs with small spatial and temporal baselines, making it particularly suitable for detecting slow deformation. However, the velocities of active rock glaciers typically range from centimeters to meters per year ([Hu et al., 2025](#)). When SBAS incorporates interferograms with longer temporal baselines, unwrapping errors become more severe, leading to underestimated velocities ([Fan et al., 2025](#)). Some studies used Persistent Scatterer Interferometry (PSI) to measure rock glacier velocities (e.g., [Barboux et al., 2015](#); [Guerrero et al., 2025](#)). But this method relies on highly coherent scatterers, making it effective for very slow deformation but often unsuitable for active rock glaciers due to severe decorrelation in long-time-span interferograms. Stacking methods were also commonly used to measure rock glacier velocities (e.g., [Brencher et al., 2021](#); [Rouyet et al., 2021](#); [Buchelt et al., 2023](#)). However, conventional stacking typically uses interferograms from a single orbital geometry (e.g., ascending or descending), thus averaging LOS measurements in the same 1D directions.

## 3.3 Study area

The Tibetan Plateau forms an expansive high-elevation zone in Asia, with an average elevation exceeding 4,000 meters above sea level ([Bolch et al., 2019b](#)). It encompasses 13 subregions of HMA, as defined by [Bolch et al. \(2019b\)](#), along with the Qaidam Basin (Figure 3.1). This region hosts 105,427 glaciers, with the majority concentrated in the Pamir, Karakoram, and Nyainqêntanglha ([RGI Consortium, 2023](#)). Permafrost covers approximately 60% ( $1.5 \times 10^6$  km $^2$ ) of the total area ([Obu et al., 2018](#)), and 44,273 rock glaciers have been identified and outlined in this region ([Sun et al., 2024](#)).

Climatically, this region experiences a complex continental system shaped by the interplay of the Indian monsoon, East Asian monsoon, and westerlies ([Yao et al., 2012](#)), creating a distinct southeastern-northwestern climatic contrast ([Yao et al.,](#)

[2013](#)). The southeastern part is influenced by the Indian and East Asian monsoons, which bring warm, moist air and substantial summer rainfall, while the northwestern part is dominated by the westerlies, which bring cold, dry air and minimal precipitation ([Yao et al., 2013](#)). [Huang et al. \(2023\)](#) demonstrated that the 300 mm precipitation isoline from May to September can serve as an indicator of the northern boundary of the Asian summer monsoon. Based on the interannual variability of this boundary, they divided the Tibetan Plateau region into domains of westerlies, monsoon, and westerlies-monsoon transition (Figure [3.1](#)).

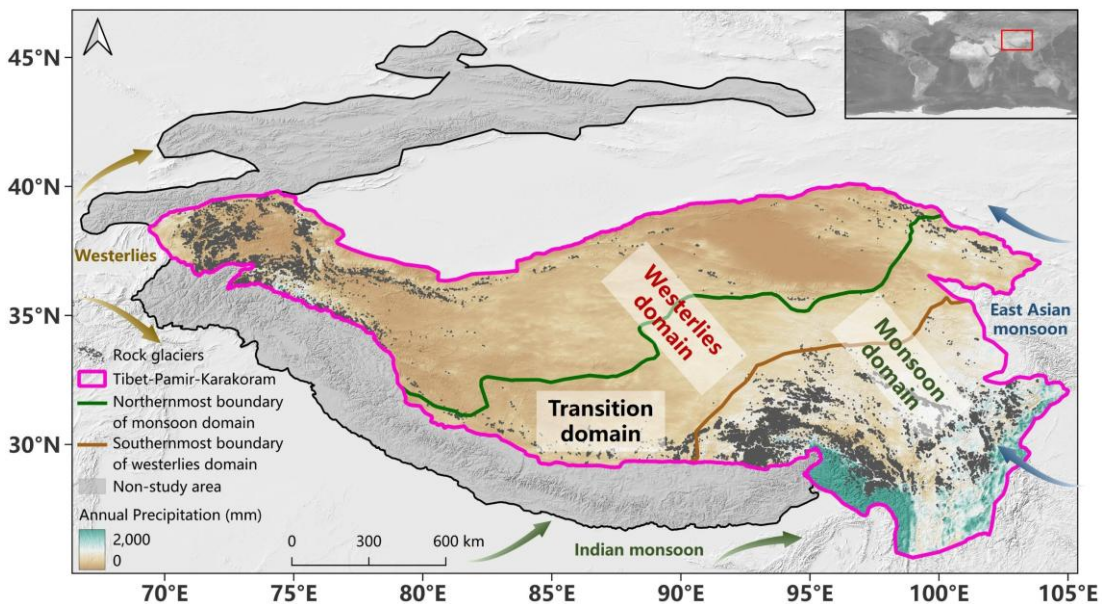


Figure 3.1: The locations of rock glaciers, mapped in the TPRoGI by [Sun et al. \(2024\)](#), on the Tibetan Plateau. The northernmost boundary of monsoon domain and the southernmost boundary of westerlies domain are from [Huang et al. \(2023\)](#). Also shown are mean annual precipitation from 1979 to 2020 obtained from [Jiang et al. \(2023\)](#).

## 3.4 Methods and materials

### 3.4.1 Assessing rock glacier velocities using multi-temporal and multi-geometry InSAR

We developed a multi-temporal and multi-geometry InSAR approach for assessing rock glacier velocities (Figure [3.2](#)). Our approach begins with the generation of unwrapped interferograms and associated products using the Alaska Satellite Facility Hybrid Pluggable Processing Pipeline (ASF HyP3) service ([Hogenson et al., 2020](#)). C-band Sentinel-1 SAR images were configured as interferometric pairs with a

temporal baseline of 12 days. We applied a multi-looking of  $10 \times 2$  and set the strength of the Goldstein-Werner adaptive phase filter as 0.3 to mitigate noise while preserving local-scale deformation signals on rock glaciers ([Goldstein and Werner, 1998](#)). HyP3 uses the 30-m-resolution Copernicus GLO-30 Digital Elevation Model (DEM) ([European Space Agency, 2024](#)) to remove topographic phases.

We developed a method to automatically remove locally uniform atmospheric errors over rock glaciers. Atmospheric errors are recognized as one of the primary sources of errors in rock glacier velocity measurements derived from InSAR ([Liu et al., 2013](#)). While datasets from global weather models such as ERA5 ([Hersbach et al., 2020](#)) and the Generic Atmospheric Correction Online Service (GACOS) ([Yu et al., 2018a](#)) are commonly employed to mitigate these errors, their efficacy in mountainous regions remains limited. Products from ERA5 often exhibit biases or artifacts in alpine environments ([Cao et al., 2020; Huang et al., 2022; Li et al., 2022](#)), compounded by a coarse spatial resolution ( $0.1^\circ$ , ~10 km) that may inadequately resolve atmospheric variability in highly variable terrain. The performance of GACOS depends on the density of GNSS stations ([Yu et al., 2018b](#)), which are however, usually very sparse in mountainous regions. Previous studies have mitigated the impact of spatially long-wavelength atmospheric artifacts in rugged terrain by selecting a stable reference point and using its phase to adjust for these errors ([Liu et al., 2013; Wang et al., 2017; Reinosch et al., 2021; Hu et al., 2023a](#)). However, manually identifying suitable reference points for rock glaciers across large areas is labor-intensive. We utilized InSAR coherence maps to automatically identify stable reference pixels. We set a 10-pixel (~400 meters) buffer zone around each rock glacier, which is sufficiently small compared to the spatial scales of atmospheric conditions and thus the atmospheric delays can be approximated as the same as the rock glaciers. Within this buffer zone, we selected the pixels with coherence values exceeding 0.5 and the 75th percentile values of all the pixels. The mean phase values of the selected stable pixels were subtracted from the unwrapped phases to correct for atmospheric errors.

We used the phases after atmosphere error correction to determine the surface downslope velocities of rock glaciers. We first calculated surface deformations from the corrected phases using radar wavelength. Dividing the deformations by time interval gives the line-of-sight (LOS) velocities  $V_{\text{LOS}}$ , which were projected onto a

surface-parallel (downslope) direction to obtain rock glacier downslope velocities  $V_{\text{RoG}}$  ([Liu et al., 2013](#)):

$$V_{\text{RoG}} = \frac{V_{\text{LOS}}}{\beta} \quad (3.1)$$

where  $\beta$  indicates the geometry conversion factor, which can be calculated using the heading and incidence angles of the radar satellite as well as the aspect and slope angles of rock glaciers:

$$\beta = \sin(\alpha - \varphi) \sin \theta_{\text{inc}} \cos \theta_{\text{slp}} + \cos \theta_{\text{inc}} \sin \theta_{\text{slp}} \quad (3.2)$$

where  $\varphi$  is the heading of the satellite flight path,  $\theta_{\text{inc}}$  is the radar's incidence angle, and  $\alpha$  and  $\theta_{\text{slp}}$  are the mean aspect and median slope angles of a rock glacier extracted from the Copernicus DEM. The computation was performed at the pixel level, producing one downslope velocity field per rock glacier from a single interferogram.

To ensure high data quality, we performed quality control on the derived downslope velocity fields. Due to constraints in viewing geometry, quantifying the kinematics of rock glaciers moving close to parallel satellite flight direction can introduce significant uncertainty ([Liu et al., 2013](#); [RGIK, 2022a](#)). In such cases, the geometry conversion factor can be exceedingly small, resulting in an unreasonably high estimate of downslope velocity. To mitigate this issue, we only calculated the downslope velocities for rock glaciers where  $|\beta|$  exceeds 0.2 ([RGIK, 2022a](#)). Furthermore, the quantification of velocity can be highly uncertain in cases of low coherence and poor viewing geometry arising from shadow and layover effects that may result in a negative downslope velocity ([Liu et al., 2013](#)). We only selected valid pixels exhibiting a positive downslope velocity and a coherence value greater than 0.3.

Finally, we aggregated the downslope velocity fields derived from multi-temporal and multi-geometry interferograms. The downslope velocity fields derived from individual interferometric pairs often display noticeable gaps after filtering out invalid pixels. Furthermore, relying solely on a single geometry from either an ascending or descending orbit can result in many unsuccessful assessments due to unfavorable geometric conditions ([Eriksen et al., 2017](#); [Cai et al., 2024](#)). To overcome this challenge, we utilized multiple pairs with diverse geometries, frames,

and acquisition dates. The results were aggregated by computing the mean velocity at each pixel from various downslope velocity fields obtained from different pairs. The pixels were resampled and aligned to the Copernicus DEM before aggregation, and we finally generated a 30-m-resolution downslope velocity field for each rock glacier.

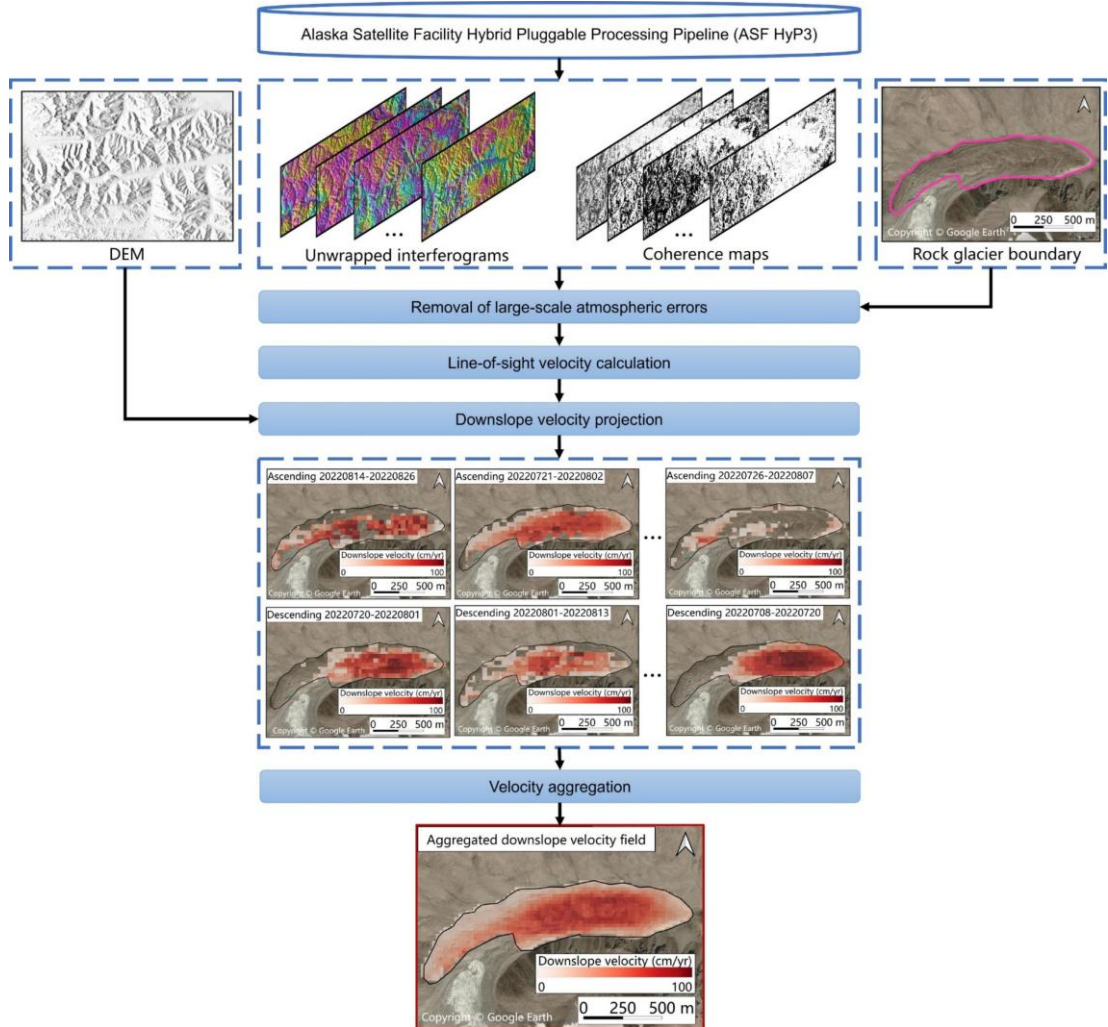


Figure 3.2: Workflow of the InSAR approach for assessing rock glacier velocities using multi-temporal and multi-geometry interferograms.

For the Tibetan Plateau region, we used a total of 153 Sentinel-1 SAR frames in Interferometric Wide mode, consisting of 77 in ascending orbits and 76 in descending orbits, to provide comprehensive coverage of nearly all the rock glaciers compiled in TPRoGI (Figure 3.3). Given our objective to reveal large-scale rock glacier velocity patterns, we selected a two-month period, i.e., July to August, which was sufficient to produce spatially complete velocity fields. We chose these two

snow-free summer months to ensure high coherence ([Delaloye et al., 2008](#); [Strozzi et al., 2020](#)). After reviewing data availability across different years, we found that 2022 has the most data available.

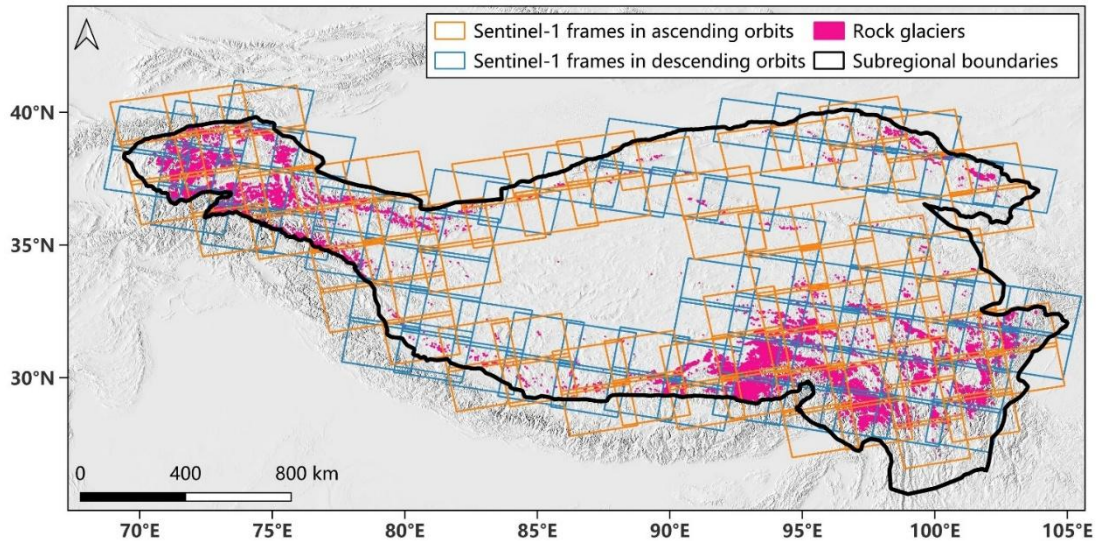


Figure 3.3: Distribution of rock glaciers presented in TPRoGI [v1.0] and Sentinel-1 frames in ascending and descending orbits.

For comparative validation, we additionally selected four frames in the Northern Tien Shan (two ascending and two descending; July–August 2022; Figure 3.4) to compare with the results derived from very-high-resolution Pléiades satellite imagery by [Wood et al. \(2025\)](#), 19 SAR frames in the U.S. (eight ascending and 11 descending; July–August 2020; Figure 3.5) to compare with the results derived from aerial imagery by [Kääb and Røste \(2024\)](#), and seven frames in the Swiss Alps (three ascending and four descending; July–August 2022; Figure 3.6) to compare with the GNSS-derived results provided by Swiss Permafrost Monitoring Network (PERMOS) ([PERMOS, 2024](#)).

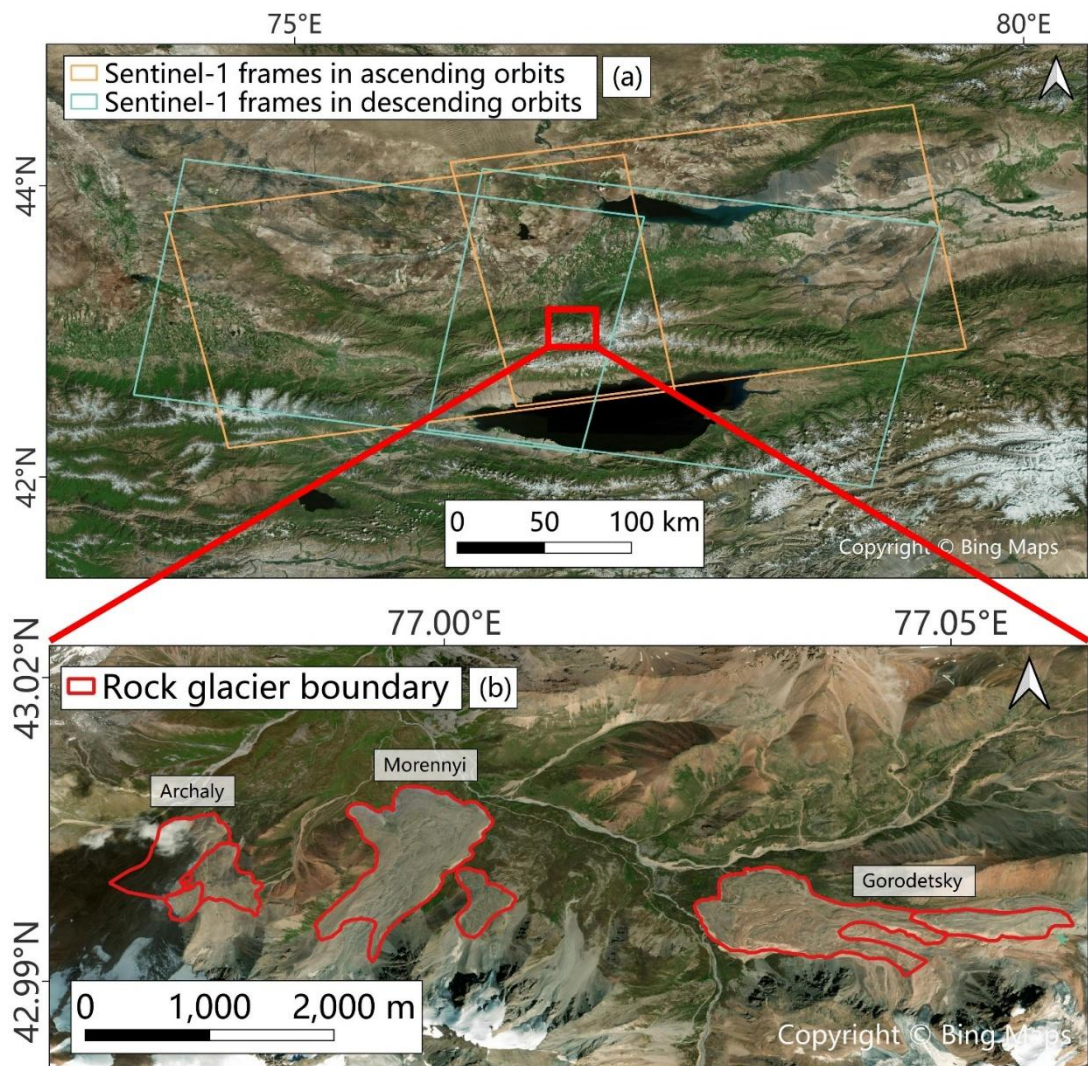
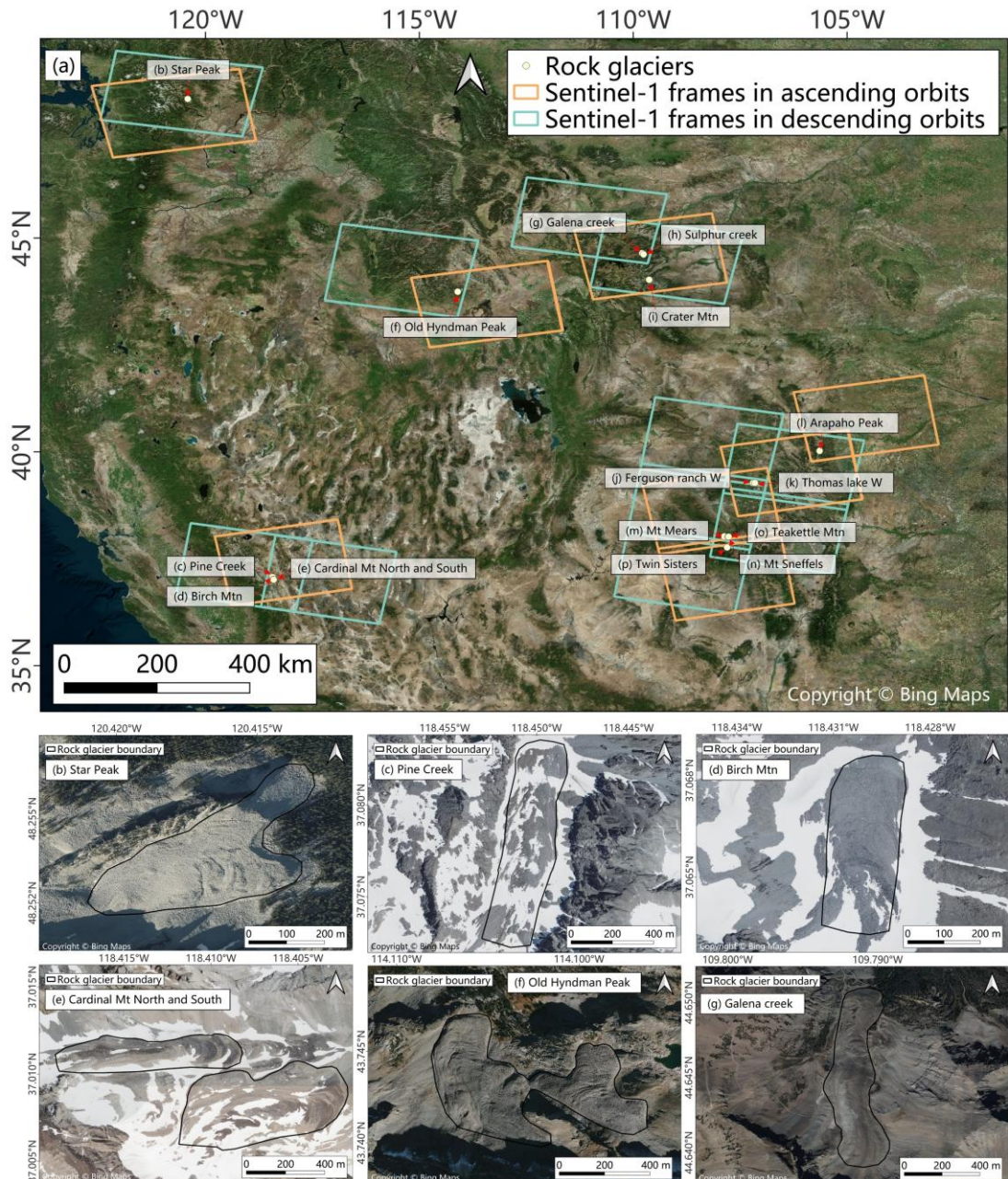


Figure 3.4: Sentinel-1 frames in ascending and descending orbits in the Northern Tien Shan.  
(b) Enlarged view of the studied rock glaciers. The basemap is from Bing Maps.



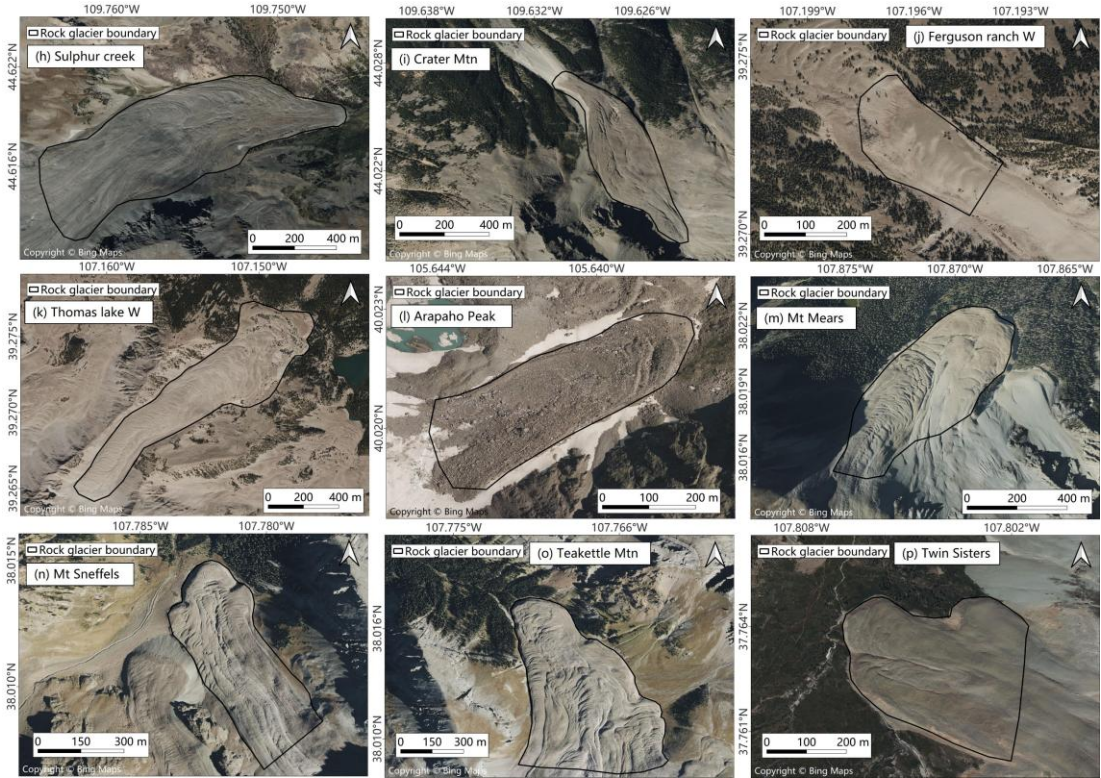


Figure 3.5: (a) Distribution of 16 rock glaciers studied by Kääb and Røste (2024) and Sentinel-1 frames in ascending and descending orbits in the United States. Enlarged views of the rock glaciers: (b) Star Peak, (c) Pine Creek, (d) Birch Min, (e) Cardinal Mt North and South, (f) Old Hyndman Peak, (g) Galena creek, (h) Sulphur creek, (i) Cater Mtn, (j) Ferguson ranch W, (k) Thomas lake W, (l) Arapaho Peak, (m) Mt Mears, (n) Mt Sneffels, (o) Teakettle Mtn, (p) Twin Sisters. The basemap is Bing Maps.

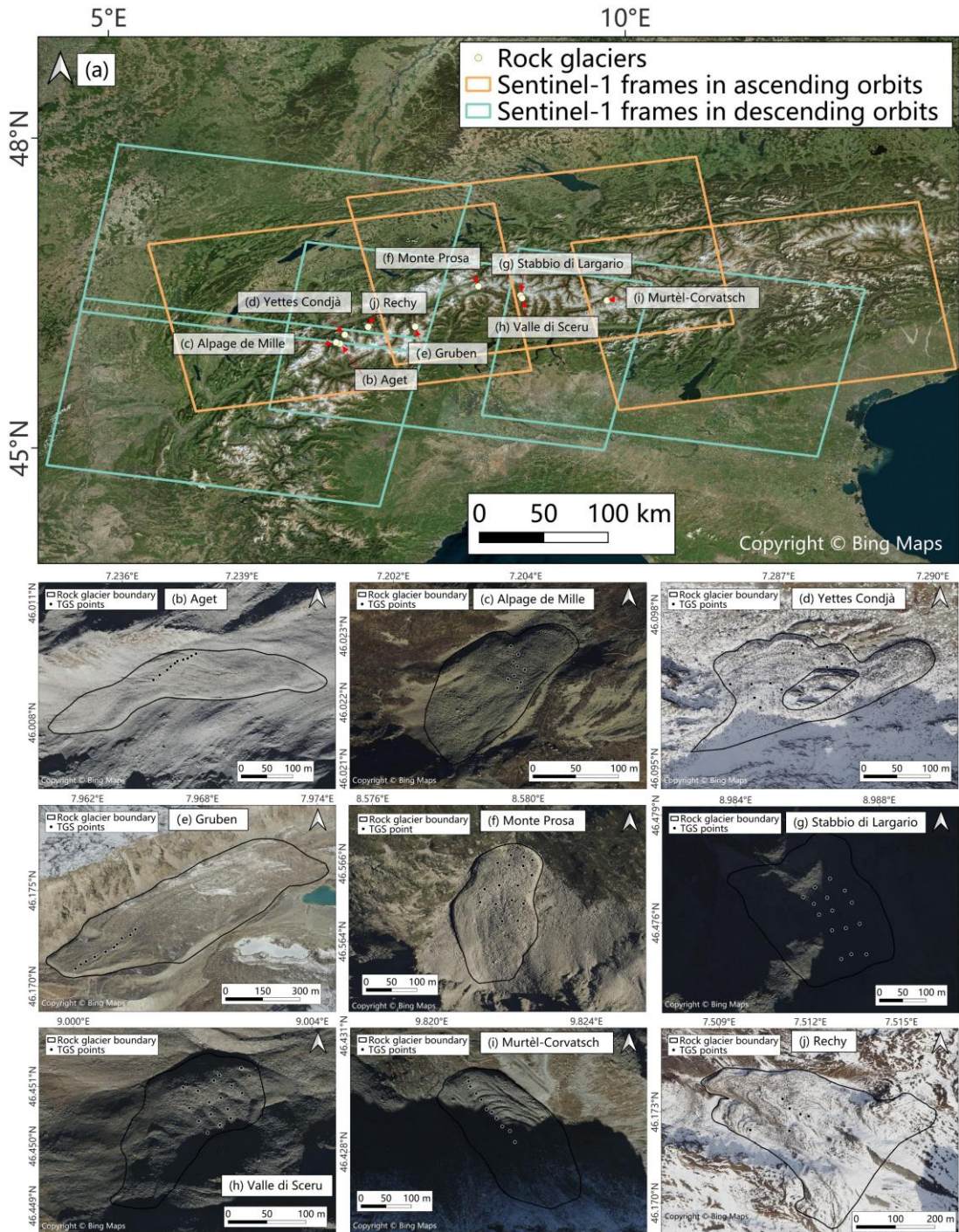


Figure 3.6: (a) Distribution of nine rock glaciers and Sentinel-1 frames in ascending and descending orbits in the Swiss Alps. Enlarged views of the rock glaciers: (b) Aget, (c) Alpage de Mille, (d) Yettes Condjà, (e) Gruben, (f) Monte Prosa, (g) Stabbio di Largario, (h) Valle di Sceru, (i) Murtèl-Corvatsch, (j) Rechy. The basemap is Bing Maps.

### 3.4.2 Comparing InSAR-derived velocities with other velocity datasets

To validate our method and demonstrate its transferability, we compared our InSAR-derived velocities with three independent velocity datasets derived from very-high-resolution optical images (Pléiades satellite images, aerial images) and in-situ GNSS measurements across diverse geographical regions worldwide. We compared our results with velocity data from aerial imagery in the U.S. and GNSS measurements in the Swiss Alps, as no similarly high-quality rock glacier velocity data exist for High Mountain Asia.

We used Pléiades satellite images (0.5 m resolution) acquired on June 20, 2013 and September 5, 2019 in the Muztagh Ata (Eastern Pamir), on September 5, 2019 and September 27, 2022 in the western Nyainqêntanglha (Southeastern Tibet), and on August 27, 2016 and September 16, 2020 in the central Ile Alatau (Northern Tien Shan). These images were orthorectified within an earlier study assessing glacier changes by [Bhattacharya et al. \(2021\)](#). The velocities were derived through a feature tracking method (cf. [Wood et al., 2025](#)). We compared the velocities of three rock glaciers in the Muztagh Ata, three in the western Nyainqêntanglha, and seven in the central Ile Alatau. The velocities for the rock glaciers in the Muztagh Ata and western Nyainqêntanglha were derived in this study, and the velocities for those in the central Ile Alatau were obtained from a previous study by [Wood et al. \(2025\)](#). When comparing the velocity magnitudes, we used the 75th percentile pixel values from the InSAR- and feature tracking-derived velocity fields.

We utilized the most recent velocities of 16 rock glaciers in the U.S. provided by [Kääb and Røste \(2024\)](#) (Figure 3.5) to validate our method. These velocities were derived by applying digital image matching ([Kääb and Vollmer, 2000](#); [Heid and Kääb, 2012](#)) between pairs of high-resolution orthorectified aerial images from the U.S. Geological Survey.

Additionally, we collected GNSS-measured velocities between 2021 and 2022 from nine Swiss Alpine rock glaciers (Figure 3.6) provided by [PERMOS \(2024\)](#) to validate our approach. The datasets were compiled through surface velocity measurements at TGS points, recording annual differences in the east, north, and up directions ( $E_{\text{diff}}$ ,  $N_{\text{diff}}$ ,  $U_{\text{diff}}$ ) ([PERMOS, 2024](#); Table 3.1), which were converted to annual downslope velocities  $V_{\text{TGS}}$ :

$$V_{\text{TGS}} = \sin \alpha \cos \theta_{\text{slp}} E_{\text{diff}} + \cos \alpha \cos \theta_{\text{slp}} N_{\text{diff}} - \sin \theta_{\text{slp}} U_{\text{diff}} \quad (3.3)$$

Other rock glaciers monitored by PERMOS were excluded from the analysis as their velocities are higher than 100 cm/yr, which exceed the detection capability of InSAR. For each rock glacier, we obtained the GNSS measurements at reference points due to their higher quality than those at survey points. To compare with GNSS-derived velocities provide by [PERMOS \(2024\)](#), we first sampled the pixel values from the InSAR-derived velocity fields at each TGS point. For each rock glacier, we calculated the GNSS- and InSAR-derived mean velocity and standard deviation using the GNSS-measured and sampled InSAR-derived velocities at all the TGS points, respectively.

Table 3.1: Information of nine rock glaciers and terrestrial survey point (TGS) points in Swiss Alps.

Rock glacier	TGS site	Latitude	Longitude	Number of TGS points	TGS point
Aget	AGE	46.009774°N	7.240549°E	10	AGE_121, AGE_122, AGE_123, AGE_124, AGE_125, AGE_126, AGE_127, AGE_128, AGE_129, AGE_130
Murtèl-Corvatsch	COR	46.428387°N	9.822111°E	10	COR_018, COR_019, COR_020, COR_021, COR_022, COR_023, COR_024, COR_025, COR_026, COR_027
Gruben	GRU	46.173987°N	7.967232°E	10	GRU_030, GRU_031, GRU_032, GRU_033, GRU_034, GRU_035, GRU_036, GRU_037, GRU_038, GRU_039
Stabbio di Largario	LAR	46.476326°N	8.986290°E	15	LAR_007, LAR_008, LAR_009, LAR_010, LAR_011, LAR_012, LAR_015, LAR_016, LAR_017, LAR_020, LAR_021, LAR_022, LAR_024, LAR_025, LAR_026
Alpage de Mille	MIL	46.022178°N	7.203342°E	9	MIL_010, MIL_011, MIL_017, MIL_018, MIL_019, MIL_026, MIL_027, MIL_030, MIL_031
Rechy	REC	46.172379°N	7.723988°E	6	REC_0165, REC_0192, REC_0205, REC_0325, REC_0343, REC_0344
Valle di Sceru	SCE	46.450392°N	9.001874°E	17	SCE_001, SCE_002, SCE_006, SCE_007, SCE_008, SCE_009, SCE_010, SCE_011, SCE_012, SCE_013, SCE_014, SCE_015, SCE_016, SCE_017, SCE_017, SCE_019, SCE_220
Monte Prosa	MPR	46.564521°N	8.579329°E	16	MPR_A008, MPR_A010, MPR_A013, MPR_A014, MPR_A015, MPR_A016, MPR_A020, MPR_A021, MPR_A022, MPR_A024, MPR_A025, MPR_A026, MPR_A027, MPR_A030, MPR_A031, MPR_A032
Yettes Condjà	YET	46.096435°N	7.287290°E	11	YET_011, YET_053, YET_054, YET_055, YET_057, YET_058, YET_100, YET_101, YET_102, YET_013, YET_104

### 3.4.3 Assessing rock glacier velocities on the Tibetan Plateau

To evaluate the capability of our method for large-scale assessment, we applied it to TPRoGI [v1.0], a plateau-wide inventory covering our study region. This inventory includes 44,273 rock glaciers identified and outlined using a deep learning approach with manual postprocessing ([Sun et al., 2024](#); Figure 3.1). Given that InSAR performance may degrade on smaller rock glaciers due to aliasing effects caused by sparse pixel coverage, we restricted our analysis to rock glaciers with areas exceeding 0.1 km<sup>2</sup>. Consequently, we selected 19,940 rock glaciers and generated their downslope velocity fields. However, some velocity fields exhibited significant gaps, prompting us to further filter the dataset to include only those rock glaciers with valid pixel coverage exceeding 30%.

To represent active areas, we used the 75th percentile pixel values from the downslope velocity fields as the representative for each rock glacier by following the practices of [Zhang et al. \(2021\)](#) and [Brencher et al. \(2021\)](#). For large-scale spatial pattern analysis, we calculated mean velocities within 50 km × 50 km grid cells based on the velocities of individual rock glaciers. To examine latitudinal and longitudinal trends, we computed mean velocities and standard deviations in 50 km bins along these directions. Additionally, to explore the relationships between rock glacier velocities and environmental factors, we generated box plots to analyze velocity distributions across ranges of areas, minimum elevations, and slopes. These environmental attributes are from TPRoGI.

## 3.5 Results

### 3.5.1 Comparison with other velocity datasets

#### 3.5.1.1 Comparison with velocities derived from Pléiades imagery in Muztagh Ata, western Nyainqêntanglha, and central Ile Alatau

Figure 3.7 shows the rock glacier velocity field examples derived from Pléiades imagery and InSAR. The velocity fields derived from both methods exhibit similar spatial patterns at all the three local regions. The InSAR and feature tracking methods consistently capture the active areas on the rock glaciers. They also successfully distinguish the rock glaciers with different activities. However, for Morennyi\_RGU1, the method only detects flow in the northeastern direction but fails to capture the northern flow and the rapid movement on the ‘thumb’ lobe. This is

attributed to the inherent constraints of InSAR, which lacks the sensitivity to detect deformation parallel to the flight direction ([Liu et al., 2013](#)) and often encounters phase unwrapping issues when measuring very fast movements ([Fan et al., 2025](#)).

The velocity magnitudes exhibit a statistically significant positive correlation (slope =  $0.8 \pm 0.1$ ,  $R^2 = 0.88$ ,  $p < 0.01$ , Fig. 4a), indicating a consistent order of magnitude. However, our method tends to underestimate the magnitudes for fast-moving rock glaciers. The InSAR-derived velocities are on average 21% smaller than those derived from Pléiades images, with a mean absolute difference of 13 cm/yr.

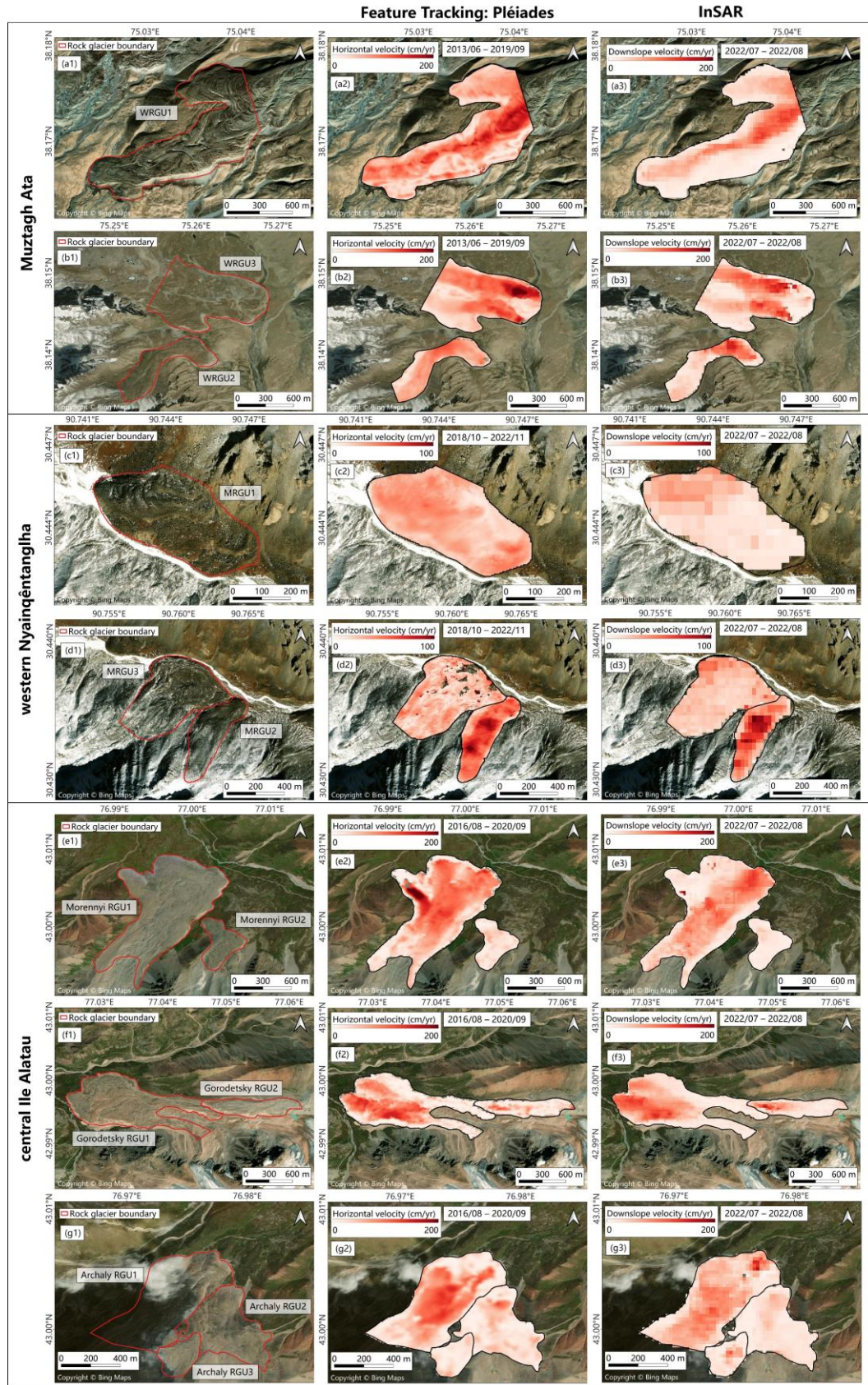


Figure 3.7: Rock glacier boundaries (first column) and velocity fields derived from Pléiades imagery (second column) and InSAR (third column) in the Muztagh Ata, western Nyainqêntanglha, and central Ile Alatau. The background images are from Bing Maps.

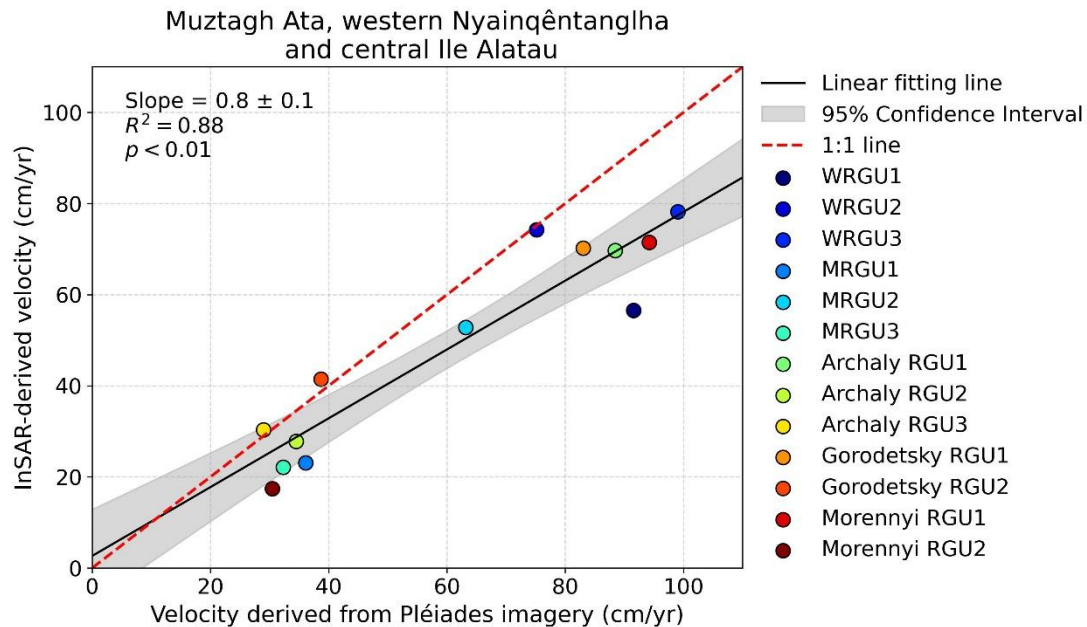


Figure 3.8: Scatter plot between the 75th percentile pixel values from the velocity fields derived from Pléiades imagery and InSAR for the rock glaciers in the Muztagh Ata, western Nyainqêntanglha, and central Ile Alatau

### 3.5.1.2 Comparison with velocities derived from aerial imagery in the western U.S.

The rock glacier velocities derived from our InSAR approach show a consistent order of magnitude with those reported by [Käab and Røste \(2024\)](#), as evidenced by a statistically significant positive correlation (slope =  $0.8 \pm 0.1$ ;  $R^2 = 0.70$ ,  $p < 0.01$ ; Figure 3.9). Half of the rock glaciers exhibit relative differences less than 20%, and seven rock glaciers show relative differences ranging between 20% and 40%. Only one rock glacier (Surphur Creek) displays a relative difference exceeding 50%. On average, the mean relative velocity difference is 23%, with a mean absolute difference of 12 cm/yr. The velocity fields obtained from our InSAR method are illustrated in Figure 3.10.

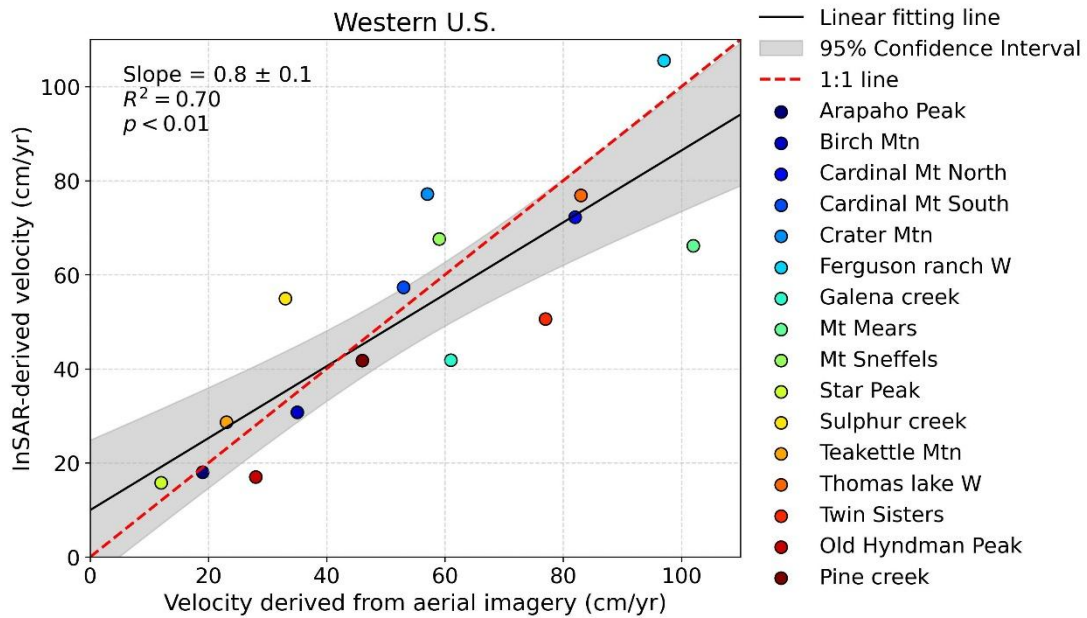


Figure 3.9: Scatter plot between the 75th percentile pixel values from the InSAR-derived velocity fields and the velocities derived from aerial imagery by [Kääb and Røste \(2024\)](#).

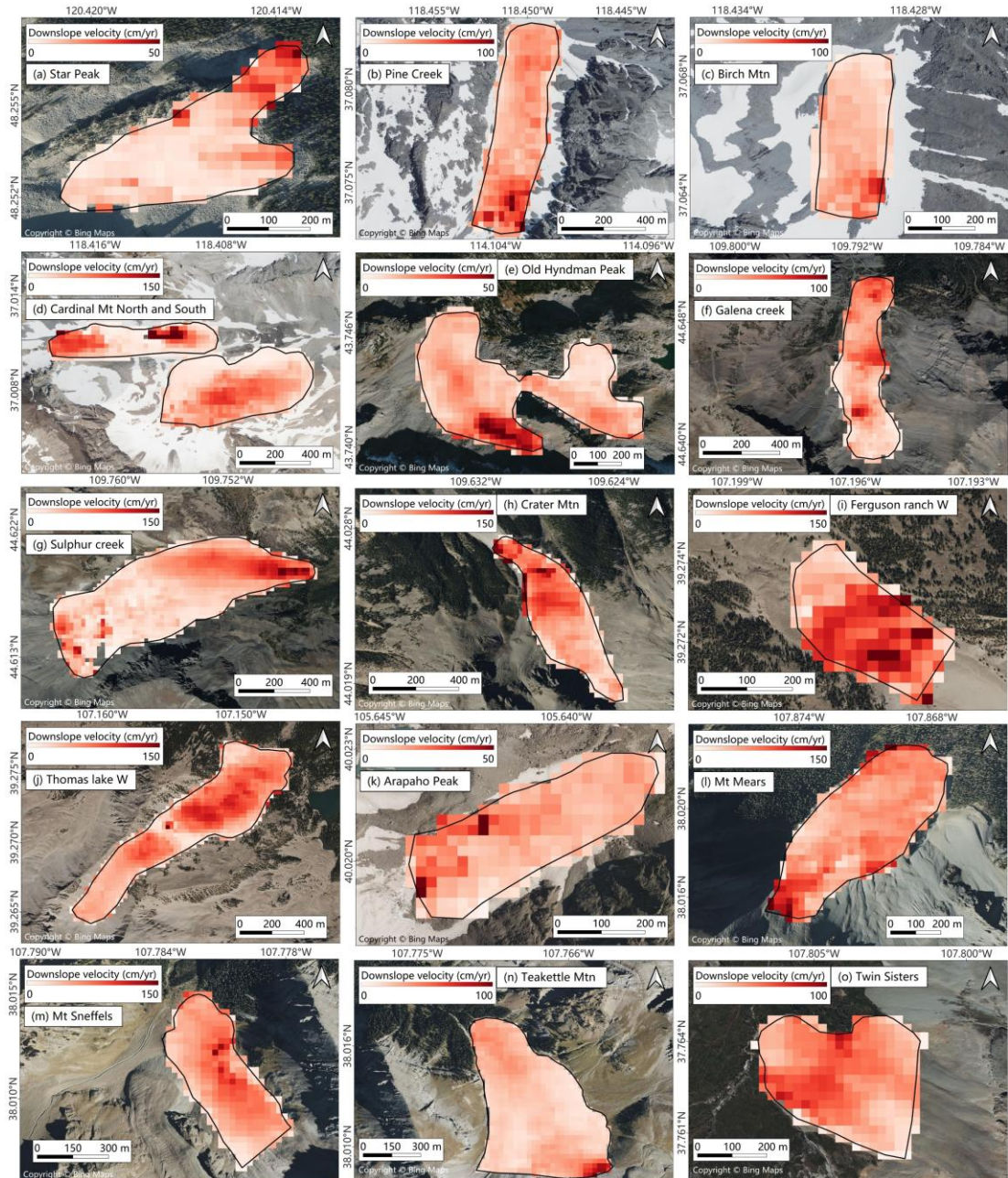


Figure 3.10: InSAR-derived velocity fields for the rock glaciers in the United States: (a) Star Peak, (b) Pine Creek, (c) Birch Min, (d) Cardinal Mt North and South, (e) Old Hyndman Peak, (f) Galena creek, (g) Sulphur creek, (h) Cater Mtn, (i) Ferguson ranch W, (j) Thomas lake W, (k) Arapaho Peak, (l) Mt Mears, (m) Mt Sneffels, (n) Teakettle Mtn, (o) Twin Sisters. The basemap is from Bing Maps.

### 3.5.1.3 Comparison with GNSS-derived velocities in the Swiss Alps

We observed weak agreement between our InSAR-derived velocities and GNSS measurements for rock glaciers in the Swiss Alps. Although velocities from both methods exhibit a consistent order of magnitude (statistically significant positive correlation: slope =  $0.4 \pm 0.1$ ;  $R^2 = 0.86$ ,  $p < 0.01$ ; Figure 3.11), our InSAR-derived velocities show significant underestimation for most rock glaciers, except for Murtèl-Corvatsch, which displays notable overestimation. Only two rock glaciers (Aget and Alpage de Mille) have relative differences below 20%, while the others exceed 50%. The average relative difference is 50%, with a mean absolute difference of 22 cm/yr. The InSAR-derived velocity fields and TGS point locations are illustrated in Figure 3.12.

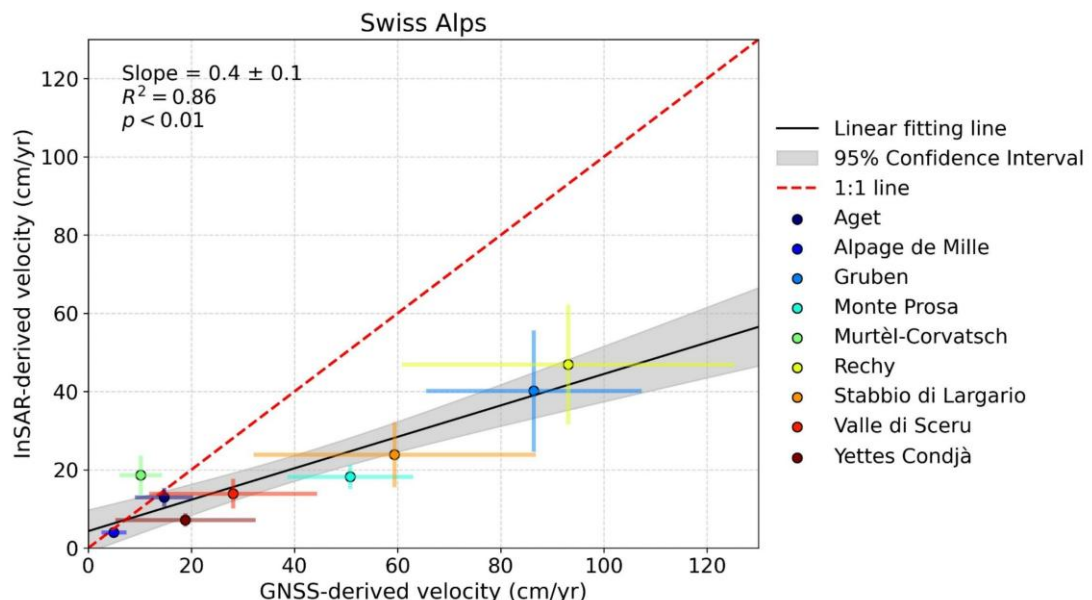


Figure 3.11: Scatter plot between the mean velocities of InSAR-derived pixel velocities and GNSS-measured point velocities. The uncertainty represents the standard deviation. The uncertainty bars in (c) indicate standard deviations derived from GNSS-measured and sampled InSAR-derived velocities at all the TGS points. The uncertainty bars in (c) indicate standard deviations derived from GNSS-measured and sampled InSAR-derived velocities at all the TGS points.

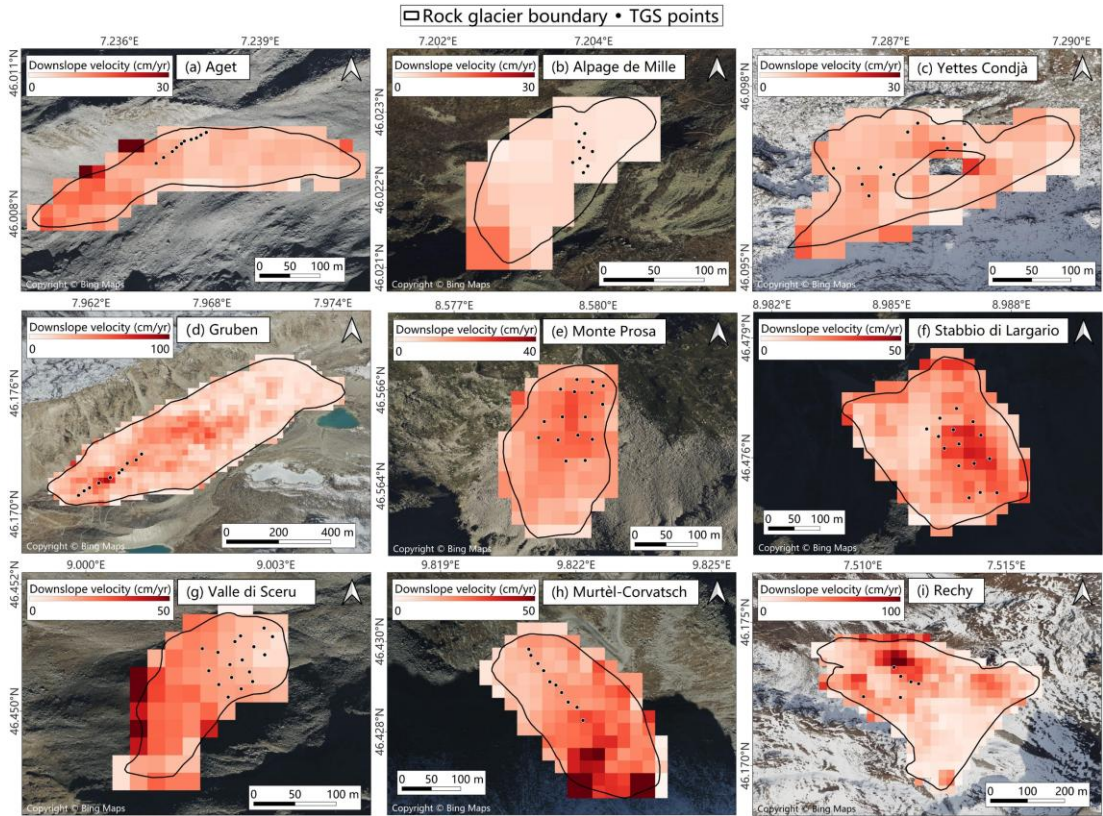


Figure 3.12: InSAR-derived velocity fields for the rock glaciers in the Swiss Alps: (a) Aget, (b) Alpage de Mille, (c) Yettes Condjà, (d) Gruben, (e) Monte Prosa, (f) Stabbio di Largario, (g) Valle di Sceru, (h) Murtèl-Corvatsch, (i) Rechy. The basemap is from Bing Maps.

### 3.5.2 Contrasting rock glacier velocity patterns on the Tibetan Plateau

We collected 489 interferograms to assess rock glacier velocities on the Tibetan Plateau. Our method generated 19,727 downslope velocity fields for nearly all rock glaciers with areas exceeding  $0.1 \text{ km}^2$  as compiled in TPRoGI (99% for the entire study region, 98% for the westerlies domain, and 99% for the monsoon domain; Table 3.2). The very few failures were mostly due to the strong decorrelations presented on rock glaciers, which resulted in significant spatial gaps in the velocity fields.

The median velocity of all assessed rock glaciers is 17 cm/yr. We found a prominent contrast in rock glacier velocities within our study region: rock glaciers in the westerlies domain creep on average faster (median = 30 cm/yr) than those in the monsoon domain (median = 13 cm/yr) (Figures 3.13a, 3.14a). Along the longitudinal direction, rock glacier velocities first increase from 25 cm/yr at  $70^\circ\text{E}$  to 60 cm/yr at  $80^\circ\text{E}$ , then decrease to 12 cm/yr at  $90^\circ\text{E}$ , and increase to 25 cm/yr at  $105^\circ\text{E}$  (Fig. 5b).

The maximum and minimum velocities are 61 cm/yr at 82.5°E and 12 cm/yr at 90°E, respectively (Figure 3.13b). Along the latitudinal direction, rock glacier velocities first increase from 9 cm/yr at 28°N to 25 cm/yr at 31.5°N, then decrease to 10 cm/yr at 33°N, subsequently increase to 52 cm/yr at 36°N, then decrease to 30 cm/yr at 37.5°N, and finally increase to 40 cm/yr at 39°N (Fig. 5c). The velocities increase at an overall rate of 2.8 cm/° from 28°N to 39°N. The maximum and minimum velocities are 52 cm/yr at 36°N and 9 cm/yr at 28°N, respectively (Figure 3.13c).

Table 3.2: Number of rock glaciers with areas larger than 0.1 km<sup>2</sup> compiled in TPRoGI [v1.0] and number with a successful generation of downslope velocity fields.

Region	Number of rock glaciers with areas larger than 0.1 km <sup>2</sup> compiled in TPRoGI [v1.0]	Number of rock glaciers with a successful generation of downslope velocity fields
Entire study region	19,940	19,727
Westerlies domain	6,964	6,823
Monsoon domain	12,981	12,909

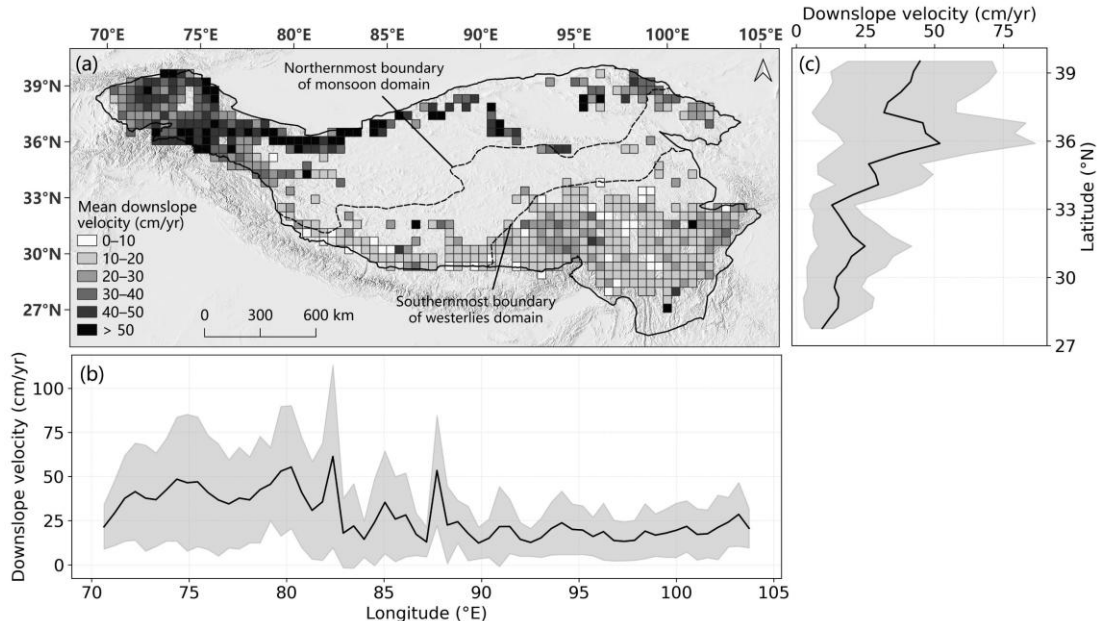


Figure 3.13: (a) Averaged rock glacier downslope velocities in grid cells of 50 km×50 km and in 50 km bins along (b) longitudinal and (c) latitudinal directions. The northernmost boundary of monsoon domain and the southernmost boundary of westerlies domain in (a) are from [Huang et al. \(2023\)](#). The gray-shaded areas in (b) and (c) denote the standard deviation of all velocities in the bins.

Rock glacier velocities increase with larger areas, showing a statistically significant positive correlation between the median areas and median velocities across different area ranges ( $R^2 = 0.89, p < 0.05$ ; Figure 3.14b). Conversely, a statistically significant negative correlation between the median minimum elevations and median velocities across different elevation ranges was found ( $R^2 = 0.99, p < 0.01$ ; Figure 3.14c). The median slopes and median velocities across different slope ranges show a statistically significant positive correlation ( $R^2 = 0.97, p < 0.01$ ; Figure 3.14d).

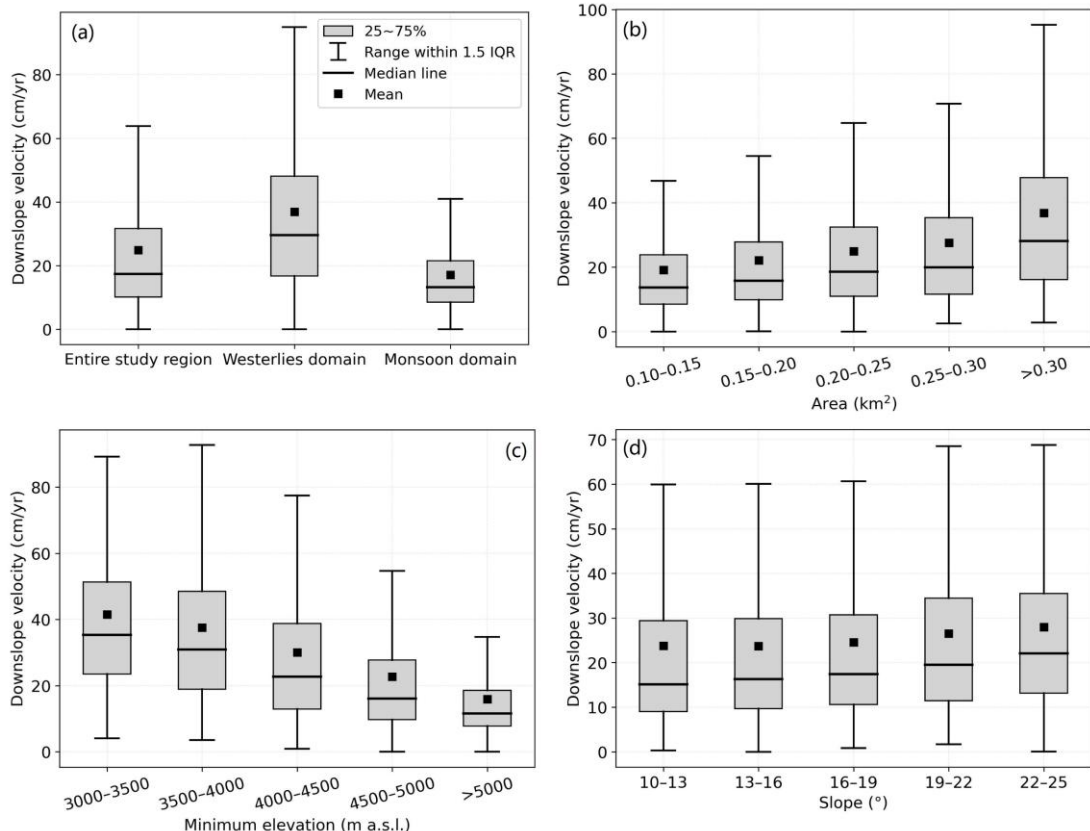


Figure 3.14: Distributions of rock glacier downslope velocities in (a) the entire study region and different climatic domains, and different ranges of (b) rock glacier area, (c) minimum elevation, and (d) slope. IQR is interquartile range.

## 3.6 Discussion

### 3.6.1 Advantages and limitations of our InSAR approach

#### 3.6.1.1 Advantages

In this study, we developed a new framework for large-scale rock glacier velocity assessment using InSAR. Our approach enables systematic evaluation, while

leveraging multi-geometry and multi-temporal interferograms to generate comprehensive velocity fields. Compared to existing InSAR methods, our approach offers several key advantages. Firstly, the wrapped method requires substantial manual effort, as assigning rock glacier velocity classes requires operators to visually interpret numerous interferograms ([Bertone et al., 2022](#)). In contrast, our approach minimizes manual intervention, enabling efficient large-scale assessments. Secondly, the rock glacier velocities derived from the single unwrapped method often exhibit large uncertainties due to the inherent limitations of using snapshot interferograms ([Liu et al., 2013](#)). In contrast, our approach generates more comprehensive and spatially complete velocity fields by utilizing interferograms from multiple acquisition dates and satellite imaging geometries. This multi-temporal, multi-geometry integration mitigates errors associated with unfavorable viewing angles, atmospheric distortions, and decorrelation ([Cai et al., 2024](#)). Thirdly, unlike SBAS and PSI, our method is better suited for measuring active rock glacier velocities. The PSI-derived velocities by [Guerrero et al. \(2025\)](#) are one order of magnitude lower than the geodetic measurements, whereas our results have a much better agreement with independent velocity datasets. Similarly, the SBAS-derived velocities typically fall within the mm/yr range ([Zhang et al., 2023; Cai et al., 2024](#)), which are below the velocities of active rock glaciers. Fourth, compared to conventional stacking approaches, our method leverages multi-geometry data to derive velocities in the downslope direction, providing more comprehensive measurements.

We compared our InSAR-derived velocities with those obtained from very-high-resolution satellite and aerial imagery, as well as GNSS measurements. The good agreement between our results and those from optical imagery across various regions demonstrates the reliability, transferability, and applicability of our method for large-scale assessments. However, the weaker agreement observed in the Swiss Alps highlights the challenges inherent to InSAR-based rock glacier velocity assessment, which will be further discussed in the following subsection.

### 3.6.1.2 Limitations

The comparison with other velocity datasets indicates that our InSAR approach tends to underestimate velocity magnitudes. This discrepancy stems probably from phase unwrapping errors, inaccuracies in atmospheric correction, and phase filtering. Firstly, we use Sentinel-1 C-band data with a 12-day temporal baseline to assess rock

glacier velocities, which impose limitations on velocity assessment for fast-moving rock glaciers with velocities exceeding 100 cm/yr. This is because when measuring the velocities of these rock glaciers, unwrapping errors caused by aliasing effects are common, which can introduce uncertainties and result in underestimated velocities ([Fan et al., 2025](#)). For instance, the InSAR-derived velocity field of the rock glacier at Muztagh Ata shows an apparent velocity underestimation over the front area which likely stems from phase unwrapping errors (Figure [3.7b3](#)). Additionally, short temporal baselines (e.g., 6 or 12 days) can cause difficulties in assessing slow-moving rock glaciers with velocities under 10 cm/yr, as noise may obscure motion signals ([Liu et al., 2013](#)). Secondly, we utilize coherence to automatically select stable reference pixels and use the phases of these pixels to correct atmospheric errors. However, we cannot rule out the possibility that some selected pixels may fall in slow-moving areas. Consequently, the phase contributions from both atmospheric effects and the deformation of these moving areas are removed, leading to underestimated velocities. Thirdly, we use the adaptive Goldstein-Werner phase filter to mitigate noise in interferograms. This filter, however, suppresses deformation signals on a local scale and contributes to an underestimation of velocities.

Our InSAR method is less effective for measuring the velocities of small rock glaciers. Firstly, the ASF HyP3 service only accepts multi-looking windows to configurations of  $10 \times 2$  and  $20 \times 4$ , producing a minimum pixel spacing of 40 m. This coarse spatial resolution may limit the ability to accurately assess velocities for small rock glaciers, as the sparse pixel coverage increases susceptibility to aliasing effects ([Pepin et al., 2024](#)). Secondly, the strong local-scale velocity variations on small rock glaciers could be largely suppressed due to unwrapping errors and phase filtering. For the nine Swiss Alpine rock glaciers, GNSS-derived velocities exhibit large standard deviations, reflecting pronounced spatial variability in movement across different locations within these small rock glaciers. In contrast, our InSAR approach underestimates this variability, as evidenced by its significantly smaller standard deviations (Figure [3.11](#)). Thirdly, our method cannot resolve velocity variations within individual pixels. In cases where rock glaciers exhibit substantial velocity differences at sub-pixel scales, our approach may fail to accurately capture these variations. These factors likely explain the reduced effectiveness of our approach in the Swiss Alps, where rock glaciers are generally smaller than those in High

Mountain Asia and the U.S.

Additionally, rock glacier movement rates vary seasonally, which are typically larger in late summer to autumn and smaller in spring ([Delaloye et al., 2010](#); [Cicoira et al., 2019b](#)). Therefore, the velocities derived from Sentinel-1 data from the two-month snow-free summer period in this study are expected to be about 20% higher than the annual velocities ([RGIK, 2022a](#)).

Given these constraints, we recommend using our InSAR-derived velocity products with caution. Empirically, we suggest that our approach yields higher reliability for rock glaciers larger than 0.1 km<sup>2</sup> and with velocities between 10 and 100 cm/yr, which constitute approximately 75% (~15,000) of all assessed rock glaciers in our study region.

Further research is needed to address the remaining challenges in InSAR-based rock glacier velocity assessment. First, integrating multi-platform interferograms, particularly from sensors with higher spatial resolution and shorter wavelengths (X-band) and longer wavelengths less prone to phase aliasing (L-band), or variable revisit times (e.g., 6, 24, 36, 60 days), has the potential to enhance the velocity detection capabilities of InSAR ([RGIK, 2022a](#)). Nonetheless, new methods must be developed to effectively aggregate and interpret these diverse datasets. Second, there is a need to develop more effective methods for atmospheric error correction, particularly in mountainous regions. For instance, more innovative strategies for automatically selecting stable reference points in non-moving areas can help improve the performance of our proposed method. Third, more evaluation and validation studies on InSAR-derived velocity products are needed for assessing the performance of different InSAR methods on rock glacier velocity assessments.

### **3.6.2 Environmental controls on rock glacier velocities**

Our large-scale regional study reveals a contrasting pattern of rock glacier velocities across different climatic domains, which is likely driven by differences in glacial influence and rock glacier areas between the two domains.

The influence from glaciers appears to significantly affect rock glacier dynamics. First, the hydrological contribution from adjacent glaciers provides a steady water supply, which sustains high creep rates in connected rock glaciers ([Croce et al., 2002](#); [Manchado et al., 2024](#)). Second, advancing glaciers can exert pressure on the root

zones of rock glaciers, leading to the formation of push moraines and debris rearrangement, which further enhances their dynamic behavior ([Bolch et al., 2019a](#)). In the Pamir-Karakoram-Western Kunlun Shan region (the westerlies domain), the abundance of glaciers likely amplifies the activity of nearby rock glaciers. In contrast, although rock glaciers are widespread in southeastern Tibet (the monsoon domain), glaciers are largely confined to the Nyainqntanglha. The scarcity of glaciers in other areas, such as the Hengduan Shan, may contribute to the slower movement of rock glaciers there. This disparity in glacial influence could help explain the contrasting velocity patterns observed in our study region.

Additionally, we found a strong positive correlation between rock glacier area and velocity (Figure [3.14b](#)), suggesting that larger rock glaciers tend to move faster. This relationship is likely driven by the greater gravitational forces acting on larger rock glaciers due to their increased mass ([Manchado et al., 2024](#)). This may also help explain why rock glaciers in the westerlies domain, which are generally larger than those in the monsoon domain ([Sun et al., 2024](#)), exhibit faster velocities.

However, rock glacier velocity patterns should result from a complex interplay between landform geometry (e.g., area and thickness), material properties (e.g., debris grain size and ice content) and environmental factors (e.g., topography, climatic conditions and influence of glaciers) ([Haeblerli et al., 2006](#); [Cicoira et al., 2021](#); [Kab and Roste, 2024](#); [Hu et al., 2025](#)). Furthermore, variations in geological and lithological settings between the westerlies and monsoon domains may also play a role in shaping rock glacier velocities. Therefore, more comprehensive studies are needed to elucidate the environmental controls governing the contrasting rock glacier velocity patterns across different climatic domains.

### **3.6.3 Significance of our large-scale rock glacier velocity dataset**

The assessment from this study holds significant value. The first large-scale regional velocity estimates provide crucial data support for investigating rock glacier dynamics, mountainous hydrology, permafrost distribution, and disaster management.

Firstly, the velocity dataset provides valuable baseline information for generating RGV products. Currently, very few RGV products are available in HMA ([Kab et al., 2021](#)), underscoring the urgency to address the data gap for this important region. Gaining preliminary insights into the kinematic status of rock glaciers is highly

beneficial before selecting RGV monitoring sites ([Kellerer-Pirkbauer et al., 2024](#); [Kääb and Røste, 2024](#)). Our dataset advances this goal by not only delivering a regional-scale overview of rock glacier velocities but also providing detailed velocity fields for individual rock glaciers. These fields enable straightforward identification of active areas within rock glaciers, thereby facilitating the selection of suitable locations for in situ monitoring instrumentation.

Secondly, our dataset offers insights into the ice content of rock glaciers. Most previous studies addressing ice volume within rock glaciers have estimated it by applying a scaling relationship based solely on area, providing only total regional estimates or information on small regions ([Bolch and Marchenko, 2009](#); [Azócar and Brenning, 2010](#); [Jones et al., 2018b, 2021](#); [Harrison et al., 2024](#); [Li et al., 2024](#)). Rock glacier kinematics could relate to interior ice storage ([Hartl et al., 2016](#); [Hu et al., 2023b](#)). Therefore, our results indicate that the rock glaciers in the westerlies domain may contain abundant ground ice despite the drier climatic environment there. The few available geophysical investigations in the Tien Shan with similar climate characteristics corroborate this finding ([Bolch et al., 2019a](#)). Consequently, the rock glaciers in the westerlies domain exhibit a high significance as water resources and might, to some extent, counterbalance the projected decrease in glacier runoff ([Janke and Bolch, 2021](#); [Harrison et al., 2021](#); [Rounce et al., 2023](#)).

Thirdly, the InSAR-derived products from this study, including the velocity dataset and coherence maps, are beneficial for inferring rock glacier activity levels ([RGIK, 2023](#)), which are essential for evaluating permafrost occurrence ([Hu et al., 2024](#)). However, our results cannot directly classify rock glacier activities based on the velocity thresholds suggested by [RGIK \(2022a\)](#) (relict: < 1 cm/yr; transitional: 1–10 cm/yr; active: > 10 cm/yr). Accurately capturing velocities below 10 cm/yr needs interferograms with longer temporal baselines (e.g., 24, 36, or 60 days), and especially for identifying relict rock glaciers, the temporal baseline of up to a year may be required ([RGIK, 2022a](#)). Despite this, previous studies have shown that incorporating InSAR-derived information into unsupervised and supervised classifiers can significantly improve the classification of rock glacier activities ([Bertone et al., 2019](#); [Crippa et al., 2024](#)). Therefore, our dataset could be a valuable input for advanced classifiers or machine learning models to enhance rock glacier activity classification.

Moreover, evaluating rock glacier kinematics is beneficial for assessing and monitoring potential disasters in high mountain environments. Rapid movement or destabilization of rock glaciers can trigger hazards such as rockfalls, debris flows, and lake outbursts, posing risks to nearby human infrastructure ([Marcer et al., 2021](#); [Janke and Bolch, 2021](#)). For instance, [Blöthe et al. \(2019\)](#) found that 5–14% of the 2,000 rock glaciers in Karakoram, Tien Shan, and Altai mountains affected 95 km of river channels. [Hassan et al. \(2021\)](#) identified one rock glacier dam in the upper Hunza Basin and noted that 35 rock glaciers could form dams while 68 have interacted with river channels. The advance of these rock glaciers may potentially trigger lake outbursts if the dams destabilize, and our velocity dataset can aid in evaluating such hazards in the broad study region.

### 3.7 Conclusion

This study presents a methodological framework for generating rock glacier velocity fields using multi-temporal and multi-geometry InSAR, enabling rapid and systematic assessment of rock glacier velocities across extensive regions. We rigorously validate our approach using diverse velocity datasets derived from very-high-resolution optical images (satellite Pléiades and aerial images) and in-situ GNSS measurements. To demonstrate the applicability of our approach in large-scale regions, we applied it to a plateau-wide inventory and generated the first large-scale regional rock glacier velocity dataset for the Tibetan Plateau region, encompassing downslope velocity fields for almost 19,727 rock glaciers. Our main findings are as follows:

- (1) The velocities derived from our InSAR-based approach show statistically significant correlations with all comparison datasets but tend to underestimate magnitudes. The mean relative difference is approximately 20% when compared to velocities derived from Pléiades and aerial images. However, this difference increases to 50% when compared to GNSS point measurements. These discrepancies likely stem from inherent limitations of InSAR, including inaccuracies in atmospheric error correction and phase unwrapping errors in interferograms. The weaker agreement with the GNSS dataset could also be due to the different scales by comparing point measurements with grid cells. These findings underscore the need for further work on InSAR-based rock glacier velocity assessment. In the future, all

available GNSS points will be used to compare with the velocities.

(2) The overall median velocity of all assessed rock glaciers on the Tibetan Plateau is 17 cm/yr. A contrasting velocity pattern across different climatic domains was found: rock glaciers in the westerlies domain move on average faster (median = 30 cm/yr) than those in the monsoon domain (median = 13 cm/yr). We attribute this disparity to differences in glacial influence and rock glacier sizes between the two climatic domains.

This study conducts the first comprehensive comparison of InSAR-derived velocities with those obtained from other data sources. We emphasize accurate atmospheric correction and phase unwrapping issues as critical challenges for InSAR in achieving high-accuracy velocity estimates, which are essential for producing high-quality RGV products. The large-scale velocity dataset generated in this study holds significant value for future research, including the selection of RGV monitoring sites, mountain hydrology assessments, permafrost modeling, and disaster evaluation. Furthermore, this work provides valuable insights into the environmental controls on regional-scale spatial patterns of rock glacier velocities.

# Chapter 4 Assessing rock glacier water storage in High Mountain Asia

---

## Abstract

The climate-driven cryosphere decline in High Mountain Asia (HMA) underscores the urgent need to comprehensively assess water availability in this vulnerable region. While rock glaciers act as critical long-term water reservoirs, their hydrological roles in HMA remains poorly quantified and is often overlooked in hydrological models and water management strategies. Here, we integrate deep learning techniques with high-resolution satellite imagery to map rock glaciers and, for the first time, comprehensively evaluate their water storage across the entire HMA region. To mitigate the estimation uncertainty of water storage caused by mapping inaccuracies, we calibrated our results using a Tibetan Plateau rock glacier inventory. Rock glaciers in HMA collectively store  $189.7 \pm 21.7 \text{ km}^3$  of water volume equivalent (WVEQ), representing ~2.5% (1:39 ratio) of the water stored in glaciers. Notably, the Hengduan Shan holds the largest rock glacier WVEQ ( $22.0 \pm 8.9 \text{ km}^3$ ) and exhibits the highest rock-glacier-to-glacier storage ratio (1:3), driven by the widespread presence of rock glaciers and limited glacier coverage. Moreover, as climate change accelerates glacier mass loss, the relative hydrological importance of rock glaciers is likely to grow in the coming decades. Our findings reveal that although rock glaciers cannot replace glaciers as a regional water source in HMA, their localized contributions can be substantial and warrant greater attention. These results highlight the necessity of considering these ‘hidden’ water reservoirs to refine current hydrological models and inform local water resource adaptation strategies.

## 4.1 Introduction

High Mountain Asia (HMA), often termed the "Asian Water Tower," hosts the largest volume of frozen water outside the polar regions, sustaining nearly 2 billion people downstream ([Immerzeel et al., 2020](#); [Yao et al., 2022](#)). Since the 1980s, climate change has driven regional warming at rates double the global average ([Yao et al., 2019](#)), triggering accelerated losses in key cryospheric components. Glaciers have undergone intensified mass loss in recent decades ([Bhattacharya et al., 2021](#);

[Hugonet et al., 2021](#)), with projections indicating severe depletion by 2100 ([Kraaijenbrink et al., 2017](#); [Rounce et al., 2023](#)). Snowpacks are melting across much of HMA, and their meltwater contributions are projected to decline sharply ([Smith and Bookhagen, 2018](#); [Kraaijenbrink et al., 2021](#)). Permafrost degradation is similarly pronounced, marked by rising ground temperatures, shrinking spatial extent, thickening active layer, and the proliferation of thermokarst lakes and thaw slumps ([Zhao et al., 2020](#); [Mu et al., 2020](#); [Xia et al., 2024](#)). These cascading changes amplify concerns about water sustainability in HMA, highlighting the urgency to comprehensively quantify cryospheric water reserves to inform adaptive management strategies.

Rock glaciers are defined as debris landforms shaped by gravity-driven creep in permafrost environments ([RGIK, 2023](#)). They are known to store ground ice from field-based or geophysical measurements (e.g., [Corte, 1976](#); [Arenson et al., 2002](#); [Croce and Milana, 2002](#); [Hausmann et al., 2007, 2012](#); [Bolch et al., 2019a](#)), suggesting their potential as water reservoirs ([Rangecroft et al., 2015](#); [Jones et al., 2019a](#); [Wagner et al., 2020a](#)). Moreover, the degradation of rock glaciers occurs slower than that of glaciers due to insulation by surface debris ([Haeberli et al., 2006](#); [Janke and Bolch, 2021](#); [Harrison et al., 2021](#)), implying their increasingly hydrological importance in the future under warming climates ([Jones et al., 2019a](#); [Schaffer et al., 2019](#)). However, the role of rock glaciers is often overlooked in hydrological models and water management strategies.

While the hydrological significance of rock glaciers as water stores has been extensively studied in the Andes ([Corte, 1976](#); [Brenning, 2005a](#); [Azócar and Brenning, 2010](#); [Bodin et al., 2010](#); [Perucca and Esper Angillieri, 2011](#); [Rangecroft et al., 2015](#); [Janke et al., 2017](#); [Schaffer et al., 2019](#)), relevant researches in HMA remain fragmented, with most focusing on the Himalaya region ([Jones et al., 2018b, 2021](#)) and localized assessments ([Bolch and Marchenko, 2009](#); [Hu et al., 2023b](#); [Li et al., 2024](#); [Pandey et al., 2024](#)). The hydrological importance of rock glaciers in most regions of HMA remains underexplored and poorly quantified.

To quantify the water storage of rock glaciers, mapping their spatial distribution and extent is a critical first step. While regional rock glacier inventories exist (e.g., [Jones et al., 2021](#); [Sun et al., 2024](#)), a comprehensive inventory for the entire HMA region has remained absent. To address this gap, we used a deep learning model to map rock

glaciers from high-resolution satellite imagery and derived an initial water storage estimate from the mapped polygons. Considering the uncertainties in water storage estimation due to the inaccurate mapping from the deep learning model, we used a Tibetan Plateau rock glacier inventory (i.e., TPRoGI developed in our first work) to calibrate the results for the Hindu Kush Himalaya and Tien Shan regions. We then evaluate their significance as water resources by comparing the water storage to that of glaciers. Our study provides the first comprehensive assessment of rock glacier water storage and hydrological significance relative to glaciers across the entire HMA region.

## 4.2 Study area and data

### 4.2.1 Study area

HMA encompasses an extensive and geographically diverse expanse of approximately 4 million square kilometers, spanning Central and South Asia. Characterized by rugged topography, deep valleys, and the expansive Tibetan Plateau, it incorporates surrounding high-mountain ranges such as the Himalayas, Karakoram, Hindu Kush, Pamirs, and Tien Shan ([Bolch et al., 2019b](#)). Our study focuses on the 22 HMA subregions defined by [Bolch et al. \(2019b\)](#), along with the Qaidam Basin (Figure [4.1](#)). Climatically, HMA exhibits pronounced heterogeneity due to the interplay of the Indian monsoon, East Asian monsoon, and mid-latitude westerly winds. This creates stark regional contrasts, ranging from arid and semi-arid conditions in the western ranges to more humid environments in the east ([Yao et al., 2022](#)). The region's high elevation and climatic complexity sustain a globally significant cryosphere, featuring extensive glaciers, rock glaciers, and permafrost systems ([Bolch et al., 2019b](#); [Zou et al., 2017](#); [Sun et al., 2024](#)).

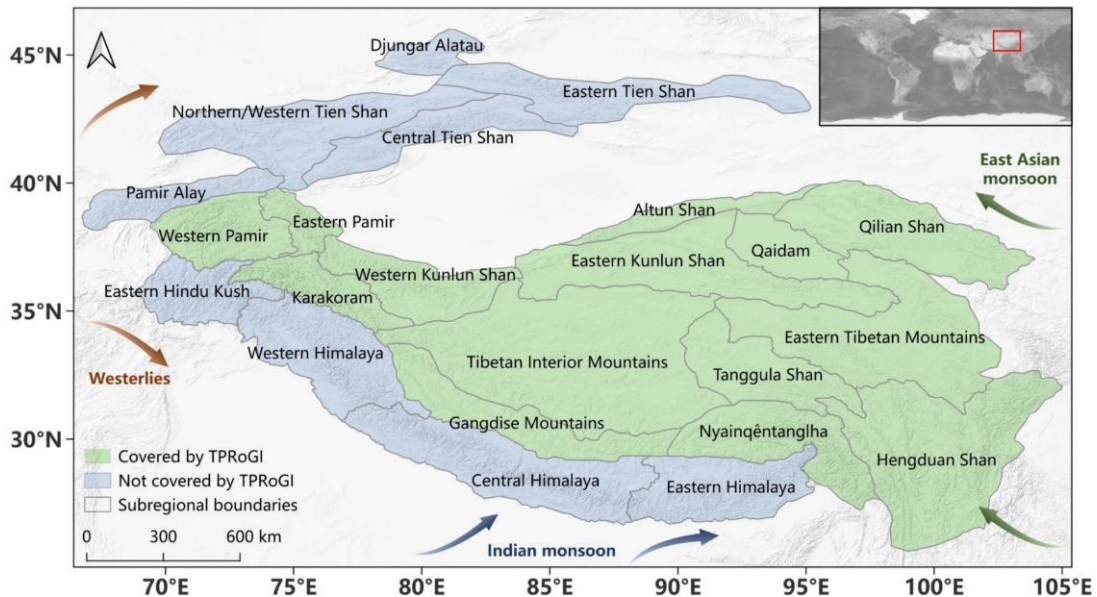


Figure 4.1: (a) Study area (High Mountain Asia).

#### 4.2.2 Data

We employed high-resolution (~5 m) optical satellite imagery from Planet Basemaps to map rock glaciers across HMA. Datasets from the third (July–September) and fourth (October–December) quarters of 2021 were downloaded and preprocessed to generate natural-color composites using the Red, Green, and Blue (RGB) spectral bands. These quarterly products leveraged advanced fusion algorithms to enhance visual consistency and mitigate cloud cover by aggregating multi-temporal imagery ([Nass et al., 2019](#)).

We used TPRoGI (v1.0, [Sun et al., 2024](#)), an inventory covering the Tibetan Plateau, to calibrate the deep-learning-derived region-wide WVEQs for the Hindu Kush Himalaya and Tien Shan regions. This inventory contains 44,273 rock glaciers, which was compiled using a deep learning approach with manual postprocessing ([Sun et al., 2024](#)).

We used permafrost extent and glacier outlines to remove false positives predicted by the deep learning model. The permafrost extent for HMA was extracted from the Northern Hemisphere permafrost distribution map produced by [Obu et al. \(2018\)](#). For glacier data, we utilized the Randolph Glacier Inventory (RGI v6.0; [RGI Consortium, 2017](#)), which includes 95,536 glaciers in HMA. While RGI v7.0 ([RGI Consortium, 2023](#)) offers updated glacier outlines, we retained RGI v6.0 because the thickness dataset we used from [Farinotti et al. \(2019\)](#) and [Millan et al. \(2022\)](#) are

based on this inventory.

We used ice thickness datasets produced by [Farinotti et al. \(2019\)](#) and [Millan et al. \(2022\)](#) to estimate glacier water storage. [Farinotti et al. \(2019\)](#) used an ensemble of up to five models to provide a consensus estimate for the ice thickness of glaciers in RGI v6.0. [Millan et al. \(2022\)](#) generated a comprehensive high-resolution mapping of ice motion and used these datasets to reconcile ice thickness distribution with glacier dynamics and surface topography. The glacier mass projections for 2100 under the SSP1-2.6, SSP3-7.0, and SSP5-8.5 scenarios from [Rounce et al. \(2023\)](#) were used to estimate future glacier water storage.

## 4.3 Methods

### 4.3.1 Mapping rock glaciers using deep learning

In a prior study, we developed a deep learning model for mapping rock glaciers ([Sun et al., 2024](#)) based on DeepLabv3+ neural network architecture ([Chen et al., 2018](#)). This model was trained using optical imagery from Planet Basemaps (the third quarter of 2021) and local rock glacier inventories from six areas, which was subsequently applied to map rock glaciers for the Tibetan Plateau region. In this study, we expanded the mapping scope from the Tibetan Plateau to the entire HMA region. To overcome limitations such as cloud cover and topographic shadows in single-season imagery, particularly in challenging subregions in the Himalaya, we applied the deep-learning model to Planet Basemaps datasets from both the third and fourth quarters of 2021. Predictions from the two quarters were merged, dissolved, and refined through a three-step false-positive removal protocol:

- Size filtering: Polygons smaller than 0.01 km<sup>2</sup> were discarded ([RGIK, 2023](#)).
- Permafrost extent masking: Polygons outside the [Obu et al. \(2018\)](#) permafrost zone were excluded, with a 10 km buffer applied to account for permafrost model uncertainties and potential rock glacier occurrence outside permafrost areas ([Bolch and Gorbunov, 2014](#)).
- Glacier exclusion: Overlaps with glacier boundaries (RGI v6.0; [RGI Consortium, 2017](#)) were removed.

This workflow retained 183,489 polygons, covering a total area of 24,670 km<sup>2</sup> (Figure 4.2), which were used to derive the initial rock glacier WVEQ estimates.

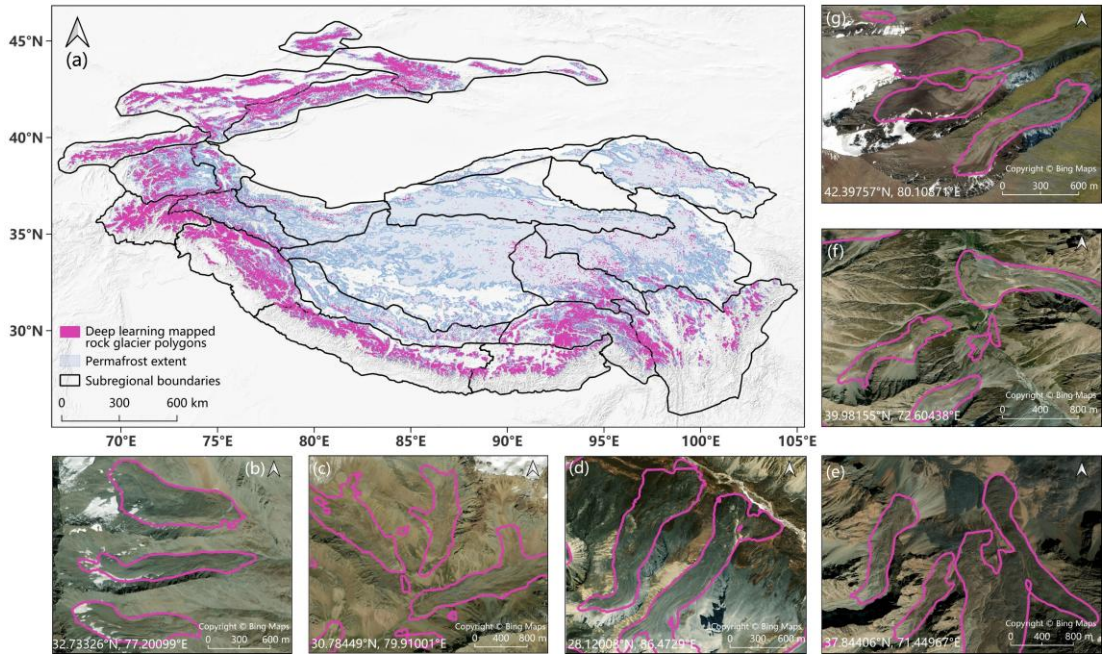


Figure 4.2: (a) Deep-learning-mapped rock glacier polygons across High Mountain Asia (HMA). (b-g) Examples of deep-learning-mapped rock glacier polygons.

### 4.3.2 Estimating water storage

The water volume equivalent (WVEQ) of a rock glacier  $V_{\text{RoG}}$  can be calculated by multiplying the surface area  $A_{\text{RoG}}$ , mean thickness  $\bar{H}_{\text{RoG}}$ , ice content  $w_i$ , and an ice density conversion factor  $f_i$ , which equals 0.9 considering an ice density of 900 kg/m<sup>3</sup> ([Paterson, 1994](#)):

$$V_{\text{RoG}} = A_{\text{RoG}} \bar{H}_{\text{RoG}} w_i f_i \quad (4.1)$$

Obtaining rock glacier thickness is challenging due to the practicalities for performing field-based or geophysical measurements ([Cicoira et al., 2021](#)), and thus empirical models are desirable. The most widely used empirical model is the area-thickness power-law relationship established by [Brenning \(2005b\)](#) based on field data in the Andes of Central Chile:

$$\bar{H}_{\text{RoG}} = 50 A_{\text{RoG}}^{0.2} \quad (4.2)$$

The units of  $\bar{H}_{\text{RoG}}$  and  $A_{\text{RoG}}$  are in m and km<sup>2</sup>, respectively. This model has been widely applied to estimate rock glacier thickness worldwide ([Azócar and Brenning, 2010](#); [Bodin et al., 2010](#); [Perucca and Esper Angillieri, 2011](#); [Rangecroft et al., 2015](#); [Janke et al., 2017](#); [Millar and Westfall, 2019](#); [Jones et al., 2018b, 2021](#); [Wagner et al., 2021](#); [Li et al., 2024](#); [Pandey et al., 2024](#)).

[Cicoira et al. \(2021\)](#) recently proposed new methods to estimate rock glacier thickness based on surface slope angles, using detailed observations of surface creep rates, slope angles, and thickness on 23 and 5 rock glaciers from the Alps and the Andes, respectively. Among the three models they developed, the first assumes constant thickness, and the second can yield negative values in our case. Therefore, we adopted their third model, which uses a perfectly plastic model to estimate slope-dependent thickness:

$$\bar{H}_{\text{RoG}} = \frac{\tau}{\rho_{\text{RoG}} g \sin \alpha} \quad (4.3)$$

Where  $g$  is the gravitational acceleration ( $9.79 \text{ m/s}^2$ ),  $\alpha$  is the surface slope angle, and  $\tau$  is the driving stress on rock glaciers caused by gravitational force. By analyzing rock glacier datasets, [Cicoira et al. \(2021\)](#) determined a mean driving stress of 92 kPa. While this value may differ for rock glaciers in HMA, the lack of datasets makes it challenging to estimate a precise value for our study area. We therefore adopted the 92 kPa value as the driving stress in our analysis.  $\rho_{\text{RoG}}$  is the density of rock glaciers, which is given by the contribution of volumetric debris  $w_d$  and ice content  $w_i$  and their densities ( $\rho_i = 900 \text{ kg/m}^3$ ,  $\rho_d = 2700 \text{ kg/m}^3$ ):

$$\rho_{\text{RoG}} = \rho_d w_d + \rho_i w_i \quad (4.4)$$

Field measurements and geophysical data from diverse climatic regions indicate that rock glaciers typically contain 40–60% ice by volume (e.g., [Elconin and LaChapelle, 1997](#): >50%; [Arenson et al., 2002](#): 40–70%; [Croce and Milana, 2002](#): ~55%; [Hausmann et al., 2007](#): 45–60%, [2012](#): 40–60%; Halla et al., 2021: 42–44%; Mathys et al., 2024: 38–60%). Based on these findings, studies commonly adopt ice content estimates of 40% (lower bound), 50% (mean), and 60% (upper bound) to calculate the rock glacier WVEQ ([Bodin et al., 2010](#); [Rangecroft et al., 2015](#); [Jones et al., 2018b, 2021](#); [Li et al., 2024](#)). However, [Arenson and Jakob \(2010\)](#) argue for distinguishing ice content by activity status, proposing ranges of 25–45% for active rock glaciers and 10–25% for inactive ones. [Wagner et al. \(2021\)](#) later revised the inactive threshold to 20%, reflecting the observed lower ice content in the Austrian Alps. Recent work by [Panday et al. \(2024\)](#) further categorizes ice content by rock glacier type: 40–60% for glacier-connected and glacier forefield-connected systems, and 20–40% for talus-connected and debris-mantled slope-connected systems.

To address uncertainties in ice content, we simulated 1,000 values sampled from a normal distribution (mean = 50%, standard deviation = 10%). Therefore, for each rock glacier, 2,000 WVEQ estimates were computed by combining these ice content values with thickness estimates derived from the two empirical models ([Brenning, 2005b](#); [Cicoira et al., 2021](#)). By aggregating WVEQ estimates across all the individual rock glaciers within each subregion and  $1^\circ \times 1^\circ$  grids, we calculated subregion-based and grid-based WVEQs, respectively. The resulting WVEQ distributions formed by the 2000 estimates display a bimodal pattern, which is attributable to systematic discrepancies between the two empirical thickness models. This is because these models were calibrated using data from contrasting regions: the semi-arid/semi-humid Andes of Central Chile, where rock glaciers average  $\sim 30$  m in thickness ([Brenning, 2005b](#)), and the temperate, more humid Alps, where rock glaciers are thinner ( $\sim 20$  m; [Cicoira et al., 2021](#)). This regional divergence introduces a  $\sim 10$  m difference in thickness estimates. To conservatively capture this variability, we calculated the mean and standard deviation of WVEQ using all the 2,000 WVEQ estimates, where the standard deviation could serve as uncertainty.

Assuming a 100% ice content by volume, the ice volume of a glacier can be calculated by summing up all the thickness of each pixel  $h$  and multiplying with the size of one pixel  $a$ , which can then be converted into glacier WVEQ  $V_G$  by applying the ice density conversion factor:

$$V_G = \sum h a f_i \quad (4.5)$$

We used both the ice thickness datasets from [Farinotti et al. \(2019\)](#) and [Millan et al. \(2022\)](#) and averaged the results to obtain glacier WVEQ.

### 4.3.3 Refining estimates using Tibetan Plateau inventory

The inaccurate mapping results from the deep learning model can introduce significant uncertainties into water storage estimates. To refine our estimates, we calibrated the results using the Tibetan Plateau rock glacier inventory developed in our first work (TPRoGI, [Sun et al., 2024](#)) which includes 44,273 rock glaciers across 14 subregions. The workflow is illustrated in Figure [4.3](#). We excluded Qaidam due to the absence of rock glaciers and estimated subregion-based and grid-based WVEQs for the remaining 13 subregions using the rock glaciers compiled in TPRoGI

following the same procedure described in Section 4.3.2. Statistically significant linear correlations were observed between the WVEQs estimated from deep-learning-mapped polygons and inventory-compiled rock glacier boundaries for both the subregion-based ( $R^2 = 0.81, p < 0.01$ ; Figure 4.4) and grid-based ( $R^2 = 0.84, p < 0.01$ ; Figure 4.5) cases. For both cases, we fitted an empirical linear relationship and applied it to scale the deep-learning-derived WVEQ estimates for the remaining nine subregions (the Hindu Kush Himalaya and Tien Shan regions).

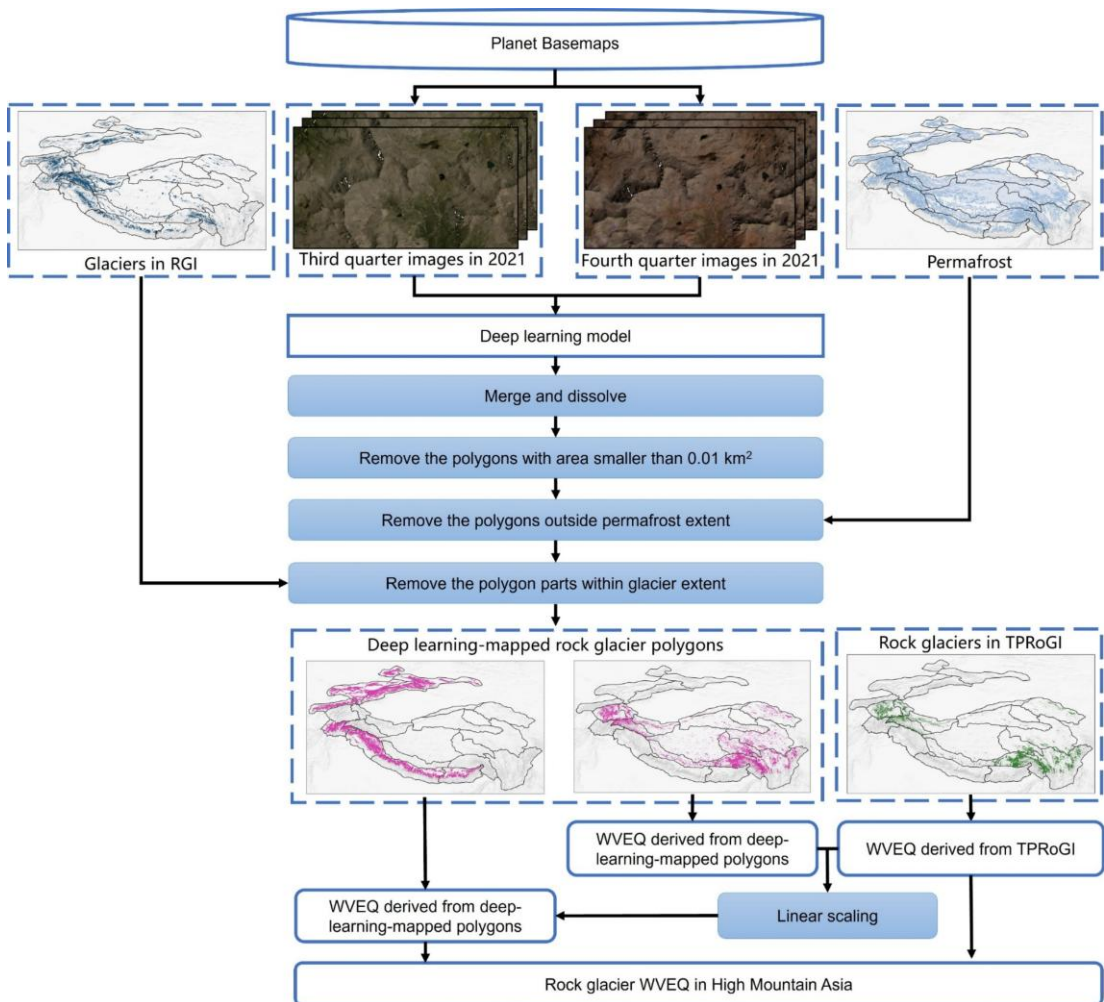


Figure 4.3: Workflow of assessing rock glacier water storage in High Mountain Asia using deep learning. The Tibetan Plateau inventory (TPRoGI) is employed to calibrate the WVEQ estimates from deep-learning-mapped polygons using a linear scaling approach.

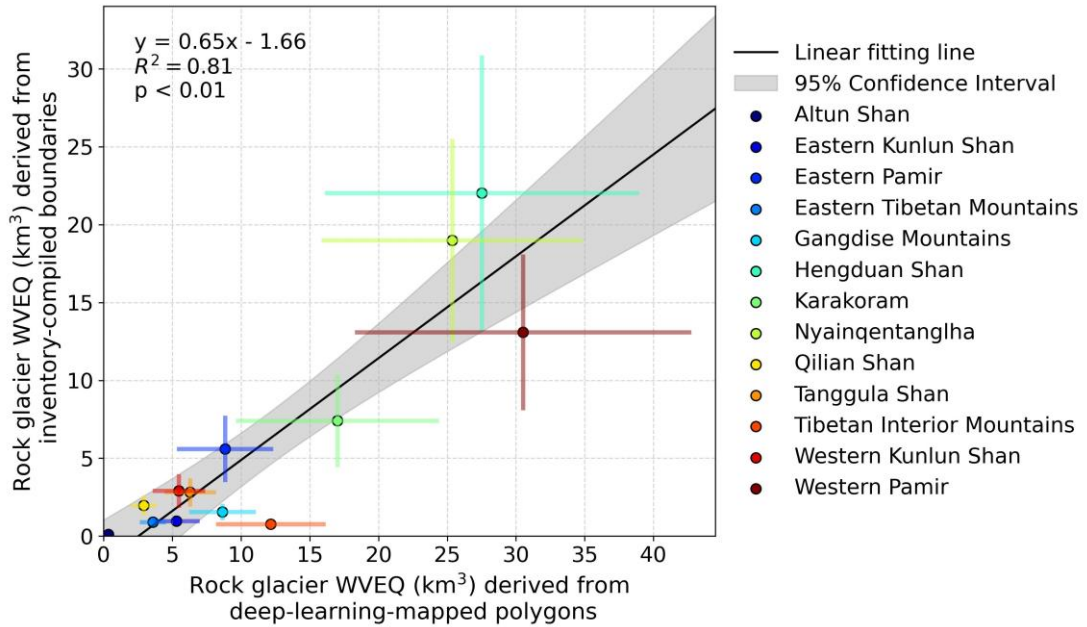


Figure 4.4: Subregion-based linear relationship between rock glacier WVEQs derived from rock glacier inventory (TPRoGI) and deep-learning-mapped polygons.

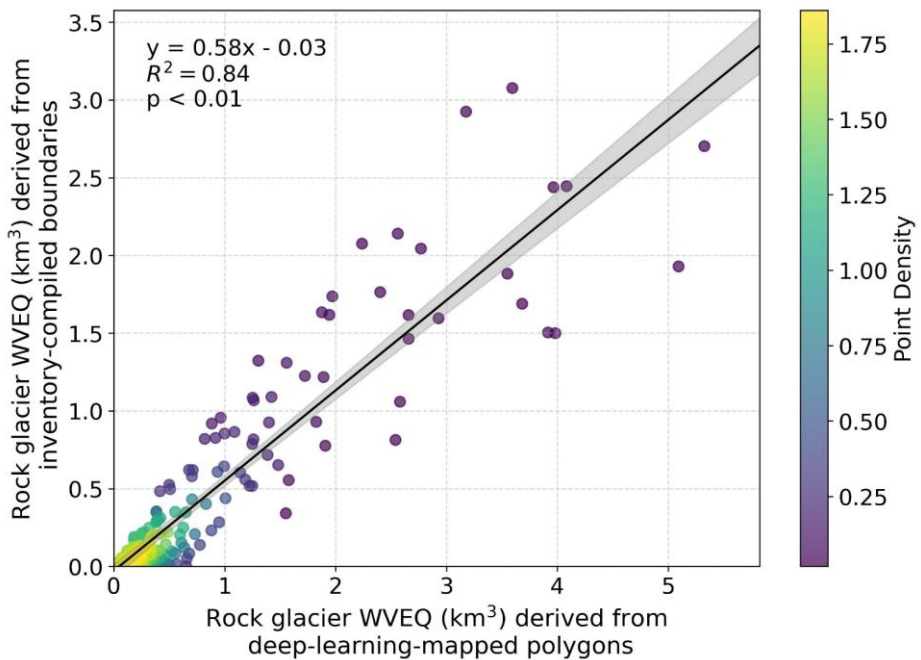


Figure 4.5: Grid-based linear relationship between rock glacier WVEQs derived from rock glacier inventory (TPRoGI) and deep-learning-mapped polygons.

## 4.4 Results

### 4.4.1 Rock glacier WVEQ

The total rock glacier WVEQ in HMA is estimated at  $189.7 \pm 21.7 \text{ km}^3$  (Table 4.1). Regionally, WVEQs exhibit significant spatial variability (Figures 4.6, 4.7). Across

the HMA, WVEQs are smaller in the inner Tibetan Plateau, and larger in the surrounding mountainous regions. The Hengduan Shan holds the largest WVEQ at  $22.0 \pm 8.9 \text{ km}^3$ , followed by the Eastern Hindu Kush ( $21.6 \pm 10.1 \text{ km}^3$ ) and Western Himalaya ( $21.4 \pm 9.0 \text{ km}^3$ ). Four other subregions with WVEQs higher than  $10 \text{ km}^3$  are Nyainqêntanglha ( $19.0 \pm 6.5 \text{ km}^3$ ), Northern/Western Tien Shan ( $17.1 \pm 6.2 \text{ km}^3$ ), Central Himalaya ( $16.8 \pm 6.7 \text{ km}^3$ ), and Western Pamir ( $13.1 \pm 5.0 \text{ km}^3$ ).

At regional scales, our estimates align well with previous inventory-based studies. In the Himalayas, our estimate of  $45.7 \pm 11.7 \text{ km}^3$  shows close agreement (12% difference) with [Jones et al.'s \(2021\)](#) inventory-derived value of  $51.8 \pm 10.4 \text{ km}^3$ . Similarly, for the Northwestern Himalaya, our result of  $25.1 \pm 10.7 \text{ km}^3$  falls within [Pandey et al.'s \(2024\)](#) estimated range of  $17.9\text{--}28.4 \text{ km}^3$  (8% difference). In the Guokalariju region, our estimate of  $2.0 \pm 1.4 \text{ km}^3$  compares favorably (18% difference) with [Li et al.'s \(2024\)](#) range of  $1.3\text{--}3.6 \text{ km}^3$ . These consistencies demonstrate that our deep-learning-based scaling approach produces reliable regional estimates of rock glacier water storage across HMA.

#### 4.4.2 Rock-glacier-to-glacier WVEQ ratios

The total glacier WVEQ in HMA is estimated at  $6,377.3 \text{ km}^3$  and  $8,324.3 \text{ km}^3$  based on ice thickness data from [Farinotti et al. \(2019\)](#) and [Millan et al. \(2022\)](#), respectively, with an average of  $7,350.8 \text{ km}^3$  (Table 4.1). The rock-glacier-to-glacier WVEQ ratio for the entire HMA is 1:39 (Figure 4.6, Table 4.1), indicating that the hydrological significance of rock glaciers as water stores is  $\sim 2.5\%$  of glaciers in HMA. However, the ratios vary significantly across different regions. In the inner Tibetan Plateau and glacier-abundant regions such as Karakoram and Western Kunlun Shan, the ratios are smaller than 1:100, whereas in some surrounding mountainous regions, the ratios are higher than 1:10. The Hengduan Shan stands out with the highest ratio at 1:3, highlighting the critical role of rock glaciers as water reservoirs in this area (approximately 30% of glaciers), which is attributed to the extensive distribution of rock glaciers ([Sun et al., 2024](#)) coupled with the limited presence of glaciers. Other regions where rock glaciers hold considerable water stores with ratios exceeding 1:10 include the Northern/Western Tien Shan (1:7), Djungar Alatau (1:8), and Eastern Hindu Kush (1:9). Especially in some local regions of the Hengduan Shan, the ratios exceed 1:1, indicating that rock glaciers store more water than glaciers there (Figures 4.7).

## CHAPTER 4. WATER STORAGE

Table 4.1: Rock glacier water volume equivalents (WVEQs), glacier WVEQs, and rock-glacier-to-glacier WVEQ ratios of different subregions in HMA.

Subregion	Method for deriving rock glacier WVEQ <sup>1</sup>	Rock glacier WVEQ (km <sup>3</sup> )		Glacier WVEQ (km <sup>3</sup> )		Rock-glacier-to-glacier WVEQ ratio
		Mean	Standard deviation	Farinotti et al. (2019)	Millan et al. (2022)	
Hengduan Shan	Inventory	22.0	8.9	52.4	76.9	64.6
Eastern Hindu Kush	Deep learning	21.6	10.1	170.3	233.2	201.8
Western Himalaya	Deep learning	21.4	9.0	460.5	539.9	500.2
Nyainqntanglha	Inventory	19.0	6.5	372.7	607.5	490.1
Northern/Western Tien Shan	Deep learning	17.1	6.2	89.3	141.0	115.2
Central Himalaya	Deep learning	16.8	6.7	500.5	525.5	513.0
Western Pamir	Inventory	13.1	5.0	556.5	771.0	663.8
Central Tien Shan	Deep learning	9.8	3.6	459.6	672.6	566.1
Eastern Himalaya	Deep learning	7.5	3.2	166.0	193.4	179.7
Eastern Tien Shan	Deep learning	7.4	2.7	106.9	86.3	96.6
Karakoram	Inventory	7.4	3.0	1916.3	2495.5	2205.9
Pamir Alay	Deep learning	6.5	3.2	87.0	144.9	115.9
Eastern Pamir	Inventory	5.6	2.1	114.3	152.4	133.4
Western Kunlun Shan	Inventory	2.9	1.1	595.1	895.8	745.4
Tanggula Shan	Inventory	2.8	0.9	127.8	125.1	126.4
Dzungar Alatau	Deep learning	2.4	1.3	19.9	20.3	20.1
Qilian Shan	Inventory	2.0	0.6	67.3	78.2	72.8
Gangdise Mountains	Inventory	1.6	0.5	46.5	49.3	47.9
Eastern Kunlun Shan	Inventory	1.0	0.3	206.4	207.9	207.1
Eastern Tibetan Mountains	Inventory	0.9	0.3	13.9	16.2	15.1

## ***CHAPTER 4. WATER STORAGE***

Tibetan Interior Mountains	Inventory	0.8	0.3	237.1	282.2	259.6	1:337
Altun Shan	Inventory	0.1	0.0	11.2	9.2	10.2	1:93
Total		189.7	21.7	6377.3	8324.3	7350.8	1:39

<sup>1</sup>Inventory: the subregion is covered by the Tibetan Plateau inventory (TPRoGI, [Sun et al., 2024](#)) and thus the WVEQ is estimated using the rock glacier boundaries from this inventory; Deep learning: the subregion is not covered by TPRoGI and thus the WVEQ is estimated using a scaling approach based on the estimates from deep-learning-mapped polygons.

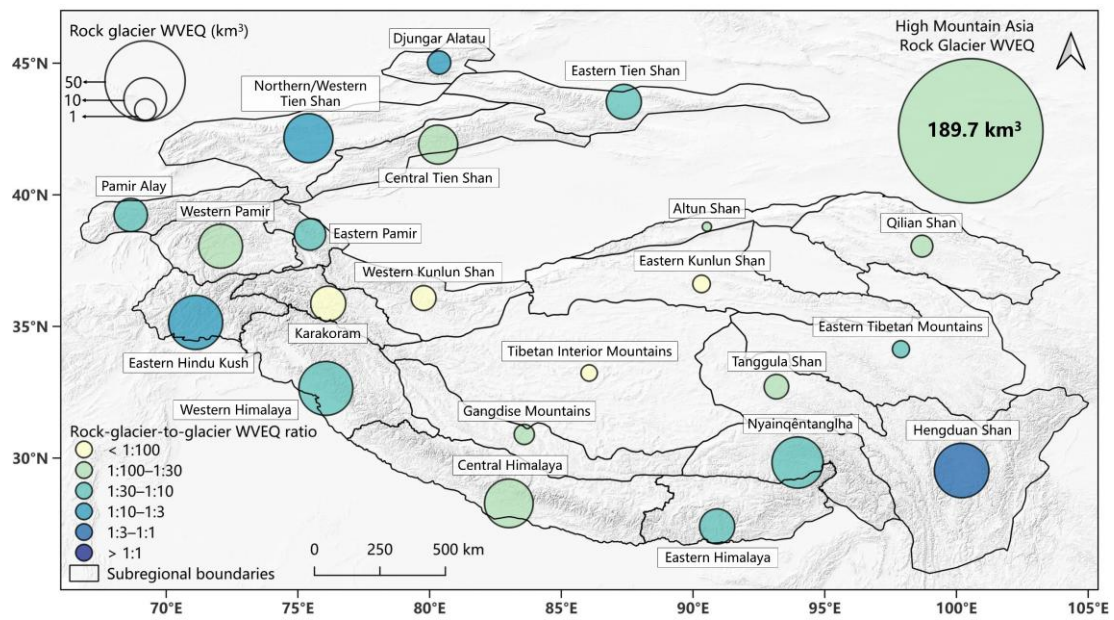


Figure 4.6: Rock glacier WVEQs and rock-glacier-to-glacier WVEQ ratios of different subregions in HMA.

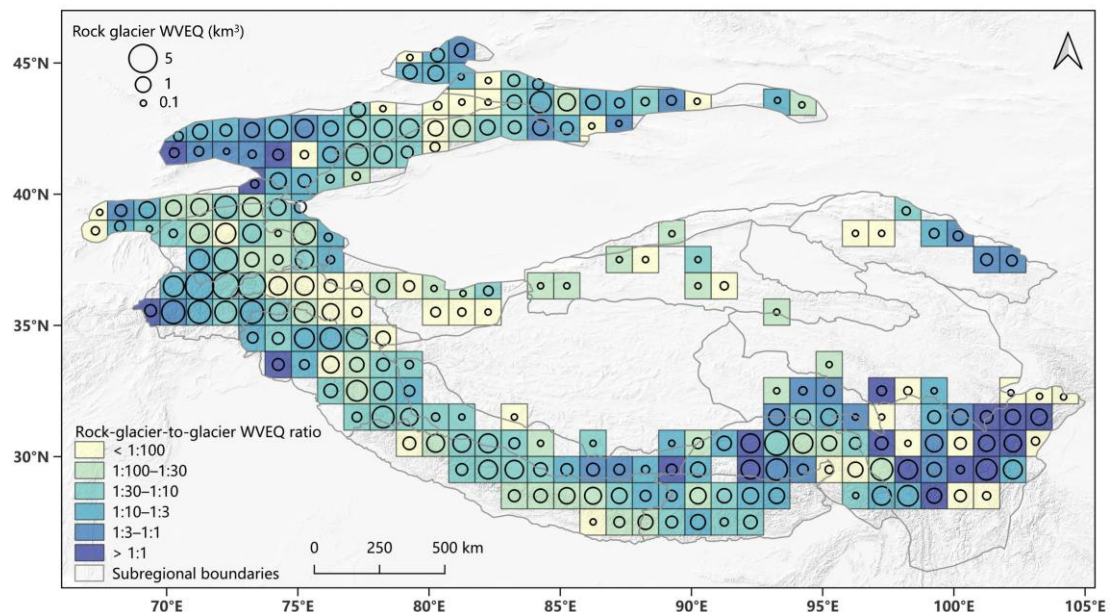


Figure 4.7: Rock glacier WVEQs and rock-glacier-to-glacier WVEQ ratios at  $1^\circ \times 1^\circ$  grids in HMA.

## 4.5 Discussion

### 4.5.1 Uncertainty and limitations

The uncertainties of estimated WVEQs stem from multiple sources, including the estimations of rock glacier ice content and thickness, as well as the limitations in the rock glacier inventory and scaling method. In this study, we focus solely on the uncertainties arising from ice content assumptions and thickness estimates. To provide a conservative assessment, we assume a normal distribution of 1,000 ice content values and employ two empirical thickness models, yielding 2,000 WVEQ estimates. The standard deviation derived from these estimates is used to quantify the uncertainty. For the entire HMA region, uncertainties across subregions are treated as independent and propagated using standard error formulas.

However, ice content within rock glaciers exhibits significant spatial heterogeneity, varying both within individual features and across different rock glaciers ([Jones et al., 2018a](#)). Factors such as activity level ([Arenson & Jakob, 2010](#); [Wagner et al., 2021](#)) and connectivity to upslope units ([Pandey et al., 2024](#)) further influence ice distribution. The lack of detailed data on internal structure and ice content impedes precise water storage assessments. Additionally, the two empirical thickness models used are inherently coarse. Brenning's ([2005b](#)) area-based model relies on a simplified volume-area scaling relationship, while Cicoira et al.'s ([2021](#)) slope-dependent model assumes constant driving stress. Both were developed using limited datasets from the Andes and the Alps, raising uncertainties when applied to HMA due to the absence of region-specific calibration.

Further uncertainties arise from the rock glacier inventory and our deep-learning-based scaling method. Firstly, TPRoGI offers comprehensive coverage but may include misclassified landforms or omit some rock glaciers. Secondly, unlike previous studies that excluded relict rock glaciers ([Jones et al., 2018a, 2021](#); [Wagner et al., 2021](#); [Li et al., 2024](#)), our inventory does not distinguish activity levels, potentially inflating water storage estimates by incorporating inactive forms. Thirdly, to extend the assessment across HMA, we employ a linear scaling method by using TPRoGI to calibrate the WVEQ estimates derived from deep-learning-mapped polygons. However, this approach remains approximate, as it inherently assumes spatial consistency in the relationship between deep-learning-based and inventory-based WVEQ estimates across different regions. Consequently, while providing a

practical solution for regional estimation, this scaling method may introduce significant uncertainties.

To improve the accuracy of rock glacier water storage estimates, future efforts should prioritize field-based data on ice content, internal structure, and thickness, particularly in HMA. Additionally, the compilation of a comprehensive rock glacier inventory for the entire HMA would significantly enhance the reliability of such assessments.

#### **4.5.2 Comparison of rock-glacier-to-glacier WVEQ ratio with other regions**

While the overall rock-glacier-to-glacier WVEQ ratio in HMA is less pronounced than in other regions worldwide (e.g., the Andes), certain subregions of HMA exhibit comparable or even higher rock glacier water storage relative to glaciers. The Hengduan Shan, for example, has a rock-glacier-to-glacier WVEQ ratio of 1:3, which is higher than most documented ratios in the Andes (e.g., 1:7 in the Andes of Santiago (33°–35°S) ([Brenning, 2005a](#)), 1:3 to 1:7 in the Chilean Andes (27°–33°S) ([Azócar and Brenning, 2010](#)), 1:8 in Cerro El Potro (28°S) ([Perucca and Esper Angillieri, 2011](#)), and 1:33 in Bolivian Andes (15°–22°S) ([Rangecroft et al., 2015](#))). Other HMA subregions, such as the Northern/Western Tien Shan (1:7), Djungar Alatau (1:8), and Eastern Hindu Kush (1:9), have WVEQ ratios comparable to those in the drier Central Andes. This suggests that, in some parts of HMA, rock glaciers play a more significant or similar hydrological role than in many Andean valleys.

#### **4.5.3 Future rock glacier water storage**

As climate change drives continued glacier melting and recession across HMA, rock glaciers are likely to assume greater hydrological importance as water reservoirs ([Jones et al., 2021](#)). To project future glacier WVEQ, we employed glacier mass loss projections for 2100 under SSP1-2.6, SSP3-7.0, and SSP5-8.5 scenarios from [Rounce et al. \(2023\)](#), converting ice mass to water volume (1 Gt ≈ 1 km<sup>3</sup>). Our analysis indicates substantial reductions in HMA glacier WVEQ by 2100: 3,109.5 km<sup>3</sup> (SSP1-2.6), 1,976.2 km<sup>3</sup> (SSP3-7.0), and 1,570.7 km<sup>3</sup> (SSP5-8.5).

While current understanding of long-term rock glacier evolution remains limited, differential DEM analyses reveal significantly lower elevation changes in rock glaciers compared to adjacent glaciers ([Müller et al., 2016](#); [Bolch et al., 2019a](#);

[Robson et al., 2022](#)). This suggests rock glaciers exhibit greater climatic resilience, with slower mass loss rates that position them as more stable, long-term water reservoirs. For conservative estimation, we projected potential ice losses of 10% (SSP1-2.6), 30% (SSP3-7.0), and 50% (SSP5-8.5) from rock glaciers by 2100. These projections yield substantially increased rock glacier-to-glacier WVEQ ratios: 1:18 (SSP1-2.6), 1:14 (SSP3-7.0), and 1:16 (SSP5-8.5), indicating a potential doubling of rock glaciers' relative hydrological importance across HMA.

The future role of rock glaciers shows particularly dramatic shifts at regional scales, with the increase of hydrological importance much higher in some regions. Under SSP1-2.6, projected glacier WVEQ declines to 6.3 km<sup>3</sup> (Hengduan Shan), 1.0 km<sup>3</sup> (Dzungar Alatau), and 9.6 km<sup>3</sup> (Northern/Western Tien Shan) ([Rounce et al., 2023](#)). Consequently, rock glacier-to-glacier ratios are expected to reach 4:1, 2:1, and 2:1 in these regions, respectively. These projections suggest that in certain subregions of HMA, rock glaciers may transition from supplementary to primary water sources, potentially surpassing glaciers as the dominant hydrological reservoirs by the end of this century.

#### 4.5.4 Implications for hydrological models and water management strategies

Our assessment reveals that while rock glaciers play a secondary hydrological role to glaciers across HMA as a whole—primarily due to the immense ice volumes stored in major glacier systems like the Karakoram and Western Kunlun Shan—their contributions in specific subregions are substantial and cannot be overlooked. For instance, the Hengduan Shan exhibits a remarkably high rock-glacier-to-glacier WVEQ ratio of 1:3, indicating that rock glaciers store one-third of the water volume contained in glaciers. In arid regions such as the Northern/Western Tien Shan, Dzungar Alatau, and Eastern Hindu Kush, where ratios exceed 1:10, rock glaciers also serve as critical water reservoirs.

Additionally, rock glaciers are frequently found in regions where glaciers are sparse or entirely absent. In such areas, rock glaciers may serve as a critical hydrological resource in sustaining local water systems. The Hengduan Shan exemplifies this pattern: numerous basins lack glaciers yet contain dense clusters of rock glaciers, resulting in very high rock-glacier-to-glacier WVEQ ratios, which even surpass 1:1 in some local regions (Figures 4.7). In these areas, rock glaciers could behave as the

dominant water reservoirs for the local hydrological systems. The pervasive presence of rock glaciers in glacier-deficient zones underscores their hydrological importance, particularly in arid or seasonally dry mountain environments where meltwater from rock glaciers may be a vital buffer against water scarcity.

Our future approximation indicates that the hydrological importance of rock glaciers as water stores relative to glaciers will grow significantly by the end of the 21st century. In subregions like the Hengduan Shan, Djungar Alatau, and Northern/Western Tien Shan, rock glaciers may transition from supplementary to primary water resources as climate-driven glacier retreat accelerates. By 2100, these resilient ice-debris landforms could surpass glaciers as the dominant hydrological reservoirs in certain areas, fundamentally altering regional water availability.

However, rock glaciers remain conspicuously absent from most hydrological models and water management policies despite their significant hydrological values for certain regions and growing importance. This oversight risks misrepresenting future water security in HMA's vulnerable mountain communities. We urge a paradigm shift in research and policy to prioritize rock glaciers, emphasizing detailed mapping, classification, in-situ measurements and monitoring of these ice-rich features in critical regions, and integration into hydrological models and regional water management strategies. Only through such measures can we ensure adaptive management of these "hidden" ice reservoirs in a warming climate.

## **4.6 Conclusions**

In this study, we leveraged deep learning techniques to map rock glaciers from high-resolution satellite imagery, enabling the first comprehensive evaluation of rock glacier water storage across the entire HMA. The main findings from our assessment are as follows:

- (1) HMA's rock glaciers hold  $189.7 \pm 21.7 \text{ km}^3$  of WVEQ, representing a rock-glacier-to-glacier WVEQ ratio of 1:39. This highlights that while glaciers dominate HMA's cryospheric water storage, rock glaciers are a non-negligible reservoir.
- (2) The Hengduan Shan hosts the largest rock glacier WVEQ ( $22.0 \pm 8.9 \text{ km}^3$ ), followed by the Eastern Hindu Kush ( $21.6 \pm 10.1 \text{ km}^3$ ) and Western Himalaya ( $21.4 \pm 9.0 \text{ km}^3$ ).

(3) The Hengduan Shan exhibits the highest relative hydrological significance, with a rock-glacier-to-glacier ratio of 1:3—surpassing most global mountain regions. Other critical areas include the Northern/Western Tien Shan (1:7), Djungar Alatau (1:8), and Eastern Hindu Kush (1:9).

(4) As climate change accelerates glacier retreat, rock glaciers are poised to become increasingly hydrologically important. Our first approximation suggests their relative contribution could double by 2100, particularly in arid and semi-arid subregions where they may transition from supplementary to primary water sources.

Overall, while rock glaciers are not a substitute water resource for vast glaciers in most of HMA, their role in specific subregions (e.g., Tien Shan, Hengduan Shan) is critical and should not be neglected. Moreover, their importance will potentially grow as glaciers diminish, yet these "hidden" ice reservoirs remain overlooked in current hydrological models and water management frameworks. Therefore, we urge prioritizing actions to enhance the monitoring of rock glaciers and integrate them into hydrological models and regional water security plans. By improving the attention on these climate-resilient water reservoirs, HMA can better adapt to the cascading impacts of glacier loss and ensure sustainable water resources for millions across the region.

# Chapter 5 Conclusions and outlook

---

## Abstract

By utilizing high-resolution satellite optical imagery, deep learning, and radar interferometry, this thesis provides a comprehensive investigation of the distribution, velocities and water storage of rock glaciers in High Mountain Asia (HMA), addressing critical knowledge gaps of rock glaciers for this important region. In this chapter, we first consolidate the key research findings from our work. Next, we highlight the innovative contributions and potential impacts of this thesis. Finally, we propose future research directions emerging from the present study.

### 5.1 Conclusions

This thesis presents three studies to comprehensively investigate the distribution, velocities, and water storage of rock glaciers across large regions in HMA.

The first study presents a deep-learning-based method leveraging the DeepLabv3+ network to map rock glaciers from Planet Basemaps. Applying this approach to the Tibetan Plateau, we created a comprehensive inventory of 44,273 rock glaciers.

In the second study, we developed a multi-temporal and multi-geometry InSAR approach for the rapid and systematic assessment of rock glacier velocities across extensive regions. Using the inventory compiled in the first study, we produced downslope velocity fields for 19,727 rock glaciers larger than 0.1 km<sup>2</sup> across the Tibetan Plateau region.

The third study extends the application of the deep learning model from the first study to the entire HMA. Combining the WVEQ derived from the deep-learning-mapped polygons and the Tibetan Plateau inventory, we assessed the water storage of rock glaciers in HMA and evaluated their hydrological significance relative to glaciers.

The key conclusions of this thesis are as follows:

#### Distribution of rock glaciers on the Tibetan Plateau

- 1) Deep learning demonstrates a promising capability in detecting and outlining rock glaciers and can serve as a valuable tool for inventorying rock glaciers

across large regions.

- 2) Rock glaciers are widespread in the northwestern and southeastern plateau and densely distributed in the Western Pamir and Nyainqêntanglha, while they are scarce in the inner plateau.
- 3) The majority of rock glaciers are situated at elevations from 4,000 to 5,500 m a.s.l. and on slopes between 10° and 25° with north and west preferences.
- 4) Rock glaciers show a north-west preference in the eastern plateau, a north-only orientation in the central plateau, and no specific preference in the western plateau.
- 5) Rock glaciers on the Tibetan Plateau cover a total area of 6,000 km<sup>2</sup> with a mean area of 0.14 km<sup>2</sup>, with rock glaciers in the western plateau exhibiting larger areas compared to those in other areas.

#### *Velocities of rock glaciers on the Tibetan Plateau*

- 1) The velocities derived from our InSAR-based approach show statistically significant correlations with all comparison datasets but tend to underestimate magnitudes.
- 2) The mean relative difference is approximately 20% when compared to velocities derived from Pléiades and aerial images, which nevertheless increases to 50% when compared to GNSS measurements.
- 3) The overall median velocity of all assessed rock glaciers for the Tibetan Plateau region is 17 cm/yr.
- 4) Rock glaciers exhibit contrasting velocities on the Tibetan Plateau with on average faster movement (median = 30 cm/yr) in the westerlies domain than those in the monsoon domain (median = 13 cm/yr).

#### *Water storage of rock glaciers in HMA*

- 1) While rock glaciers are not a substitute water resource for glaciers in most of HMA, their role in specific subregions is critical and cannot be neglected.
- 2) The total rock glacier WVEQ in HMA is  $189.7 \pm 21.7$  km<sup>3</sup>, representing ~2.5% (1:39 ratio) of the water stored in glaciers.
- 3) At the regional scale, rock glacier WVEQs exhibit significant spatial variability.

The Hengduan Shan holds the largest rock glacier WVEQ ( $22.0 \pm 8.9 \text{ km}^3$ ) and the highest rock-glacier-to-glacier ratio (1:3).

- 4) As climate change accelerates glacier mass loss, the relative hydrological importance of rock glaciers is likely to grow in the coming decades. Our first approximation indicates a potential doubling of rock glaciers' relative hydrological importance across HMA by the end of this century.

## **5.2 Innovative merits and potential impacts**

This thesis introduces novel methods for mapping rock glaciers and assessing their velocities, based on which we created benchmark datasets encompassing the locations, boundaries, velocities, and water storage of rock glaciers in HMA. The innovative contributions of this research can be summarized as follows:

### *Deep-learning-based Mapping and Inventorying*

A systematic, deep-learning-based approach for mapping and inventorying rock glaciers was developed, rigorously validated, and applied for the first time to create rock glacier inventories in previously uncharted regions. This approach not only automates the detection of rock glaciers, significantly accelerating the production of inventories in uncharted regions, but also serves as a tool to identify potentially overlooked rock glaciers in already mapped regions.

### *Comprehensive Inventory for the Tibetan Plateau*

The first comprehensive rock glacier inventory for the Tibetan Plateau region has been compiled. This inventory has the most extensive collection of rock glaciers to date, enhancing our understanding of the distribution and characteristics of rock glaciers on the Tibetan Plateau. This benchmark dataset provides a foundation for investigating various scientific questions related to rock glaciers and mountain permafrost on the Tibetan Plateau.

### *InSAR Methodology for Velocity Assessment*

A multi-temporal and multi-geometry InSAR method was developed for the systematic production of rock glacier velocity fields, enabling rapid and consistent assessments across large regions. While numerous rock glacier inventories have been compiled globally, the kinematic status of most mapped rock glaciers remains unknown. Our approach provides an effective and efficient means to assess the

kinematic status of these mapped features.

*Large-scale Rock Glacier Velocity Dataset*

The first large-scale rock glacier velocity dataset for the Tibetan Plateau region has been produced, offering unprecedented insights into the spatial patterns of rock glacier velocities across extensive areas. This groundbreaking dataset lays the foundation for establishing long-term rock glacier monitoring sites, enhances understanding of their significance as water resources, provides a basis for inferring their activity levels, and supports the assessment of potential geohazards.

*Hydrological Significance of Rock Glaciers as water stores*

The first comprehensive assessment of rock glacier water storage across the entire HMA was conducted, significantly advancing our understanding of the hydrological importance of rock glaciers in the region. The results of this assessment will enhance current climate and hydrological models, which overlook the contributions of rock glaciers, and support engagement with local communities and stakeholders to develop regional water management strategies and climate resilience initiatives.

Both the deep-learning-based mapping method and the InSAR-based velocity assessment method are readily transferable to other regions worldwide, providing powerful tools to facilitate the inventorying and velocity assessment of rock glaciers globally. The benchmark datasets produced in this thesis represent a significant contribution to the understanding, monitoring, and assessment of permafrost on the Tibetan Plateau, particularly in the context of climate change. The water storage assessment will enhance future scenario modeling, contributing to a better understanding of sustainable water management in HMA.

### **5.3 Future work**

Our work can be further improved in the following aspects: (1) Enhancement of the deep-learning-based rock glacier mapping method; (2) Enhancement and application of the InSAR-based rock glacier velocity assessment method; (3) Investigating the environmental controls on rock glacier velocities; (4) Investigating the long-term evolutions on selected rock glaciers.

### 5.3.1 Enhancement of the deep-learning-based rock glacier mapping method

While our first work has demonstrated the potential of deep learning for mapping rock glaciers in unexplored regions, the model's outputs still suffer from significant uncertainties, including imprecise boundaries, false positives, and missed detections. These limitations necessitate considerable manual correction, hindering the efficient creation of large-scale rock glacier inventories. To improve the model's accuracy and reduce reliance on labor-intensive post-processing, future efforts should focus on three key areas: leveraging multi-source satellite imagery, enhancing label data quality, and adopting more advanced deep learning architectures.

One major limitation of our current approach is its dependence on Planet Basemaps, a commercial dataset with restricted accessibility. To ensure broader applicability, we should explore open-access alternatives such as Sentinel-2 and Landsat imagery. Although these datasets offer lower spatial resolution, their global coverage and cost-free availability make them practical for large-scale applications. Preliminary experiments are needed to evaluate whether their performance is comparable to that of high-resolution commercial imagery. If successful, this shift would significantly improve the scalability of our method, particularly in data-scarce regions.

Another critical challenge lies in the inconsistency of existing label data. Our current training datasets are derived from regional inventories compiled by different institutions using varying methodologies, which may introduce noise and bias. A promising solution is the Rock Glacier Inventory Kinematics (RGIK) initiative ([Rouyet et al., 2025](#)), which provides standardized inventories for 12 global regions using unified mapping protocols. These high-quality datasets could serve as a robust benchmark for model training and validation. As more regions are inventoried under this framework, the growing volume of consistent label data will further enhance model generalizability and performance.

Finally, rapid advancements in deep learning offer opportunities to improve our model's architecture. Traditional CNNs, while effective at local feature extraction, often struggle with long-range spatial dependencies—a key limitation in delineating rock glacier boundaries. Emerging Transformer-based models, such as Swin Transformer ([Liu et al., 2021](#)) and SegFormer ([Xie et al., 2021](#)), have demonstrated superior performance in semantic segmentation by capturing global context. Hybrid architectures, such as CvT ([Wu et al., 2021](#)) and CoAtNet ([Dai et al., 2021](#)) that

combine CNNs' local precision with Transformers' global modeling could further refine boundary accuracy and reduce errors. Testing these state-of-the-art approaches may yield significant gains in automation reliability.

By integrating open-access satellite data, standardized inventories, and cutting-edge neural networks, we can develop a more accurate and scalable rock glacier mapping pipeline. This would minimize manual intervention, accelerate inventory generation, and support global monitoring efforts in periglacial environments.

### **5.3.2 Enhancement and application of the InSAR-based rock glacier velocity assessment method**

Our second study developed an InSAR-based stacking framework for large-scale rock glacier velocity assessment. However, the reliance on C-band Sentinel-1 data with a fixed 12-day temporal baseline limits the method's reliability to rock glaciers larger than 0.1 km<sup>2</sup> moving at velocities between 10 and 100 cm/yr. To enhance the framework's performance, several key challenges in InSAR-based velocity assessment must be addressed. First, more effective atmospheric error correction methods are needed, particularly for mountainous terrain. Innovative approaches for automatically selecting stable reference points in non-moving areas could significantly improve accuracy. Second, incorporating interferograms with variable temporal baselines (e.g., 6, 24, 36, or 60 days) and multi-frequency data (e.g., L-band) may enhance velocity detection capabilities (RGIK, 2022a). However, new methodologies must be developed to effectively integrate and interpret these diverse datasets. Third, more evaluation and validation studies on InSAR-derived velocity products are needed to evaluate the performance of different InSAR methods for rock glacier velocity assessment.

Our framework is readily transferable to other regions globally, enabling large-scale assessment of rock glacier velocities. Numerous regional inventories have been compiled worldwide, including in the Himalayas ([Harrison et al., 2024](#)), the United States ([Johnson et al., 2021](#)), and the Austrian Alps ([Wagner et al., 2020b](#)). While these inventories document rock glacier distribution, their kinematic status remains largely unknown. Applying our method could rapidly assess the movement rates of these compiled rock glaciers, which is beneficial for selecting detailed monitoring sites, evaluating mountain hydrology, refining permafrost models, and supporting hazard assessments in these regions.

### 5.3.3 Investigating the environmental controls on rock glacier velocities

Our second study revealed contrasting rock glacier velocity patterns across different climatic domains on the Tibetan Plateau: rock glaciers in the westerlies-dominated region move significantly faster on average than those in the monsoon-dominated region. Additionally, we identified statistically significant correlations between rock glacier velocities and several environmental variables, including positive associations with area and slope, and negative correlations with minimum elevation, Mean Annual Air Temperature (MAAT), and annual precipitation. These findings raise intriguing questions about the underlying mechanisms driving these contrasting patterns and the environmental controls on rock glacier dynamics.

To further investigate these relationships, we will use the velocity products generated in our second study, focusing on rock glaciers larger than 0.1 km<sup>2</sup> with velocities between 10 and 100 cm/yr to ensure data reliability. We will analyze six key environmental variables: rock glacier area, slope, minimum elevation, MAAT, annual precipitation, and glacial influence. The first three variables will be extracted from the inventory compiled in our first study, while MAAT and precipitation data will be sourced from the high-resolution (1/30°) climate dataset by [Jiang et al. \(2023\)](#). Given the potential impact of glaciers on nearby rock glacier dynamics, we will also classify rock glaciers based on their upslope connections (e.g., talus-connected vs. glacier-connected) to account for glacial influence.

Our analytical approach will consist of three main steps:

1. Pearson correlation analysis – We will group rock glaciers into 0.1 cm/yr velocity bins, compute mean velocities and environmental variables within each bin, and assess pairwise correlations.
2. Machine learning modeling – We will employ three models—Support Vector Machine (SVM; Cortes and Vapnik, 1995), XGBoost (Chen and Cuestrin, 2016), and Random Forest (Breiman, 2001)—to model the relationships between velocities and environmental factors.
3. SHAP analysis (Lundberg et al., 2020) – To interpret model outputs, we will quantify the relative importance of each environmental variable using SHapley Additive exPlanations (SHAP).

This multi-method approach will provide a robust assessment of the environmental

controls on rock glacier velocities, offering new insights into their dynamic behavior under varying climatic and topographic conditions.

### **5.3.4 Investigating the long-term evolutions of selected rock glaciers**

Our work presents the distribution and kinematic status of rock glaciers on the Tibetan Plateau, which serves as an important baseline information for selecting rock glaciers for more detailed long-term evolution studies. We will use declassified historical high-resolution stereo Corona Keyhole (KH-4B data from 1967-1972 with a spatial resolution of 1.8 m and contemporary high-resolution stereo satellite Pléiades imagery with a spatial resolution of 0.5 m to investigate long-term changes in surface elevation and movement rate of rock glaciers since the 1970s.

We will use the Remote Sensing Software Package Graz (RSG), developed by Joanneum Research Graz, to process the Corona KH-4B stereo panoramic imagery for generating DEMs and orthorectified images. The Corona KH-4 satellite missions acquired panoramic stereo imagery with high spatial resolution from the 1960s, which were designed primarily for strategic surveillance of the former Soviet Union during the Cold War. The potential of Corona KH-4 satellite data has yet to be leveraged since declassified due to the complexities arising from handling image geometry, film distortions, and limited metadata ([Ghuffar et al., 2022](#)).

To generate high-quality DEMs from Pléiades data, the open-source automated DEM production software Ames Stereo Pipeline (ASP) will be utilized. Developed by the National Aeronautics and Space Administration (NASA), ASP is a suite of free and open source automated stereogrammetry tools designed to process stereo images captured from satellites. This software can produce various cartographic products, including DEM and ortho-projected images ([Beyer et al., 2018](#)).

To analyze long-term surface elevation changes in rock glaciers, we will employ xDEM, an open-source package designed for robust and modular DEM analysis. The workflow begins with co-registering multi-temporal DEMs to ensure precise alignment, using stable terrain areas beyond the rock glacier boundaries. To prevent the inclusion of deforming regions in the co-registration process, a 300-meter buffer will be applied around the rock glacier outlines. Following co-registration, elevation changes will be calculated through DEM differencing, producing detailed surface elevation change maps.

Horizontal flow velocities of the rock glaciers will be derived using an image correlation approach ([Wood et al., 2025](#)). We will test varying combinations of search and reference window sizes to identify the most reliable results.

To assess long-term rock glacier evolution, we will compare their elevation changes and horizontal velocities with those of nearby cryospheric features, such as glaciers, dead ice, and debris-covered glaciers. Additionally, long-term meteorological records—including in-situ measurements and ERA5 climate reanalysis data—will be analyzed to evaluate the climatological drivers behind rock glacier dynamics.

# Outputs

---

## Publications

**Zhangyu Sun**, Yan Hu, Adina Racoviteanu, Lin Liu, Stephan Harrison, Xiaowen Wang, Jixin Cai, Xin Guo, Yujun He, and Hailun Yuan (2024). TPRoGI: A comprehensive rock glacier inventory for the Tibetan Plateau using deep learning. *Earth System Science Data*, 16(12), 5703–5721. <https://doi.org/10.5194/essd-16-5703-2024>.

**Zhangyu Sun**, Lin Liu, Chengyan Fan, Yan Hu, Francesca Baldacchino, Atanu Bhattacharya, Ella Wood, and Tobias Bolch. Unveiling large-scale velocity characteristics of rock glaciers in the Tibet-Pamir-Karakoram region using InSAR. Manuscript under review.

**Zhangyu Sun**, Lin Liu, Stephan Harrison, Tobias Bolch. Rock glaciers represent important water reservoirs in High Mountain Asia. Manuscript in preparation.

## Conferences

**Zhangyu Sun**, Lin Liu, Yan Hu, and Xiaowen Wang (2024). TPRoGI: A comprehensive rock glacier inventory for the Tibetan Plateau using deep learning. The 3rd Chinese Conference of Cryospheric Science, Lingshui, Hainan, China.

**Zhangyu Sun**, Lin Liu, Yan Hu, and Chengyan Fan (2024). Assessing rock glacier velocities on the Tibetan Plateau using satellite SAR interferometry, EGU General Assembly Conference, Vienna, Austria.

Adina Racoviteanu, **Zhangyu Sun**, Yan Hu, Lin Liu, and Stephan Harrison (2024). Rock glacier inventorying and validation across the Hindu Kush Himalaya from deep learning and high-resolution images, EGU General Assembly Conference, Vienna, Austria.

**Zhangyu Sun**, Yan Hu, Lin Liu, Adina Racoviteanu, and Stephan Harrison (2023). Mapping and inventorying rock glaciers on the Tibetan Plateau from Planet Basemaps using deep learning, International Symposium on Third Pole Environment, Chongqing, China.

**Zhangyu Sun**, Yan Hu, Lin Liu, Adina Racoviteanu, and Stephan Harrison (2023).

Mapping and inventorying rock glaciers on the Tibetan Plateau from Planet Basemaps using deep learning, EGU General Assembly Conference, Vienna, Austria.

**Zhangyu Sun**, Yan Hu, Lin Liu, Adina Racoviteanu, and Stephan Harrison (2023). Mapping and inventorying rock glaciers on the Tibetan Plateau from Planet Basemaps using deep learning, The Sixth European Conference on Permafrost (EUCOP6), Puigcerdà, Catalonia, Spain.

**Zhangyu Sun**, Yan Hu, Lin Liu, Adina Racoviteanu, and Stephan Harrison (2022). Mapping Rock Glaciers on the Tibetan Plateau from Planet Basemaps Using Deep Learning, AGU Fall Meeting, Chicago, U.S.

## **Data**

**Zhangyu Sun**, Yan Hu, Adina Racoviteanu, Lin Liu, Stephan Harrison, Xiaowen Wang, Jiaxin Cai, Xin Guo, Yujun He, and Hailun Yuan (2024). TPRoGI: a comprehensive rock glacier inventory for the Tibetan Plateau using deep learning (1.0). Zenodo. <https://doi.org/10.5281/zenodo.10732042>.

**Zhangyu Sun**. (2024). Downslope velocity fields of rock glaciers in the Tibet-Pamir-Karakoram region. Zenodo. <https://doi.org/10.5281/zenodo.13347728>.

**Zhangyu Sun**, Lin Liu, Yan Hu, and Xiaowen Wang (2024). Rock glacier inventory for the Tibetan Plateau (2021). National Tibetan Plateau / Third Pole Environment Data Center. <https://doi.org/10.11888/Cryos.tpdc.301688>.

# Bibliography

---

- Arendonk, L., Hoelzle, M., & Springman, S. (2002). Borehole deformation measurements and internal structure of some rock glaciers in Switzerland. *Permafrost and Periglacial Processes*, 13(2), 117-135. <https://doi.org/10.1002/ppp.414>.
- Arendonk, L. U., & Jakob, M. (2010). The significance of rock glaciers in the dry Andes—a discussion of Azócar and Brenning (2010) and Brenning and Azócar (2010). *Permafrost and Periglacial Processes*, 21(3), 282-285. <https://doi.org/10.1002/ppp.693>.
- Azócar, G. F., & Brenning, A. (2010). Hydrological and geomorphological significance of rock glaciers in the dry Andes, Chile (27–33 S). *Permafrost and Periglacial Processes*, 21(1), 42-53. <https://doi.org/10.1002/ppp.669>.
- Barboux, C., Delaloye, R., & Lambiel, C. (2014). Inventorying slope movements in an Alpine environment using DInSAR. *Earth surface processes and landforms*, 39(15), 2087-2099. <https://doi.org/10.1002/esp.3603>.
- Barboux, C., Strozzi, T., Delaloye, R., Wegmüller, U., & Collet, C. (2015). Mapping slope movements in Alpine environments using TerraSAR-X interferometric methods. *ISPRS journal of photogrammetry and remote sensing*, 109, 178-192. <https://doi.org/10.1016/j.isprsjprs.2015.09.010>.
- Barsch, D.: Rock glaciers, Series in Physical Environment, Springer, Berlin, 16, 331 pp, 1996.
- Berthling, I., Etzelmüller, B., Eiken, T., & Sollid, J. L. (1998). Rock glaciers on Prins Karls Forland, Svalbard. I: internal structure, flow velocity and morphology. *Permafrost and Periglacial Processes*, 9(2), 135-145. [https://doi.org/10.1002/\(SICI\)1099-1530\(199804/06\)9:2<135::AID-PPP284>3.0.CO;2-R](https://doi.org/10.1002/(SICI)1099-1530(199804/06)9:2<135::AID-PPP284>3.0.CO;2-R).
- Berthling, I. (2011). Beyond confusion: Rock glaciers as cryo-conditioned landforms. *Geomorphology*, 131(3-4), 98-106. <https://doi.org/10.1016/j.geomorph.2011.05.002>.
- Bertone, A., Zucca, F., Marin, C., Notarnicola, C., Cuozzo, G., Krainer, K., Mair, V., Riccardi, P., Callegari, M., & Seppi, R. (2019). An Unsupervised Method to Detect Rock Glacier Activity by Using Sentinel-1 SAR Interferometric Coherence: A Regional-Scale Study in the Eastern European Alps. *Remote Sensing*, 11(14), Article 14. <https://doi.org/10.3390/rs11141711>.
- Bertone, A., Barboux, C., Bodin, X., Bolch, T., Brardinoni, F., Caduff, R.,

## BIBLIOGRAPHY

- Christiansen, H. H., Darrow, M. M., Delaloye, R., Etzelmüller, B., Humlum, O., Lambiel, C., Lilleøren, K. S., Mair, V., Pellegrinon, G., Rouyet, L., Ruiz, L., & Strozzi, T. (2022). Incorporating InSAR kinematics into rock glacier inventories: Insights from 11 regions worldwide. *The Cryosphere*, 16(7), 2769–2792. <https://doi.org/10.5194/tc-16-2769-2022>.
- Beyer, R. A., Alexandrov, O., & McMichael, S. (2018). The Ames Stereo Pipeline: NASA's Open Source Software for Deriving and Processing Terrain Data. *Earth and Space Science*, 5(9), 537–548. <https://doi.org/10.1029/2018EA000409>.
- Bhattacharya, A., Bolch, T., Mukherjee, K., King, O., Menounos, B., Kapitsa, V., Neckel, N., Yang, W., & Yao, T. (2021). High Mountain Asian glacier response to climate revealed by multi-temporal satellite observations since the 1960s. *Nature Communications*, 12(1), Article 1. <https://doi.org/10.1038/s41467-021-24180-y>.
- Blöthe, J. H., Rosenwinkel, S., Höser, T., & Korup, O. (2019). Rock-glacier dams in High Asia. *Earth Surface Processes and Landforms*, 44(3), 808-824. <https://doi.org/10.1002/esp.4538>.
- Bodin, X., Rojas, F., & Brenning, A. (2010). Status and evolution of the cryosphere in the Andes of Santiago (Chile, 33.5 S.). *Geomorphology*, 118(3-4), 453-464. <https://doi.org/10.1016/j.geomorph.2010.02.016>.
- Boeckli, L., Brenning, A., Gruber, S., & Noetzli, J. (2012a). A statistical approach to modelling permafrost distribution in the European Alps or similar mountain ranges. *The Cryosphere*, 6(1), 125-140. <https://doi.org/10.5194/tc-6-125-2012>.
- Boeckli, L., Brenning, A., Gruber, S., & Noetzli, J. (2012b). Permafrost distribution in the European Alps: calculation and evaluation of an index map and summary statistics. *The Cryosphere*, 6(4), 807-820. <https://doi.org/10.5194/tc-6-807-2012>.
- Bolch, T., Marchenko, S. S. (2009): Significance of glaciers, rockglaciers and ice-rich permafrost in the Northern Tien Shan as water towers under climate change conditions. In: L. Braun, W. Hagg, I. V. Severskiy & G. J. Young (Eds.): Selected papers from the Workshop "Assessment of Snow, Glacier and Water Resources in Asia" held in Almaty, Kazakhstan, 28-30 Nov. 2006, IHP/HWRP-Berichte, 8: 132-144.
- Bolch, T., & Gorbunov, A. P. (2014). Characteristics and Origin of Rock Glaciers in Northern Tien Shan (Kazakhstan/Kyrgyzstan). *Permafrost and Periglacial Processes*, 25(4), 320–332. <https://doi.org/10.1002/ppp.1825>.
- Bolch, T., Shea, J. M., Liu, S., Azam, F. M., Gao, Y., Gruber, S., Immerzeel, W. W., Kulkarni, A., Li, H., Tahir, A. A., Zhang, G., & Zhang, Y. (2019a). Status and Change of the Cryosphere in the Extended Hindu Kush Himalaya Region. In P.

## BIBLIOGRAPHY

- Wester, A. Mishra, A. Mukherji, & A. B. Shrestha (Eds.), The Hindu Kush Himalaya Assessment: Mountains, Climate Change, Sustainability and People (pp. 209–255). Springer International Publishing. [https://doi.org/10.1007/978-3-319-92288-1\\_7](https://doi.org/10.1007/978-3-319-92288-1_7).
- Bolch, T., Rohrbach, N., Kutuzov, S., Robson, B. A., & Osmonov, A. (2019b). Occurrence, evolution and ice content of ice-debris complexes in the Ak-Shiirak, Central Tien Shan revealed by geophysical and remotely-sensed investigations. *Earth Surface Processes and Landforms*, 44(1), 129-143. <https://doi.org/10.1002/esp.4487>.
- Bolch, T., Yao, T., Bhattacharya, A., Hu, Y., King, O., Liu, L., Pronk, J. B., Rastner, P., & Zhang, G. (2022). Earth Observation to Investigate Occurrence, Characteristics and Changes of Glaciers, Glacial Lakes and Rock Glaciers in the Poiqu River Basin (Central Himalaya). *Remote Sensing*, 14(8), Article 8. <https://doi.org/10.3390/rs14081927>.
- Brardinoni, F., Scotti, R., Sailer, R., & Mair, V. (2019). Evaluating sources of uncertainty and variability in rock glacier inventories. *Earth Surface Processes and Landforms*, 44(12), 2450-2466. <https://doi.org/10.1002/esp.4674>.
- Breiman, L. (2001). Random forests. *Machine learning*, 45, 5-32. <https://doi.org/10.1023/A:1010933404324>.
- Brencher, G., Handwerger, A. L., & Munroe, J. S. (2021). InSAR-based characterization of rock glacier movement in the Uinta Mountains, Utah, USA. *The Cryosphere*, 15(10), 4823-4844. <https://doi.org/10.5194/tc-15-4823-2021>.
- Brenning, A. (2005a). Geomorphological, hydrological and climatic significance of rock glaciers in the Andes of Central Chile (33–35 S). *Permafrost and Periglacial Processes*, 16(3), 231-240. <https://doi.org/10.1002/ppp.528>.
- Brenning, A. (2005b). Climatic and geomorphological controls of rock glaciers in the Andes of Central Chile.
- Brun, F., Berthier, E., Wagnon, P., Kääb, A., & Treichler, D. (2017). A spatially resolved estimate of High Mountain Asia glacier mass balances from 2000 to 2016. *Nature geoscience*, 10(9), 668-673. <https://doi.org/10.1038/ngeo2999>.
- Buchelt, S., Blöthe, J. H., Kuenzer, C., Schmitt, A., Ullmann, T., Philipp, M., & Kneisel, C. (2023). Deciphering Small-Scale Seasonal Surface Dynamics of Rock Glaciers in the Central European Alps Using DInSAR Time Series. *Remote Sensing*, 15(12), Article 12. <https://doi.org/10.3390/rs15122982>.
- Cai, J., Wang, X., Liu, G., & Yu, B. (2021). A comparative study of active rock glaciers mapped from geomorphic-and kinematic-based approaches in daxue shan, southeast tibetan plateau. *Remote Sensing*, 13(23), 4931.

## BIBLIOGRAPHY

- <https://doi.org/10.3390/rs13234931>.
- Cai, J., Wang, X., Wu, T., Wu, R., & Liu, G. (2024). Characterizing the kinematics of active rock glaciers in Daxue Shan, southeastern Tibetan plateau, using SAR interferometry and generalized boosted modeling. *Remote Sensing of Environment*, 313, 114352. <https://doi.org/10.1016/j.rse.2024.114352>.
- Cao, B., Gruber, S., Zheng, D., & Li, X. (2020). The ERA5-Land soil temperature bias in permafrost regions. *The Cryosphere*, 14(8), 2581-2595. <https://doi.org/10.5194/tc-14-2581-2020>.
- Cao, B., Li, X., Feng, M., & Zheng, D. (2021). Quantifying overestimated permafrost extent driven by rock glacier inventory. *Geophysical Research Letters*, 48(8), e2021GL092476. <https://doi.org/10.1029/2021GL092476>.
- Capps Jr, S. R. (1910). Rock glaciers in Alaska. *The journal of Geology*, 18(4), 359-375. <https://doi.org/10.1086/621746>.
- Chen, L. C., Zhu, Y., Papandreou, G., Schroff, F., & Adam, H. (2018). Encoder-decoder with atrous separable convolution for semantic image segmentation. In *Proceedings of the European conference on computer vision (ECCV)* (pp. 801-818). <https://doi.org/10.48550/arXiv.1802.02611>.
- Chen, T., & Guestrin, C. (2016, August). Xgboost: A scalable tree boosting system. In *Proceedings of the 22nd ACM SIGKDD international conference on knowledge discovery and data mining* (pp. 785-794). <https://doi.org/10.1145/2939672.2939785>.
- Chollet, F. (2017). Xception: Deep learning with depthwise separable convolutions. In *Proceedings of the IEEE conference on computer vision and pattern recognition* (pp. 1251-1258). <https://doi.org/10.48550/arXiv.1610.02357>.
- Cicoira, A., Beutel, J., Faillettaz, J., Gärtner-Roer, I., & Vieli, A. (2019a). Resolving the influence of temperature forcing through heat conduction on rock glacier dynamics: a numerical modelling approach. *The Cryosphere*, 13(3), 927-942. <https://doi.org/10.5194/tc-13-927-2019>.
- Cicoira, A., Beutel, J., Faillettaz, J., & Vieli, A. (2019b). Water controls the seasonal rhythm of rock glacier flow. *Earth and Planetary Science Letters*, 528, 115844. <https://doi.org/10.1016/j.epsl.2019.115844>.
- Cicoira, A., Marcer, M., Gärtner-Roer, I., Bodin, X., Arenson, L. U., & Vieli, A. (2021). A general theory of rock glacier creep based on in-situ and remote sensing observations. *Permafrost and Periglacial Processes*, 32(1), 139-153. <https://doi.org/10.1002/ppp.2090>.
- Cicoira, A., Weber, S., Biri, A., Buchli, B., Delaloye, R., Da Forno, R., Gärtner-Roer,

## BIBLIOGRAPHY

- I., Gruber, S., Gsell, T., Hasler, A., Lim, R., Limpach, P., Mayoraz, R., Meyer, M., Noetzli, J., Phillips, M., Pointner, E., Raetzo, H., Scapozza, C., ... Beutel, J. (2022). In situ observations of the Swiss periglacial environment using GNSS instruments. *Earth System Science Data*, 14(11), 5061–5091.  
<https://doi.org/10.5194/essd-14-5061-2022>.
- Corte, A. (1976). The hydrological significance of rock glaciers. *Journal of Glaciology*, 17(75), 157-158. <https://doi.org/10.3189/S0022143000030859>.
- Cortes, C., & Vapnik, V. (1995). Support-vector networks. *Machine Learning*, 20(3), 273–297. <https://doi.org/10.1007/BF00994018>.
- Crippa, C., Steger, S., Cuozzo, G., Bearzot, F., Mair, V., Notarnicola, C., 2024. Optimizing rock glaciers activity classification in South Tyrol (North-East Italy): integrating multisource data with statistical modelling. *EGUsphere* 2024, 1-33.  
<https://doi.org/10.5194/egusphere-2024-1511>.
- Crippen, R., Buckley, S., Agram, P., Belz, E., Gurrola, E., Hensley, S., Kobrick, M., Lavalle, M., Martin, J., Neumann, M., Nguyen, Q., Rosen, P., Shimada, J., Simard, M., & Tung, W. (2016). NASADEM GLOBAL ELEVATION MODEL: METHODS AND PROGRESS. *ISPRS - International Archives of the Photogrammetry, Remote Sensing and Spatial Information Sciences*, XLI-B4, 125–128. <https://doi.org/10.5194/isprsarchives-XLI-B4-125-2016>.
- Croce, F. A., & Milana, J. P. (2002). Internal structure and behaviour of a rock glacier in the arid Andes of Argentina. *Permafrost and Periglacial Processes*, 13(4), 289-299. <https://doi.org/10.1002/ppp.415>.
- Cusicanqui, D., Lacroix, P., Bodin, X., Robson, B. A., Kääb, A., MacDonell, S., 2024. Detection and reconstruction of rock glaciers kinematic over 24 years (2000–2024) from Landsat imagery. *EGUsphere* 2024, 1-41.  
<https://doi.org/10.5194/egusphere-2024-2393>.
- Dai, Z., Liu, H., Le, Q. V., & Tan, M. (2021). CoAtNet: Marrying Convolution and Attention for All Data Sizes (arXiv:2106.04803). arXiv.  
<https://doi.org/10.48550/arXiv.2106.04803>.
- Dehecq, A., Gourmelen, N., Gardner, A. S., Brun, F., Goldberg, D., Nienow, P. W., Berthier, E., Vincent, C., Wagnon, P., & Trouvé, E. (2019). Twenty-first century glacier slowdown driven by mass loss in High Mountain Asia. *Nature Geoscience*, 12(1), 22–27. <https://doi.org/10.1038/s41561-018-0271-9>.
- Delaloye, R., Strozzi, T., Lambiel, C., & Perruchoud, E. (2008). Landslide-like development of rockglaciers detected with ERS-1/2 SAR interferometry. In *Proceedings ESA FRINGE Symposium 2007*.
- Delaloye, R., Lambiel, C., & Gärtner-Roer, I. (2010). Overview of rock glacier

## BIBLIOGRAPHY

- kinematics research in the Swiss Alps. *Geographica Helvetica*, 65(2), 135-145. <https://doi.org/10.5194/gh-65-135-2010>.
- Delaloye, R., Barboux, C., Bodin, X., Brenning, A., Hartl, L., Hu, Y., et al. (2018). Rock glacier inventories and kinematics: A new IPA Action Group. In 5th European conference on permafrost – Book of abstracts (pp. 391–392). Chamonix, France.
- Elconin, R. F., & LaChapelle, E. R. (1997). Flow and internal structure of a rock glacier. *Journal of Glaciology*, 43(144), 238-244. <https://doi.org/10.3189/S002214300000318X>.
- Erharder, G. H., Wagner, T., Winkler, G., & Marcher, T. (2022). Machine learning—an approach for consistent rock glacier mapping and inventorying—example of Austria. *Applied Computing and Geosciences*, 16, 100093. <https://doi.org/10.1016/j.acags.2022.100093>.
- Eriksen, H. Ø., Lauknes, T. R., Larsen, Y., Corner, G. D., Bergh, S. G., Dehls, J., & Kierulf, H. P. (2017). Visualizing and interpreting surface displacement patterns on unstable slopes using multi-geometry satellite SAR interferometry (2D InSAR). *Remote Sensing of Environment*, 191, 297-312. <https://doi.org/10.1016/j.rse.2016.12.024>.
- European Space Agency, 2024. Copernicus Global Digital Elevation Model. Distributed by OpenTopography. <https://doi.org/10.5069/G9028PQB>. Accessed: 2024-07-26.
- Fan, C., Liu, L., Zhao, Z., & Mu, C. (2025). Pronounced Underestimation of Surface Deformation Due To Unwrapping Errors Over Tibetan Plateau Permafrost by Sentinel - 1 InSAR: Identification and Correction. *Journal of Geophysical Research: Earth Surface*, 130(3), e2024JF007854. <https://doi.org/10.1029/2024JF007854>.
- Farinotti, D., Huss, M., Fürst, J. J., Landmann, J., Machguth, H., Maussion, F., & Pandit, A. (2019). A consensus estimate for the ice thickness distribution of all glaciers on Earth. *Nature Geoscience*, 12(3), 168-173. <https://doi.org/10.1038/s41561-019-0300-3>.
- Gardner, J. (1978). Wenkchemna Glacier: ablation complex and rock glacier in the Canadian Rocky Mountains. *Canadian Journal of Earth Sciences*, 15(7), 1200-1204. <https://doi.org/10.1139/e78-125>.
- Geiger, S. T., Daniels, J. M., Miller, S. N., & Nicholas, J. W. (2014). Influence of rock glaciers on stream hydrology in the La Sal Mountains, Utah. Arctic, Antarctic, and Alpine Research, 46(3), 645-658. <https://doi.org/10.1657/1938-4246-46.3.645>.

## BIBLIOGRAPHY

- Ghuffar, S., Bolch, T., Rupnik, E., & Bhattacharya, A. (2022). A Pipeline for Automated Processing of Declassified Corona KH-4 (1962–1972) Stereo Imagery. *IEEE Transactions on Geoscience and Remote Sensing*, 60, 1–14. *IEEE Transactions on Geoscience and Remote Sensing*.  
<https://doi.org/10.1109/TGRS.2022.3200151>.
- Goldstein, R. M., & Werner, C. L. (1998). Radar interferogram filtering for geophysical applications. *Geophysical research letters*, 25(21), 4035-4038.  
<https://doi.org/10.1029/98GL02557>.
- Gruber, S. (2012). Derivation and analysis of a high-resolution estimate of global permafrost zonation. *The Cryosphere*, 6(1), 221-233. <https://doi.org/10.5194/tc-6-221-2012>.
- Guerrero, J., Guerra, M., Yannick, T., Desir, G., & Colas, B. (2025). Kinematic inventory of rock glaciers in the Pyrenees based on InSAR and airborne LiDAR data. *Remote Sensing of Environment*, 326, 114798.  
<https://doi.org/10.1016/j.rse.2025.114798>.
- Haeberli, W., Hallet, B., Arenson, L., Elconin, R., Humlum, O., Kääb, A., Kaufmann, V., Ladanyi, B., Matsuoka, N., Springman, S., & Mühl, D. V. (2006). Permafrost creep and rock glacier dynamics. *Permafrost and Periglacial Processes*, 17(3), 189–214. <https://doi.org/10.1002/ppp.561>.
- Harrison, S., Jones, D., Anderson, K., Shannon, S., & Betts, R. A. (2021). Is ice in the Himalayas more resilient to climate change than we thought?. *Geografiska Annaler: Series A, Physical Geography*, 103(1), 1-7.  
<https://doi.org/10.1080/04353676.2021.1902582>.
- Harrison, S., Jones, D. B., Racoviteanu, A. E., Anderson, K., Shannon, S., Betts, R. A., & Leng, R. (2024). Rock glacier distribution across the Himalaya. *Global and Planetary Change*, 104481. <https://doi.org/10.1016/j.gloplacha.2024.104481>.
- Hartl, L., Fischer, A., Klug, C., & Nicholson, L. (2016). Can a simple numerical model help to fine-tune the analysis of ground-penetrating radar data? Hochebenkar rock glacier as a case study. *Arctic, Antarctic, and Alpine Research*, 48(2), 377-393. <https://doi.org/10.1657/AAAR0015-066>.
- Hassan, J., Chen, X., Muhammad, S., & Bazai, N. A. (2021). Rock glacier inventory, permafrost probability distribution modeling and associated hazards in the Hunza River Basin, Western Karakoram, Pakistan. *Science of The Total Environment*, 782, 146833. <https://doi.org/10.1016/j.scitotenv.2021.146833>.
- Hassan, J., Berg, D. L., Lippert, E. Y. H., Chen, X., Hassan, W., Hassan, M., Hussain, I., Bazai, N. A., & Khan, S. A. (2024). Rock glacier distribution and kinematics in Shigar and Shayok basins based on radar and optical remote sensing. *Earth*

## BIBLIOGRAPHY

- Surface Processes and Landforms, 49(7), 2278–2290.  
<https://doi.org/10.1002/esp.5820>.
- Hausmann, H., Krainer, K., Brückl, E., & Mostler, W. (2007). Internal structure and ice content of Reichenkar rock glacier (Stubai Alps, Austria) assessed by geophysical investigations. *Permafrost and Periglacial Processes*, 18(4), 351–367. <https://doi.org/10.1002/ppp.601>.
- Hausmann, H., Krainer, K., Brückl, E., & Ullrich, C. (2012). Internal structure, ice content and dynamics of Ölgrube and Kaiserberg rock glaciers (Ötztal Alps, Austria) determined from geophysical surveys. *Austrian Journal of Earth Sciences*, 105(2), 12–31.
- Heid, T., & Kääb, A. (2012). Evaluation of existing image matching methods for deriving glacier surface displacements globally from optical satellite imagery. *Remote Sensing of Environment*, 118, 339–355.  
<https://doi.org/10.1016/j.rse.2011.11.024>.
- Hersbach, H., Bell, B., Berrisford, P., Hirahara, S., Horányi, A., Muñoz-Sabater, J., Nicolas, J., Peubey, C., Radu, R., Schepers, D., Simmons, A., Soci, C., Abdalla, S., Abellan, X., Balsamo, G., Bechtold, P., Biavati, G., Bidlot, J., Bonavita, M., ... Thépaut, J. (2020). The ERA5 global reanalysis. *Quarterly Journal of the Royal Meteorological Society*, 146(730), 1999–2049.  
<https://doi.org/10.1002/qj.3803>.
- Hogenson, K., Kristenson, H., Kennedy, J., Johnston, A., Rine, J., Logan, T., Zhu, J., Williams, F., Herrmann, J., Smale, J., Meyer, F., 2020. Hybrid Pluggable Processing Pipeline (HyP3): A cloud-native infrastructure for generic processing of SAR data [Computer software].  
<https://doi.org/10.5281/zenodo.4646138>.
- Hu, Y., Liu, L., Huang, L., Zhao, L., Wu, T., Wang, X., & Cai, J. (2023a). Mapping and characterizing rock glaciers in the arid Western Kunlun Mountains supported by InSAR and deep learning. *Journal of Geophysical Research: Earth Surface*, 128(9), e2023JF007206. <https://doi.org/10.1029/2023JF007206>.
- Hu, Y., Harrison, S., Liu, L., & Wood, J. L. (2023b). Modelling rock glacier ice content based on InSAR-derived velocity, Khumbu and Lhotse valleys, Nepal. *The Cryosphere*, 17(6), 2305–2321. <https://doi.org/10.5194/tc-17-2305-2023>.
- Hu, Y., Arenson, L. U., Barboux, C., Bodin, X., Cicoira, A., Delaloye, R., Gärtner - Roer, I., Kääb, A., Kellerer - Pirklbauer, A., Lambiel, C., Liu, L., Pellet, C., Rouyet, L., Schoeneich, P., Seier, G., & Strozzi, T. (2025). Rock Glacier Velocity: An Essential Climate Variable Quantity for Permafrost. *Reviews of Geophysics*, 63(1), e2024RG000847. <https://doi.org/10.1029/2024RG000847>.

## BIBLIOGRAPHY

- Hu, Z., Yan, D., Feng, M., Xu, J., Liang, S., & Sheng, Y. (2024). Enhancing mountainous permafrost mapping by leveraging a rock glacier inventory in northeastern Tibetan Plateau. *International Journal of Digital Earth*, 17(1), 2304077. <https://doi.org/10.1080/17538947.2024.2304077>.
- Huang, L., Liu, L., Jiang, L., & Zhang, T. (2018). Automatic mapping of thermokarst landforms from remote sensing images using deep learning: A case study in the Northeastern Tibetan Plateau. *Remote Sensing*, 10(12), 2067. <https://doi.org/10.3390/rs10122067>.
- Huang, L., Luo, J., Lin, Z., Niu, F., & Liu, L. (2020). Using deep learning to map retrogressive thaw slumps in the Beiluhe region (Tibetan Plateau) from CubeSat images. *Remote Sensing of Environment*, 237, 111534. <https://doi.org/10.1016/j.rse.2019.111534>.
- Huang, X., Han, S., & Shi, C. (2022). Evaluation of three air temperature reanalysis datasets in the alpine region of the Qinghai–Tibet plateau. *Remote Sensing*, 14(18), 4447. <https://doi.org/10.3390/rs14184447>.
- Huang, L., Chen, J., Yang, K., Yang, Y., Huang, W., Zhang, X., & Chen, F. (2023). The northern boundary of the Asian summer monsoon and division of westerlies and monsoon regimes over the Tibetan Plateau in present-day. *Science China Earth Sciences*, 66(4), 882–893. <https://doi.org/10.1007/s11430-022-1086-1>.
- Huffman, G. J., Stocker, E. F., Bolvin, D. T., Nelkin, E. J., Tan, J., 2023. GPM IMERG Final Precipitation L3 1 month 0.1 degree x 0.1 degree V07, Greenbelt, MD, Goddard Earth Sciences Data and Information Services Center (GES DISC). Accessed: 2024-01-01. <https://doi.org/10.5067/GPM/IMERG/3B-MONTH/07>.
- Hugonnet, R., McNabb, R., Berthier, E., Menounos, B., Nuth, C., Girod, L., Farinotti, D., Huss, M., Dussaillant, I., Brun, F., & Kääb, A. (2021). Accelerated global glacier mass loss in the early twenty-first century. *Nature*, 592(7856), 726–731. <https://doi.org/10.1038/s41586-021-03436-z>.
- Hungr, O., Leroueil, S., & Picarelli, L. (2014). The Varnes classification of landslide types, an update. *Landslides*, 11, 167-194. <https://doi.org/10.1038/s41586-021-03436-z>.
- Immerzeel, W. W., Lutz, A. F., Andrade, M., Bahl, A., Biemans, H., Bolch, T., Hyde, S., Brumby, S., Davies, B. J., Elmore, A. C., Emmer, A., Feng, M., Fernández, A., Haritashya, U., Kargel, J. S., Koppes, M., Kraaijenbrink, P. D. A., Kulkarni, A. V., Mayewski, P. A., ... Baillie, J. E. M. (2020). Importance and vulnerability of the world's water towers. *Nature*, 577(7790), 364–369. <https://doi.org/10.1038/s41586-019-1822-y>.

## BIBLIOGRAPHY

- Janke, J. R., Bellisario, A. C., & Ferrando, F. A. (2015). Classification of debris-covered glaciers and rock glaciers in the Andes of central Chile. *Geomorphology*, 241, 98–121. <https://doi.org/10.1016/j.geomorph.2015.03.034>.
- Janke, J. R., Ng, S., & Bellisario, A. (2017). An inventory and estimate of water stored in firn fields, glaciers, debris-covered glaciers, and rock glaciers in the Aconcagua River Basin, Chile. *Geomorphology*, 296, 142-152. <https://doi.org/10.1016/j.geomorph.2017.09.002>.
- Janke, J. R., & Bolch, T. (2021). Rock glaciers. Reference module in Earth systems and environmental sciences. <https://doi.org/10.1016/B978-0-12-818234-5.000187-5>.
- Jiang, Y., Yang, K., Qi, Y., Zhou, X., He, J., Lu, H., Li, X., Chen, Y., Li, X., Zhou, B., Mamtimin, A., Shao, C., Ma, X., Tian, J., & Zhou, J. (2023). TPHiPr: A long-term (1979–2020) high-accuracy precipitation dataset (1 / 30°, daily) for the Third Pole region based on high-resolution atmospheric modeling and dense observations. *Earth System Science Data*, 15(2), 621–638. <https://doi.org/10.5194/essd-15-621-2023>.
- Johnson, G., Chang, H., & Fountain, A. (2021). Active rock glaciers of the contiguous United States: Geographic information system inventory and spatial distribution patterns. *Earth System Science Data*, 13(8), 3979–3994. <https://doi.org/10.5194/essd-13-3979-2021>.
- Jones, D. B., Harrison, S., Anderson, K., & Betts, R. A. (2018a). Mountain rock glaciers contain globally significant water stores. *Scientific Reports*, 8(1), 2834. <https://doi.org/10.1038/s41598-018-21244-w>.
- Jones, D. B., Harrison, S., Anderson, K., Selley, H. L., Wood, J. L., & Betts, R. A. (2018b). The distribution and hydrological significance of rock glaciers in the Nepalese Himalaya. *Global and Planetary Change*, 160, 123-142. <https://doi.org/10.1016/j.gloplacha.2017.11.005>.
- Jones, D. B., Harrison, S., Anderson, K., & Whalley, W. B. (2019a). Rock glaciers and mountain hydrology: A review. *Earth-Science Reviews*, 193, 66-90. <https://doi.org/10.1016/j.earscirev.2019.04.00>.
- Jones, D. B., Harrison, S., & Anderson, K. (2019b). Mountain glacier-to-rock glacier transition. *Global and Planetary Change*, 181, 102999. <https://doi.org/10.1016/j.gloplacha.2019.102999>.
- Jones, D. B., Harrison, S., Anderson, K., Shannon, S., & Betts, R. A. (2021). Rock glaciers represent hidden water stores in the Himalaya. *Science of The Total Environment*, 793, 145368. <https://doi.org/10.1016/j.scitotenv.2021.145368>.
- Kääb, A., & Vollmer, M. (2000). Surface geometry, thickness changes and flow

## BIBLIOGRAPHY

- fields on creeping mountain permafrost: automatic extraction by digital image analysis. *Permafrost and Periglacial Processes*, 11(4), 315-326. [https://doi.org/10.1002/1099-1530\(200012\)11:4<315::AID-PPP365>3.0.CO;2-J](https://doi.org/10.1002/1099-1530(200012)11:4<315::AID-PPP365>3.0.CO;2-J).
- Kääb, A., Strozzi, T., Bolch, T., Caduff, R., Trefall, H., Stoffel, M., & Kokarev, A. (2021). Inventory and changes of rock glacier creep speeds in Ile Alatau and Kungöy Ala-Too, northern Tien Shan, since the 1950s. *The Cryosphere*, 15(2), 927-949. <https://doi.org/10.5194/tc-15-927-2021>.
- Kääb, A., Røste, J., 2024. Rock glaciers across the United States predominantly accelerate coincident with rise in air temperatures. *Nat. Commun.* 15(1), 7581. <https://www.nature.com/articles/s41467-024-52093-z>.
- Kaufmann, V., Ladstädter, R., 2003. Quantitative analysis of rock glacier creep by means of digital photogrammetry using multi-temporal aerial photographs: two case studies in the Austrian Alps. In: Proceedings of the 8th International Conference on Permafrost, Vol. 1, Zurich, Switzerland: AA Balkema Publishers.
- Kellerer-Pirklbauer, A., Bodin, X., Delaloye, R., Lambiel, C., Gärtner-Roer, I., Bonnefoy-Demongeot, M., Carturan, L., Damm, B., Eulensteiner, J., Fischer, A., Hartl, L., Ikeda, A., Kaufmann, V., Krainer, K., Matsuoka, N., Morra Di Cella, U., Noetzli, J., Seppi, R., Scapozza, C., ... Zumiani, M. (2024). Acceleration and interannual variability of creep rates in mountain permafrost landforms (rock glacier velocities) in the European Alps in 1995–2022. *Environmental Research Letters*, 19(3), 034022. <https://doi.org/10.1088/1748-9326/ad25a4>.
- Kenner, R., Phillips, M., Beutel, J., Hiller, M., Limpach, P., Pointner, E., & Volken, M. (2017). Factors controlling velocity variations at short-term, seasonal and multiyear time scales, Ritigraben rock glacier, Western Swiss Alps. *Permafrost and Periglacial Processes*, 28(4), 675-684. <https://doi.org/10.1002/ppp.1953>.
- Kraaijenbrink, P. D. A., Bierkens, M. F. P., Lutz, A. F., & Immerzeel, W. W. (2017). Impact of a global temperature rise of 1.5 degrees Celsius on Asia's glaciers. *Nature*, 549, 257–260. <https://doi.org/10.1038/nature23878>.
- Kraaijenbrink, P. D., Stigter, E. E., Yao, T., & Immerzeel, W. W. (2021). Climate change decisive for Asia's snow meltwater supply. *Nature Climate Change*, 11(7), 591-597. <https://doi.org/10.1038/s41558-021-01074-x>.
- Kumar, L., Skidmore, A. K., & Knowles, E. (1997). Modelling topographic variation in solar radiation in a GIS environment. *International journal of geographical information science*, 11(5), 475-497. <https://doi.org/10.1080/136588197242266>.
- Lambiel, C., & Delaloye, R. (2004). Contribution of real-time kinematic GPS in the study of creeping mountain permafrost: Examples from the Western Swiss Alps. *Permafrost and periglacial processes*, 15(3), 229-241.

## BIBLIOGRAPHY

- [https://doi.org/10.1002/ppp.496.](https://doi.org/10.1002/ppp.496)
- Li, M., Yang, Y., Peng, Z., & Liu, G. (2024). Assessment of rock glaciers and their water storage in Guokalariju, Tibetan Plateau. *The Cryosphere*, 18(1), 1-16. <https://doi.org/10.5194/tc-18-1-2024>.
- Li, Y., Qin, X., Liu, Y., Jin, Z., Liu, J., Wang, L., & Chen, J. (2022). Evaluation of long-term and high-resolution gridded precipitation and temperature products in the Qilian Mountains, Qinghai–Tibet Plateau. *Frontiers in environmental science*, 10, 906821. <https://doi.org/10.3389/fenvs.2022.906821>.
- Liu, L., Millar, C. I., Westfall, R. D., & Zebker, H. A. (2013). Surface motion of active rock glaciers in the Sierra Nevada, California, USA: inventory and a case study using InSAR. *The Cryosphere*, 7(4), 1109-1119. <https://doi.org/10.5194/tc-7-1109-2013>.
- Liu, Z., Lin, Y., Cao, Y., Hu, H., Wei, Y., Zhang, Z., Lin, S., & Guo, B. (2021). Swin Transformer: Hierarchical Vision Transformer using Shifted Windows (arXiv:2103.14030). arXiv. <https://doi.org/10.48550/arXiv.2103.14030>.
- Luckman, A., Quincey, D., & Bevan, S. (2007). The potential of satellite radar interferometry and feature tracking for monitoring flow rates of Himalayan glaciers. *Remote sensing of Environment*, 111(2-3), 172-181. <https://doi.org/10.1016/j.rse.2007.05.019>.
- Lundberg, S. M., Erion, G., Chen, H., DeGrave, A., Prutkin, J. M., Nair, B., Katz, R., Himmelfarb, J., Bansal, N., & Lee, S.-I. (2020). From local explanations to global understanding with explainable AI for trees. *Nature Machine Intelligence*, 2(1), 56–67. <https://doi.org/10.1038/s42256-019-0138-9>.
- Ma, Q., & Oguchi, T. (2024). Rock Glacier Inventory of the Southwestern Pamirs Supported by InSAR Kinematics. *Remote Sensing*, 16(7), 1185. <https://doi.org/10.3390/rs16071185>.
- Manchado, A. M. T., Allen, S., Cicoira, A., Wiesmann, S., Haller, R., & Stoffel, M. (2024). 100 years of monitoring in the Swiss National Park reveals overall decreasing rock glacier velocities. *Communications Earth & Environment*, 5(1), 138. <https://doi.org/10.1038/s43247-024-00540-6>.
- Marcer, M., Bodin, X., Brenning, A., Schoeneich, P., Charvet, R., & Gottardi, F. (2017). Permafrost favorability index: spatial modeling in the French Alps using a rock glacier inventory. *Frontiers in Earth Science*, 5, 105. <https://doi.org/10.3389/feart.2017.00105>.
- Marcer, M. (2020). Rock glaciers automatic mapping using optical imagery and convolutional neural networks. *Permafrost and periglacial processes*, 31(4), 561-566. <https://doi.org/10.1002/ppp.2076>.

## BIBLIOGRAPHY

- Marcer, M., Cicoira, A., Cusicanqui, D., Bodin, X., Echelard, T., Obregon, R., & Schoeneich, P. (2021). Rock glaciers throughout the French Alps accelerated and destabilised since 1990 as air temperatures increased. *Communications Earth & Environment*, 2(1), 81. <https://doi.org/10.1038/s43247-021-00150-6>.
- McNally, A. et al.: FLDAS Noah Land Surface Model L4 Global Monthly 0.1 x 0.1 degree (MERRA-2 and CHIRPS), Greenbelt, MD, USA, Goddard Earth Sciences Data and Information Services Center (GES DISC), <https://doi.org/10.5067/5NHC22T9375G> (last access: 1 January 2024), 2018.
- Millan, R., Mouginot, J., Rabatel, A., & Morlighem, M. (2022). Ice velocity and thickness of the world's glaciers. *Nature Geoscience*, 15(2), 124-129. <https://doi.org/10.1038/s41561-021-00885-z>.
- Millar, C. I., & Westfall, R. D. (2019). Geographic, hydrological, and climatic significance of rock glaciers in the Great Basin, USA. *Arctic, Antarctic, and Alpine Research*, 51(1), 232-249. <https://doi.org/10.1080/15230430.2019.1618666>.
- Mu, C., Abbott, B. W., Norris, A. J., Mu, M., Fan, C., Chen, X., Jia, L., Yang, R., Zhang, T., Wang, K., Peng, X., Wu, Q., Guggenberger, G., & Wu, X. (2020). The status and stability of permafrost carbon on the Tibetan Plateau. *Earth-Science Reviews*, 211, 103433. <https://doi.org/10.1016/j.earscirev.2020.103433>.
- Müller, J., Vieli, A., & Gärtner-Roer, I. (2016). Rock glaciers on the run—understanding rock glacier landform evolution and recent changes from numerical flow modeling. *The Cryosphere*, 10(6), 2865-2886. <https://doi.org/10.5194/tc-10-2865-2016>.
- Munroe, J. S. (2018). Distribution, evidence for internal ice, and possible hydrologic significance of rock glaciers in the Uinta Mountains, Utah, USA. *Quaternary Research*, 90(1), 50-65. <https://doi.org/10.1017/qua.2018.24>.
- Nass, A., Manaud, N., van Gasselt, S., & Hare, T. M. (2019). Towards a new face for Planetary Maps: Design and web-based Implementation of Planetary Basemaps. *Advances in Cartography and GIScience of the ICA*, 1, 15. <https://doi.org/10.5194/ica-adv-1-15-2019>.
- Necsoiu, M., Onaca, A., Wigginton, S., & Urdea, P. (2016). Rock glacier dynamics in Southern Carpathian Mountains from high-resolution optical and multi-temporal SAR satellite imagery. *Remote sensing of environment*, 177, 21-36. <https://doi.org/10.1016/j.rse.2016.02.025>.
- Obu, J., Westermann, S., Kääb, A., & Bartsch, A. (2018). Ground Temperature Map: 2000-2016: Northern Hemisphere Permafrost. *Pangaea*. <https://doi.pangaea.de/10.1594/PANGAEA.888600>.

## BIBLIOGRAPHY

- Pandey, P. (2019). Inventory of rock glaciers in Himachal Himalaya, India using high-resolution Google Earth imagery. *Geomorphology*, 340, 103-115. <https://doi.org/10.1016/j.geomorph.2019.05.001>.
- Pandey, P., Ali, S. N., Das, S. S., & Khan, M. A. R. (2024). Rock glaciers of the semi-arid northwestern Himalayas: distribution, characteristics, and hydrological significance. *Catena*, 238, 107845. <https://doi.org/10.1175/2023BAMSStateoftheClimate.1>.
- Paterson, W. S. B. (1994). Physics of glaciers. Butterworth-Heinemann.
- Pepin, K., & Zebker, H. (2024). Aliasing in InSAR 2-D Phase Unwrapping and Time Series. *IEEE Transactions on Geoscience and Remote Sensing*, 62, 1–17. <https://doi.org/10.1109/TGRS.2024.3359482>.
- PERMOS. (2024). In Swiss permafrost bulletin 2023 (eds.), J. Noetzli & C. Pellet (Vol. 5, pp. 25). <https://doi.org/10.13093/permos-bull-24>.
- Perucca, L., & Esper Angillieri, M. Y. (2011). Glaciers and rock glaciers' distribution at 28 SL, Dry Andes of Argentina, and some considerations about their hydrological significance. *Environmental earth sciences*, 64, 2079-2089. <https://doi.org/10.1007/s12665-011-1030-z>.
- Pfeffer, W. T., Arendt, A. A., Bliss, A., Bolch, T., Cogley, J. G., Gardner, A. S., Hagen, J.-O., Hock, R., Kaser, G., Kienholz, C., Miles, E. S., Moholdt, G., Mölg, N., Paul, F., Radić, V., Rastner, P., Raup, B. H., Rich, J., Sharp, M. J., & The Randolph Consortium. (2014). The Randolph Glacier Inventory: A globally complete inventory of glaciers. *Journal of Glaciology*, 60(221), 537–552. <https://doi.org/10.3189/2014JoG13J176>.
- Pritchard, H. D. (2019). Asia's shrinking glaciers protect large populations from drought stress. *Nature*, 569(7758), 649–654. <https://doi.org/10.1038/s41586-019-1240-1>.
- Racoviteanu, A. E., Nicholson, L., Glasser, N. F., Miles, E., Harrison, S., & Reynolds, J. M. (2022). Debris-covered glacier systems and associated glacial lake outburst flood hazards: challenges and prospects. *Journal of the Geological Society*, 179(3), jgs2021-084. <https://doi.org/10.1144/jgs2021-084>.
- Ran, Y., Cheng, G., Dong, Y., Hjort, J., Lovecraft, A. L., Kang, S., Tan, M., & Li, X. (2022). Permafrost degradation increases risk and large future costs of infrastructure on the Third Pole. *Communications Earth & Environment*, 3(1), 238. <https://doi.org/10.1038/s43247-022-00568-6>.
- Ran, Z., & Liu, G. (2018). Rock glaciers in Daxue Shan, south-eastern Tibetan Plateau: An inventory, their distribution, and their environmental controls. *The Cryosphere*, 12(7), 2327-2340. <https://doi.org/10.5194/tc-12-2327-2018>.

## BIBLIOGRAPHY

- Rangecroft, S., Harrison, S., & Anderson, K. (2015). Rock glaciers as water stores in the Bolivian Andes: an assessment of their hydrological importance. *Arctic, Antarctic, and Alpine Research*, 47(1), 89-98.  
<https://doi.org/10.1657/AAAR0014-029>.
- Reinosch, E., Gerke, M., Riedel, B., Schwalb, A., Ye, Q., & Buckel, J. (2021). Rock glacier inventory of the western Nyainqntanglha Range, Tibetan Plateau, supported by InSAR time series and automated classification. *Permafrost and Periglacial Processes*, 32(4), 657-672. <https://doi.org/10.1002/ppp.2117>.
- Ren, M., Zeng, W., Yang, B., & Urtasun, R. (2018, July). Learning to reweight examples for robust deep learning. In International conference on machine learning (pp. 4334-4343). PMLR. <https://proceedings.mlr.press/v80/ren18a.html>.
- RGI Consortium (2017). Randolph Glacier Inventory - A Dataset of Global Glacier Outlines, Version 6. [Indicate subset used]. Boulder, Colorado USA. NSIDC: National Snow and Ice Data Center. <https://doi.org/10.7265/4m1f-gd79>.
- RGI 7.0 Consortium (2023). Randolph Glacier Inventory - A Dataset of Global Glacier Outlines, Version 7.0. Boulder, Colorado USA. NSIDC: National Snow and Ice Data Center. <https://doi.org/10.5067/f6jmovy5navz>.
- RGIK (2022a). Optional kinematic attribute in standardized rock glacier inventories (version 3.0.1).  
[https://bigweb.unifr.ch/Science/Geosciences/Geomorphology/Pub/Website/IPA/RGK/RockGlacierKinematics\\_V3.pdf](https://bigweb.unifr.ch/Science/Geosciences/Geomorphology/Pub/Website/IPA/RGK/RockGlacierKinematics_V3.pdf).
- RGIK (2022b). Rock Glacier Velocity as an associated parameter of ECV Permafrost (Version 3.1).  
[https://bigweb.unifr.ch/Science/Geosciences/Geomorphology/Pub/Website/IPA/RGV/RockGlacierVelocity\\_V3.1.pdf](https://bigweb.unifr.ch/Science/Geosciences/Geomorphology/Pub/Website/IPA/RGV/RockGlacierVelocity_V3.1.pdf).
- RGIK (2023). Guidelines for inventorying rock glaciers: baseline and practical concepts (version 1.0), 25 pp. <https://doi.org/10.51363/unifr.srr.2023.002>.
- Rice, L., Wong, E., & Kolter, Z. (2020, November). Overfitting in adversarially robust deep learning. In International conference on machine learning (pp. 8093-8104). PMLR. <https://proceedings.mlr.press/v119/rice20a>.
- Rangecroft, S., Harrison, S., Anderson, K., Magrath, J., Castel, A. P., & Pacheco, P. (2014). A First Rock Glacier Inventory for the Bolivian Andes. *Permafrost and Periglacial Processes*, 25(4), 333–343. <https://doi.org/10.1002/ppp.1816>.
- Robson, B. A., Bolch, T., MacDonell, S., Hlbling, D., Rastner, P., & Schaffer, N. (2020). Automated detection of rock glaciers using deep learning and object-based image analysis. *Remote sensing of environment*, 250, 112033.  
<https://doi.org/10.1016/j.rse.2020.112033>.

## BIBLIOGRAPHY

- Robson, B. A., MacDonell, S., Ayala, Á., Bolch, T., Nielsen, P. R., & Vivero, S. (2022). Glacier and rock glacier changes since the 1950s in the La Laguna catchment, Chile. *The Cryosphere*, 16(2), 647-665. <https://doi.org/10.5194/tc-16-647-2022>.
- Rounce, D. R., Hock, R., Maussion, F., Hugonnet, R., Kochtitzky, W., Huss, M., Berthier, E., Brinkerhoff, D., Compagno, L., Copland, L., Farinotti, D., Menounos, B., & McNabb, R. W. (2023). Global glacier change in the 21st century: Every increase in temperature matters. *Science*, 379(6627), 78–83. <https://doi.org/10.1126/science.abo1324>.
- Rouyet, L., Karjalainen, O., Niittynen, P., Aalto, J., Luoto, M., Lauknes, T. R., Larsen, Y., & Hjort, J. (2021a). Environmental Controls of InSAR-Based Periglacial Ground Dynamics in a Sub-Arctic Landscape. *Journal of Geophysical Research: Earth Surface*, 126(7), e2021JF006175. <https://doi.org/10.1029/2021JF006175>.
- Rouyet, L., Lilleøren, K. S., Böhme, M., Vick, L. M., Delaloye, R., Etzelmüller, B., Lauknes, T. R., Larsen, Y., & Blikra, L. H. (2021b). Regional Morpho-Kinematic Inventory of Slope Movements in Northern Norway. *Frontiers in Earth Science*, 9. <https://doi.org/10.3389/feart.2021.681088>.
- Rouyet, L., Bolch, T., Brardinoni, F., Caduff, R., Cusicanqui, D., Darrow, M., Delaloye, R., Echelard, T., Lambiel, C., Ruiz, L., Schmid, L., Sirbu, F., & Strozzi, T. (2025). Rock Glacier Inventories (RoGI) in 12 areas worldwide using a multi-operator consensus-based procedure. <https://doi.org/10.5194/essd-2024-598>.
- Schaffer, N., MacDonell, S., Réveillet, M., Yáñez, E., & Valois, R. (2019). Rock glaciers as a water resource in a changing climate in the semiarid Chilean Andes. *Regional Environmental Change*, 19, 1263-1279. <https://doi.org/10.1007/s10113-018-01459-3>.
- Schmid, M. O., Baral, P., Gruber, S., Shahi, S., Shrestha, T., Stumm, D., & Wester, P. (2015). Assessment of permafrost distribution maps in the Hindu Kush Himalayan region using rock glaciers mapped in Google Earth. *The Cryosphere*, 9(6), 2089-2099. <https://doi.org/10.5194/tc-9-2089-2015>.
- Shean, D. E., Bhushan, S., Montesano, P., Rounce, D. R., Arendt, A., & Osmanoglu, B. (2020). A systematic, regional assessment of high mountain Asia glacier mass balance. *Frontiers in Earth Science*, 7, 363. <https://doi.org/10.3389/feart.2019.00363>.
- Smith, T., & Bookhagen, B. (2018). Changes in seasonal snow water equivalent distribution in High Mountain Asia (1987 to 2009). *Science advances*, 4(1), e1701550. <https://doi.org/10.1126/sciadv.1701550>.

## BIBLIOGRAPHY

- Scotti, R., Brardinoni, F., Alberti, S., Frattini, P., & Crosta, G. B. (2013). A regional inventory of rock glaciers and protalus ramparts in the central Italian Alps. *Geomorphology*, 186, 136–149.  
<https://doi.org/10.1016/j.geomorph.2012.12.028>.
- Spencer, A. C. (1900). A peculiar form of talus. *Science*, 11(266), 188.
- Strozzi, T., Caduff, R., Jones, N., Barboux, C., Delaloye, R., Bodin, X., Kääb, A., Mätzler, E., & Schrott, L. (2020). Monitoring Rock Glacier Kinematics with Satellite Synthetic Aperture Radar. *Remote Sensing*, 12(3), Article 3.  
<https://doi.org/10.3390/rs12030559>.
- Sun, Z., Hu, Y., Racoviteanu, A., Liu, L., Harrison, S., Wang, X., Cai, J., Guo, X., He, Y., & Yuan, H. (2024). TPRoGI: A comprehensive rock glacier inventory for the Tibetan Plateau using deep learning. *Earth System Science Data*, 16(12), 5703–5721. <https://doi.org/10.5194/essd-16-5703-2024>.
- Vivero, S., Bodin, X., Farías-Barahona, D., MacDonell, S., Schaffer, N., Robson, B. A., & Lambiel, C. (2021). Combination of aerial, satellite, and UAV photogrammetry for quantifying rock glacier kinematics in the Dry Andes of Chile (30 S) since the 1950s. *Frontiers in Remote Sensing*, 2, 784015.  
<https://doi.org/10.3389/frsen.2021.784015>.
- Wagner, T., Pauritsch, M., & Winkler, G. (2016). Impact of relict rock glaciers on spring and stream flow of alpine watersheds: Examples of the Niedere Tauern Range, Eastern Alps (Austria). *Austrian Journal of Earth Sciences*, 109(1).  
<https://doi.org/10.17738/ajes.2016.0006>.
- Wagner, T., Brodacz, A., Krainer, K., & Winkler, G. (2020a). Active rock glaciers as shallow groundwater reservoirs, Austrian Alps. *Grundwasser*, 25(3), 215-230.  
<https://doi.org/10.1007/s00767-020-00455-x>.
- Wagner, T., Pleschberger, R., Kainz, S., Ribis, M., Kellerer-Pirklbauer, A., Krainer, K., Philippitsch, R., & Winkler, G. (2020b). The first consistent inventory of rock glaciers and their hydrological catchments of the Austrian Alps. *Austrian Journal of Earth Sciences*, 113(1), 1–23.  
<https://doi.org/10.17738/ajes.2020.0001>.
- Wagner, T., Seelig, S., Helffricht, K., Fischer, A., Avian, M., Krainer, K., & Winkler, G. (2021). Assessment of liquid and solid water storage in rock glaciers versus glacier ice in the Austrian Alps. *Science of the Total Environment*, 800, 149593.  
<https://doi.org/10.1016/j.scitotenv.2021.149593>.
- Wahrhaftig, C., & Cox, A. (1959). Rock glaciers in the Alaska Range. *Geological Society of America Bulletin*, 70(4), 383-436. [https://doi.org/10.1130/0016-7606\(1959\)70\[383:Rgitar\]2.0.Co;2](https://doi.org/10.1130/0016-7606(1959)70[383:Rgitar]2.0.Co;2).

- Wang, X., Liu, L., Zhao, L., Wu, T., Li, Z., & Liu, G. (2017). Mapping and inventorying active rock glaciers in the northern Tien Shan of China using satellite SAR interferometry. *The Cryosphere*, 11(2), 997-1014. <https://doi.org/10.5194/tc-11-997-2017>.
- Whalley, W. B. (2020). Gruben glacier and rock glacier, Wallis, Switzerland: glacier ice exposures and their interpretation. *Geografiska Annaler: Series A, Physical Geography*, 102(2), 141-161. <https://doi.org/10.1080/04353676.2020.1765578>.
- Wirz, V., Beutel, J., Gruber, S., Gubler, S., & Purves, R. S. (2014). Estimating velocity from noisy GPS data for investigating the temporal variability of slope movements. *Natural Hazards and Earth System Sciences*, 14(9), 2503-2520. <https://doi.org/10.5194/nhess-14-2503-2014>.
- Wirz, V., Gruber, S., Purves, R. S., Beutel, J., Gärtner-Roer, I., Gubler, S., & Vieli, A. (2016). Short-term velocity variations at three rock glaciers and their relationship with meteorological conditions. *Earth Surface Dynamics*, 4(1), 103-123. <https://doi.org/10.5194/esurf-4-103-2016>.
- Wood, E., Bolch, T., & Streeter, R. (2025). Insights from feature tracking of optical satellite data for studying rock glacier kinematics in the Northern Tien Shan. *Frontiers in Earth Science*, 12, 1518390. <https://doi.org/10.3389/feart.2024.1518390>.
- Wu, H., Xiao, B., Codella, N., Liu, M., Dai, X., Yuan, L., & Zhang, L. (2021). CvT: Introducing Convolutions to Vision Transformers (arXiv:2103.15808). arXiv. <https://doi.org/10.48550/arXiv.2103.15808>.
- Xia, Z., Liu, L., Mu, C., Peng, X., Zhao, Z., Huang, L., Luo, J., & Fan, C. (2024). Widespread and Rapid Activities of Retrogressive Thaw Slumps on the Qinghai-Tibet Plateau From 2016 to 2022. *Geophysical Research Letters*, 51(17), e2024GL109616. <https://doi.org/10.1029/2024GL109616>.
- Xie, E., Wang, W., Yu, Z., Anandkumar, A., Alvarez, J. M., & Luo, P. (2021). SegFormer: Simple and Efficient Design for Semantic Segmentation with Transformers (arXiv:2105.15203). arXiv. <https://doi.org/10.48550/arXiv.2105.15203>.
- Yao, T., Thompson, L., Yang, W., Yu, W., Gao, Y., Guo, X., Yang, X., Duan, K., Zhao, H., Xu, B., Pu, J., Lu, A., Xiang, Y., Kattel, D. B., & Joswiak, D. (2012). Different glacier status with atmospheric circulations in Tibetan Plateau and surroundings. *Nature Climate Change*, 2(9), 663–667. <https://doi.org/10.1038/nclimate1580>.
- Yao, T., Masson-Delmotte, V., Gao, J., Yu, W., Yang, X., Risi, C., Sturm, C., Werner, M., Zhao, H., He, Y., Ren, W., Tian, L., Shi, C., & Hou, S. (2013). A

## BIBLIOGRAPHY

- review of climatic controls on  $\delta$  18 O in precipitation over the Tibetan Plateau: Observations and simulations. *Reviews of Geophysics*, 51(4), 525–548.  
<https://doi.org/10.1002/rog.20023>.
- Yao, T., Xue, Y., Chen, D., Chen, F., Thompson, L., Cui, P., Koike, T., Lau, W. K.-M., Lettenmaier, D., Mosbrugger, V., Zhang, R., Xu, B., Dozier, J., Gillespie, T., Gu, Y., Kang, S., Piao, S., Sugimoto, S., Ueno, K., ... Li, Q. (2019). Recent Third Pole's Rapid Warming Accompanies Cryospheric Melt and Water Cycle Intensification and Interactions between Monsoon and Environment: Multidisciplinary Approach with Observations, Modeling, and Analysis. *Bulletin of the American Meteorological Society*, 100(3), 423–444.  
<https://doi.org/10.1175/BAMS-D-17-0057.1>.
- Yao, T., Bolch, T., Chen, D., Gao, J., Immerzeel, W., Piao, S., Su, F., Thompson, L., Wada, Y., Wang, L., Wang, T., Wu, G., Xu, B., Yang, W., Zhang, G., & Zhao, P. (2022). The imbalance of the Asian water tower. *Nature Reviews Earth & Environment*, 3(10), Article 10. <https://doi.org/10.1038/s43017-022-00299-4>.
- Yu, L., & Gong, P. (2012). Google Earth as a virtual globe tool for Earth science applications at the global scale: progress and perspectives. *International Journal of Remote Sensing*, 33(12), 3966–3986.  
<https://doi.org/10.1080/01431161.2011.636081>.
- Yu, C., Li, Z., Penna, N. T., & Crippa, P. (2018a). Generic Atmospheric Correction Model for Interferometric Synthetic Aperture Radar Observations. *Journal of Geophysical Research: Solid Earth*, 123(10), 9202–9222.  
<https://doi.org/10.1029/2017JB015305>.
- Yu, C., Li, Z., & Penna, N. T. (2018b). Interferometric synthetic aperture radar atmospheric correction using a GPS-based iterative tropospheric decomposition model. *Remote Sensing of Environment*, 204, 109–121.  
<https://doi.org/10.1016/j.rse.2017.10.038>.
- Zhang, Q., Jia, N., Xu, H., Yi, C., Wang, N., & Zhang, L. (2022). Rock glaciers in the Gangdise Mountains, southern Tibetan Plateau: Morphology and controlling factors. *CATENA*, 218, 106561. <https://doi.org/10.1016/j.catena.2022.106561>.
- Zhang, X., Feng, M., Zhang, H., Wang, C., Tang, Y., Xu, J., Yan, D., & Wang, C. (2021). Detecting Rock Glacier Displacement in the Central Himalayas Using Multi-Temporal InSAR. *Remote Sensing*, 13(23), Article 23.  
<https://doi.org/10.3390/rs13234738>.
- Zhang, X., Feng, M., Xu, J., Yan, D., Wang, J., Zhou, X., Li, T., & Zhang, X. (2023). Kinematic inventory of rock glaciers in the Nyainqêntanglha Range using the MT-InSAR method. *International Journal of Digital Earth*, 16(1), 3923–3948.  
<https://doi.org/10.1080/17538947.2023.2260778>.

## BIBLIOGRAPHY

- Zhao, L., Zou, D., Hu, G., Du, E., Pang, Q., Xiao, Y., ... & Liu, S. (2020). Changing climate and the permafrost environment on the Qinghai–Tibet (Xizang) plateau. *Permafrost and Periglacial Processes*, 31(3), 396-405.  
<https://doi.org/10.1002/ppp.2056>.
- Zhao, L., Zou, D., Hu, G., Wu, T., Du, E., Liu, G., Xiao, Y., Li, R., Pang, Q., Qiao, Y., Wu, X., Sun, Z., Xing, Z., Sheng, Y., Zhao, Y., Shi, J., Xie, C., Wang, L., Wang, C., & Cheng, G. (2021). A synthesis dataset of permafrost thermal state for the Qinghai–Tibet (Xizang) Plateau, China. *Earth System Science Data*, 13(8), 4207–4218. <https://doi.org/10.5194/essd-13-4207-2021>.
- Zou, D., Zhao, L., Sheng, Y., Chen, J., Hu, G., Wu, T., Wu, J., Xie, C., Wu, X., Pang, Q., Wang, W., Du, E., Li, W., Liu, G., Li, J., Qin, Y., Qiao, Y., Wang, Z., Shi, J., & Cheng, G. (2017). A new map of permafrost distribution on the Tibetan Plateau. *The Cryosphere*, 11(6), 2527–2542. <https://doi.org/10.5194/tc-11-2527-2017>.
- Zou, D., Pang, Q., Zhao, L., Wang, L., Hu, G., Du, E., Liu, G., Liu, S., & Liu, Y. (2024). Estimation of permafrost ground ice to 10 m depth on the Qinghai – Tibet Plateau. *Permafrost and Periglacial Processes*, 35(3), 423-434.  
<https://doi.org/10.1002/ppp.2226>.